AN ABSTRACT OF THE THESIS OF

Jebediah Wilson for the Master of Science in Civil Engineering and Wood Science presented on September 26, 2008.

Title: Behavior of a 1/6th Scale, Two-Story, Wood Framed Residential Structure Under Surge Wave Loading

Abstract approved: ______________________________
Rakesh Gupta

The goal of this study was to develop an understanding of the nature of surge wave loading on wood framed residential structures for a variety of building configurations and test conditions. The objectives of the study were: (1) to measure forces on a 1/6th scale wood framed residential structure, (2) to evaluate qualitatively the structural response to different loading conditions, (3) to compare the effects of different structural configurations on the structural response, (4) to develop an equation to predict wave forces, and (5) to compare predicted/measured forces with existing building code.

Testing was performed on a 1/6th scale 2-story wood-framed residential structure. The design of the structural model was performed by a Colorado State University research team under the supervision of Dr. John van de Lindt, the details of which can be found in Garcia (2008). The structure was prefabricated at Colorado State University and shipped to Oregon State University's Wood Science and Engineering (WSE) Structures Laboratory for final assembly. The 1/6th scale model was tested in the Tsunami Wave Basin at the O.H. Hinsdale Wave Research Laboratory. The structure was tested in both a flooded and non-flooded condition with the following solitary wave heights: 10 cm, 20 cm, 30 cm, 40 cm, 50 cm, and 60 cm. Additional push over testing was conducted in the WSE Structures Laboratory on a nominally identical model to quantify the stiffness of the structure.

This research was successful at developing an experimental setup to capture surge wave forces on the model structure. The measured forces were mainly overturning moments and

uplift forces due to wave loading. The qualitative analysis of the data showed that differences in structural stiffness throughout the structure will cause a different load distribution in the structure, e.g. overhanging eaves above the garage can provide unanticipated loading conditions, water traveling beneath the structure generates predominantly uplift forces, and the effect of waves breaking on or near the structure greatly increases the loading. The average difference in total load from the 0° to 90° orientation (approximately 2:1 aspect ratio) had a ratio of approximately 4:1. However, the building code equations to predict surge loading does not take this into account. The ratio of force from the windows closed condition to the windows open condition is approximately 2.5:1, a reduction of 40%.

The relationships in equations (1) and (2), developed from analysis of push over testing, were used to determine the lateral wave loading. Calculation of the wave force (P_W) on the structure was then accomplished using deflection due to wave loading (Δ_W) and bore height (h) as inputs into (1) and (2).

$$P_W = \Delta_W \cdot 746 \cdot exp^{-0.03648 \cdot h} \qquad (1)$$

$$P_W = \Delta_W \cdot 4036 \cdot exp^{-0.04677 \cdot h} \qquad (2)$$

This wave force was then compared to theoretical force calculations in (3) from the City and County of Honolulu Building Code.

$$F_S = 4.5 \cdot \rho \cdot g \cdot h^2 \qquad (3)$$

Comparing predicted/measured force data with the theoretical values from (3) shows that there are large differences with changes in structural configuration. As this is the only wave loading guideline accepted for use with building codes, there is clearly a need for additional research in this area.

Behavior of a 1/6th Scale, Two-Story, Wood Framed Residential Structure Under Surge Wave Loading

by
Jebediah Wilson

A THESIS

submitted to

Oregon State University

in partial fulfillment of
the requirements for the
degree of

Master of Science

Presented September 26, 2008
Commencement June 2009

Master of Science thesis of Jebediah Wilson presented on September 26, 2008

APPROVED:

Major Professor, representing Wood Science

Major Professor, representing Civil Engineering

Head of the School of Civil and Construction Engineering

Head of the Department of Wood Science and Engineering

Dean of the Graduate School

I understand that my thesis will become part of the permanent collection of Oregon State University libraries. My signature below authorizes release of my thesis to any reader upon request.

Jebediah Wilson, Author

ACKNOWLEDGEMENTS

The author wishes to thank the following individuals for support in completion of this project:

Rakesh Gupta - Major Professor and principal investigator

John van de Lindt - Principal investigator

Milo Clauson - Mentor and friend

Rachel Garcia - Research collaborator

Faculty and Staff at the O.H. Hinsdale Wave Research Laboratory

Faculty and Staff in the Civil and Construction Engineering and Wood Science and Engineering Departments

Darrah Lemmon - Spouse and support throughout my education

NSF Award CMS-0530759 (SGER NEESR Payload Project to NEESR SG Award)

NEES, Grant No. CMMI-0402490 (NEES Operations)

TABLE OF CONTENTS

TABLE OF CONTENTS (Continued)

LIST OF FIGURES

LIST OF FIGURES (Continued)

LIST OF TABLES

LIST OF APPENDICES

LIST OF APPENDIX FIGURES

LIST OF APPENDIX FIGURES (Continued)

LIST OF APPENDIX TABLES

BEHAVIOR OF A 1/6TH SCALE, TWO-STORY, WOOD FRAMED RESIDENTIAL STRUCTURE UNDER SURGE WAVE LOADING

INTRODUCTION

Infrastructure within human societies serves a variety of purposes including shelter, bridges, roadways, water supply, as well as recreational and emergency services. Nature is constantly at work taking apart this infrastructure through a variety of forces; earthquakes, tornadoes, hurricanes and tsunamis are amongst the most significant of these forces. Certain areas on the planet are more prone to these natural forces, and in these areas special consideration must be taken with the construction of important infrastructure.

Throughout history humans have settled in coastal areas for access to food and ease of transportation. The human population is continuing to climb, while simultaneously a higher percentage of people are settling in coastal regions. The United Nations (UN) reported in 2001 that over half the world's population live within 200 kilometers of the coast (GESAMP, 2001) and the National Oceanic and Atmospheric Administration (NOAA) reported in 2004 that 53% of the United States population lives in coastal counties (NOAA, 2004). The increase in human settlements along coastal regions has a larger impact on the local environment including degradation of several key natural mechanisms (coral reefs/mangroves/marshes) for limiting coastal destruction during extreme weather events (Dahdouh-Guebas, 2006).

On August 23rd Hurricane Katrina formed off the Gulf Coast of the United States and moved inland with wind speeds as high as 225 km/hour (National Weather Service, 2005). The effects of its devastation were seen as far as 160 km inland, with the worst damage seen in New Orleans, Louisiana. Professor Rakesh Gupta of Oregon State University (OSU) and Professor John van de Lindt of Colorado State University (CSU) lead an in-depth examination of the effects of wind loading on structures in the Gulf Coast region in the aftermath of Hurricane Katrina (van de Lindt et al, 2007). They determined that although wind was a significant destructive force, the damage from waves posed a much higher threat to light-frame wood structures not designed for wave loading. In some cases waves were seen to completely remove structures from their foundations, and reduced homes into piles of disconnected lumber, as shown in Figure 1. The destroyed house in Figure 1 was located approximately 1 km from the coastline in one of the hardest hit communities, Waveland, MS.

According to NOAA's Technical Report 2005-01 there were more than 1800 deaths, with damages estimated around $125 billion dollars (National Weather Service, 2005). Hurricane Katrina was rated as one of the five deadliest hurricanes in recorded history (Knabb et al, 2005). Even deadlier and more destructive was the 1998 Hurricane Mitch or the 1928 Okeechobee Hurricane. Hurricane Mitch resulted in over 11,000 lives lost and costs rising over $8 billion, and the Okeechobee Hurricane resulted in greater than 4000 deaths, hundreds of thousands left homeless and costs exceeding $33 billion (Pielke et al, 2008).

Figure 1: Hurricane Katrina wave damage in Waveland, MS

On December 26th, 2004 a powerful subduction earthquake occurred off the West Coast of Indonesia. The earthquake generated a succession of tsunamis which struck landmasses along the Indian Ocean and became known as the Asian Tsunami or Boxing Day Tsunami.

The Asian Tsunami was the most powerful tsunami ever recorded, generated by an earthquake which registered a magnitude between 9.1 and 9.3 on the Richter scale. The tsunami created a wave around 10 meters high which traveled inland at speeds up to 450 km/hour. The energy released by the tsunami was compared to 5 megatons of TNT (Nirupama et al, 2006). According to the UN there were more than 200,000 dead or missing and over 1.7 million people displaced (Clinton, 2006). Clearly these natural forces are great in magnitude, but there are steps that engineers can take to improve the life safety of building occupants in these extreme cases.

As higher percentages of the United States (US) population move into coastal regions, the need to build infrastructure to withstand wave and surge loading becomes more important. Engineers design buildings to resist a variety of loading conditions including dead, live, soil, flood, wind, snow, rain, atmospheric ice, and earthquake loads. The methods for determining these loads are complicated and are detailed in ASCE/SEI 7-05 (ASCE, 2005). This publication has 60 pages detailing wind loading and more than 100 pages on seismic loading (over 12 Chapters). The same document has only 5 pages on flood loading, with 2 pages specifically on wave loading. The wave guidelines detailed in ASCE 7-05 only discuss breaking waves with no details on loading calculations for broken waves or on how to apply the loading to wood framed structures. The City and County of Honolulu Building Code (HBC) has developed more detailed design guidelines for wave loading, yet evidence indicates this over-predicts forces (Yeh et al, 2005). There is much need for further research to understand and detail the forces involved in wave loading. Although home owners may not be required to build structures to withstand the force of many natural disasters, increased research may enable further protection of lives from these events.

Objectives

This study aimed to further understand wave loading on wood framed structures. Specifically, the objectives of this project were:

(1) To measure bore forces on a 1/6th scale, two-story, wood framed residential structure.

(2) To evaluate qualitatively the structural response to different loading conditions.

(3) To compare the effects of different structural configurations on the structural response.

(4) To develop an equation to predict wave forces.

(5) To compare predicted/measured forces with existing building code.

Literature Review

In the past wave loading was studied as it pertained to off shore structures. In general, historical research has primarily dealt with waves breaking on structures at sea or on seawalls or vertical breakwaters. Wave mechanics have been studied extensively from as early as 1802 (Gerstner, 1802) yet this research does little to help understand the effects of impinging surges inland. Little research has been done involving broken waves impacting upon structures. This is mainly because structures are built far enough from shore to avoid these conditions, yet tsunamis and hurricanes bring these waves inland. It is also difficult to study this type of loading as the facilities are few and expensive.

The Coastal Construction Manual (FEMA, 2005) was first issued in 1985, and has been updated as of 2005. This manual includes provisions for identifying hazards, how to build in coastal areas, and provides some provision for calculating design loads including flood loads. The CCM doesn't deal with loading from solitary bores in a non-flooded condition, and thus is of little use in estimating surge forces for this study. ASCE 7-05 also deals with flood loading, but includes details on breaking wave loads which is more suited to offshore structures. Neither fit the broken wave conditions of this research.

Kenneth Wydajewski, a former graduate student at OSU, worked in a similar research area testing prototype scale breakaway walls of wood construction (Wydajewski, 1998). Wydajewski worked with non-breaking waves, breaking waves and broken waves, the latter is similar to this research. The study specifically involves breakaway walls, where the intent of the walls design and construction is to collapse under specific lateral (wind and water) loading conditions without causing collapse, displacement, or other structural damage to the elevated portion of the building or supporting foundation system (FEMA, 2005). Prior to this research no measured forces on breakaway walls had been collected to compare with (Wydajewski, 1998).

In his paper Wydajewski develops theoretical force predictions and makes comparisons to measured forces and moments. Theoretical forces are determined by relating equations for hydrodynamic and hydrostatic pressure. To collect load data the researchers setup a load frame with four load cells, collecting wave height data from resistive wave height gauges similar to those used in this study. Wydajewski warns of difficulty knowing if a wave is fully broken or still breaking, leading to large differences in measured forces. The structure was placed close to the still water line, and although the waves appeared to have broken prior to impacting the structure, the structure could have been moved further away from the still water line. One of the advantages of his experimental setup was the ability to directly measure the horizontal loading. This would have been a preferred method of measuring force for future studies.

Jerald Ramsden's paper, "Force's on a Vertical Wall Due to Long Waves, Bores, and Dry-Bed Surges" presents similar techniques to those used in this experiment (Ramsden, 1993). Like Wydajewski, Ramsden directly measures the lateral force instead of calculating the force from pressure measurements as was done in many previous studies. Ramsden has the advantage of getting accurate wave height measurements using a laser-induced fluorescence system, yet despite this technology there is still related difficulty in determining the maximum runup height on the vertical wall. Ramsden used theoretical equations from Goring (1979) for determining the force and moment, which were compared to measured values. One of the major conclusions from this work indicate that force computed assuming purely hydrostatic conditions and utilizing the maximum runup height exceeded the maximum measured values in all cases. This was thought to be due to part of the force being vertical during wave runup.

Ramsden found that the theoretical equations developed by Su and Mirie (1980), in their paper "On Head-On Collision Between Two Solitary Waves ", were the closest fit to the measured values of force and moment. For comparison the work on dry bed surges most closely resembles the wave conditions in this study, yet the wave was generated by the dam-break method. The dam break method is very different from the tsunami wave generator in the TWB, but the wave profile is similar.

Halldór Árnason's PhD dissertation, "Interactions Between an Incident Bore and a Free-Standing Coastal Structure," also tested structures impacted by broken bores (Arnason, 2005). In Árnason's research circular and square columns were loaded by bores generated in a narrow wave flume. Similarly, load cells were used to directly measure the force of the wave. The load cells used in this research measure load in three directions, as well as the moment around three axes. This type of instrumentation is preferable, because it can capture all of the loading and is easily interpreted. Árnason's work also focuses on qualitative observations regarding the structures response to wave loading. In the controlled environment of a small wave flume, theoretical predictions of wave height and force aligned well with theory. Yet having a narrow channel means the water didn't travel naturally around the structure as would happen if the structure were isolated. Future studies might test several structures side by side, as might be found in a housing community to see how loading was affected.

Most closely related to this study is the recent work of Thusyanthan and Madabhushi (2008), "Tsunami Wave Loading on Coastal Houses: A Model Approach." This research utilizes a small tsunami wave tank measuring 4.5 m long, with waves generated by dropping a 100 kg block in the water. Model coastal structures scaled at 1:25 were tested. One structure was designed similar to a common Sri Lankan house and one structure attempted to model a new tsunami resistant structure. Water was allowed to pass through and under the tsunami resistant model, effectively reducing the loading. Pressure sensors were used at two locations on the face of the model and at one location on the back. Results indicate that the tsunami resistant model was successful at reducing forces and survived the wave impact, while the typical Sri Lankan model was destroyed or displaced from its foundation. This indicates a need to examine how building configuration affects wave loading.

MATERIALS AND METHODS

The study utilized a structurally compliant 1/6th scale model of a two-story residential structure. The structure was constructed using light-framed wood construction similar to that found in coastal regions in the US, as seen in Figure 2. Architectural plans, shown in Figures 3 and 4, were drafted by Colorado State University graduate student Rachel Garcia, who also performed the scaling procedures which allowed approximate structural compliance (Garcia, 2008). Testing took place at the O.H. Hinsdale Wave Research Laboratory (HWRL), as well as in the Structures Laboratory at the Department of Wood Science and Engineering (WSE).

Model Structure Construction

The design of the structural model was performed by the Colorado State University research team under the supervision of Dr. John van de Lindt, the details of which can be found in Garcia (2008). A CSU undergrad worker constructed four sets of identical wall panels, three roof diaphragms and three floor diaphragms. The wall framing members were constructed of 0.953 cm x 1.91 cm pine boards, and the roof framing members were constructed of 1.27 cm x 1.91 cm pine boards. Figure 2 shows the partially assembled structure prior to the installation of the exterior sheathing.

Figure 2: Model structure with exterior sheathing removed (Garcia, 2008)

The scaled wall sheathing was made from Oriented Strand Board (OSB) cut to 0.5 cm thick x 20.3 cm wide x 42.9 cm high, effectively modeling a 122 cm x 244 cm wall panel typical of exterior sheathing. Roof and floor diaphragm sheathing was made from 0.635 cm plywood. The framing connections were made with 1 mm x 25.4 mm staples, with wall sheathing attached using 0.85 mm x 12.7 mm steel brad nails. Three sets of walls, two roof diaphragms, and one floor diaphragm were then shipped to OSU for final assembly.

The walls were assembled on a 1.27 cm x 114 cm x 244 cm steel plate, attached using 3.18 mm x 25.4 mm stainless steel anchor bolts through the bottom plate of the walls, at the prescribed spacing for 209 km/hour (130 mph) prescriptive code (AFPA, 2006). The second floor diaphragm was then attached using thin gauge sheet metal plates every 30 cm. The second floor walls were stapled to the second floor diaphragm using 1 mm x 25.4 mm staples, again using spacing from 209 km/hour prescriptive code. The roof diaphragm was then attached using thin gauge sheet metal joist hangers. The final dimensions of the structure are 244 cm long x 114 cm wide x 116 cm high. A fully assembled structure is shown in Figure 5.

Testing

Testing took place in two parts. The first took place at the Oregon State University Tsunami Wave Basin (TWB), and involved impacting the wood structure with a series of waves and recording the force in four load cells *(LC1, LC2, LC3, LC4),* deflection (Δ_W), acceleration, bore height and wave velocity. See Figures 6 & 7 for the wave lab testing instrumentation details. The second portion of the study took place at the WSE Structures Laboratory, which involved push over tests to quantify the relationship between input loading (P_P) and the structures deflection (Δ_P), recording force *(*P_P*, LC1, LC2, LC3, LC4)* and deflection (Δ_P). See Figure 8 for the push over testing instrumentation details.

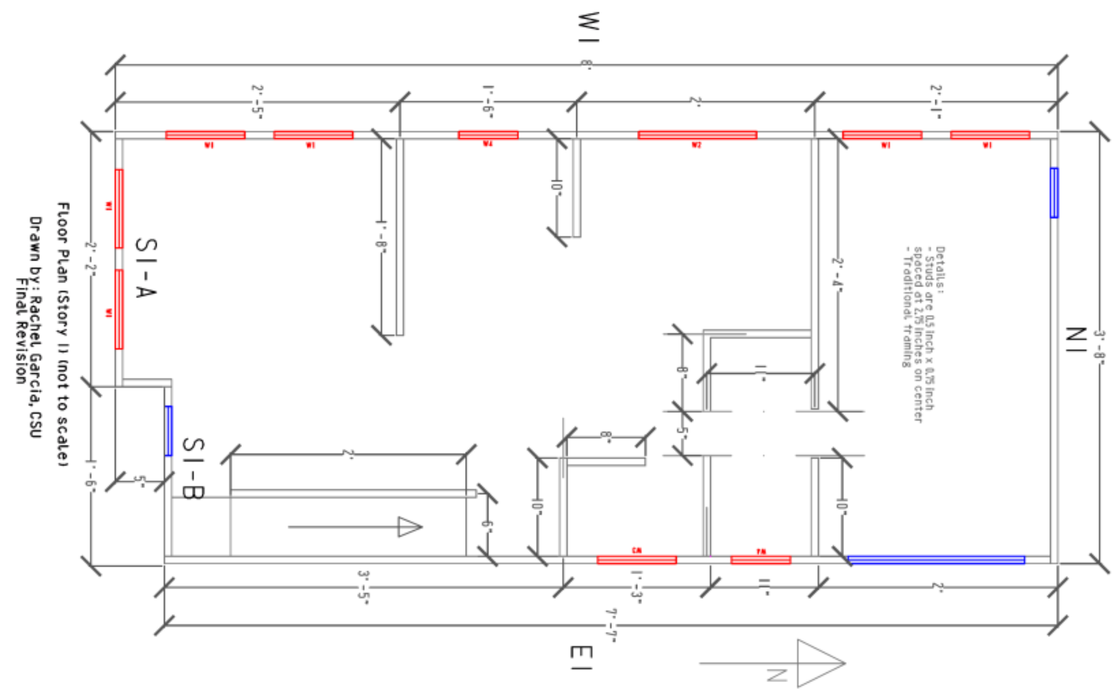

Figure 3: First story floor plan (Garcia, 2008)

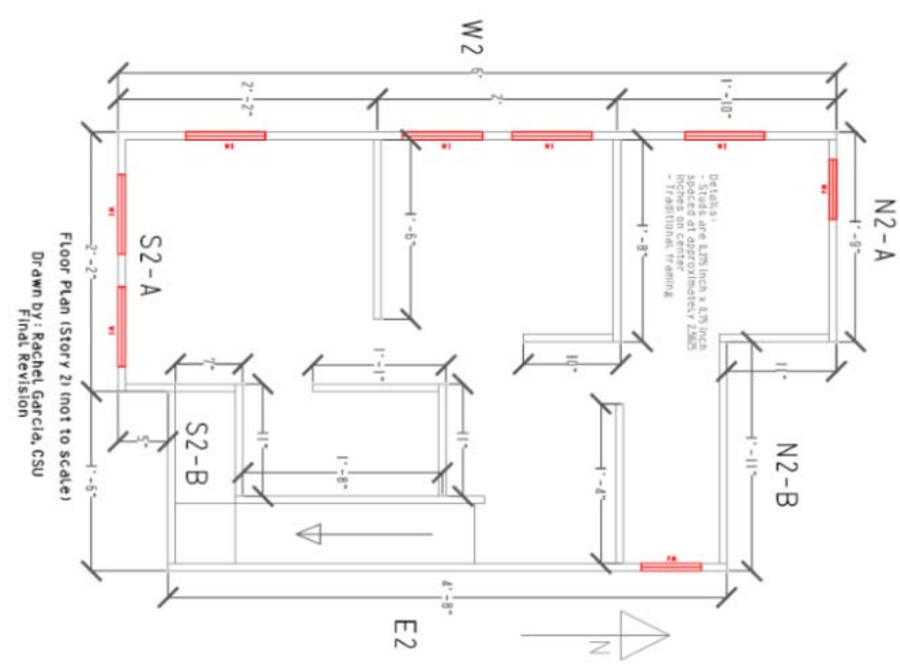

Figure 4: Second story floor plan (Garcia, 2008)

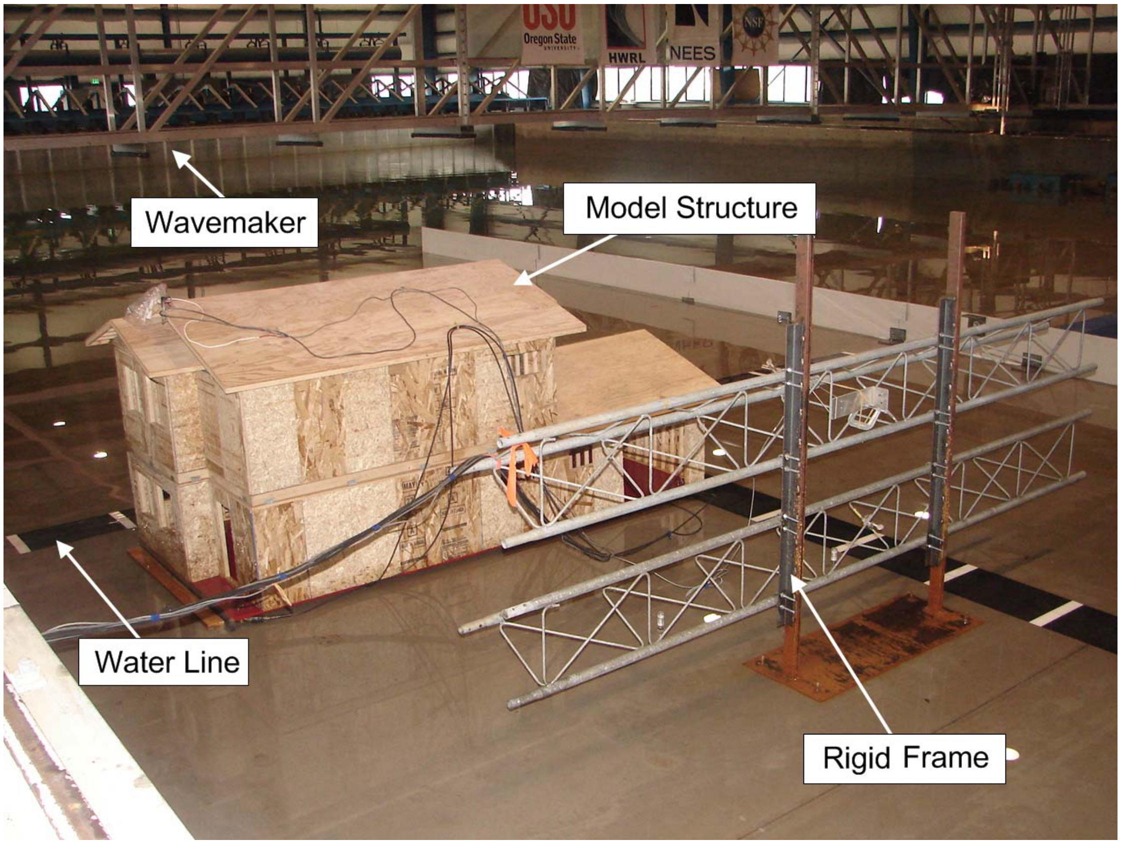

Figure 5: Assembled model structure in place in the Tsunami Wave Basin at the OH Hinsdale wave lab.

Wave Lab Tests

Test Setup

The TWB layout, showing plan and profile views of the testing area, is shown in Figure A6 in the Appendix. In this study the wave maker generated 10 cm, 20 cm, 30 cm, 40 cm, 50 cm, and 60 cm solitary waves in both a 1 m and 1.1 m water depth. The structure was placed on a flat testing area with its front edge 10 cm back from the water's edge. This was done so the waves would have developed into broken bores, yet would still have much of their initial energy.

The model structure, constructed at the WSE Structures Laboratory, was delivered to the TWB for testing. Four load cells were attached beneath the steel baseplate, one in each corner, as shown in Figure 6. The structure was anchored to the concrete basin through the use of stainless steel threaded rods attached to the four load cells, ensuring the load path was directed through the load cells. The stainless steel threaded rods, measuring 0.635 cm x 15.24 cm (1/4-20 thread pitch), were set into the concrete by drilling oversized holes and affixed using epoxy. A nut and washer was used above and below each load cell for leveling the structure and balancing the load cells. A rigid testing frame was bolted to the concrete floor behind the structure for mounting wiring and instrumentation.

As this was a preliminary study, the goal was to examine many different testing configurations to determine the most suitable for data collection. The structure was tested with its long face towards the oncoming waves, hereby referred to as the 0° orientation, as well as rotated 90° to put the short face to the oncoming waves, hereby referred to as the 90° orientation, as shown in Figure 6.

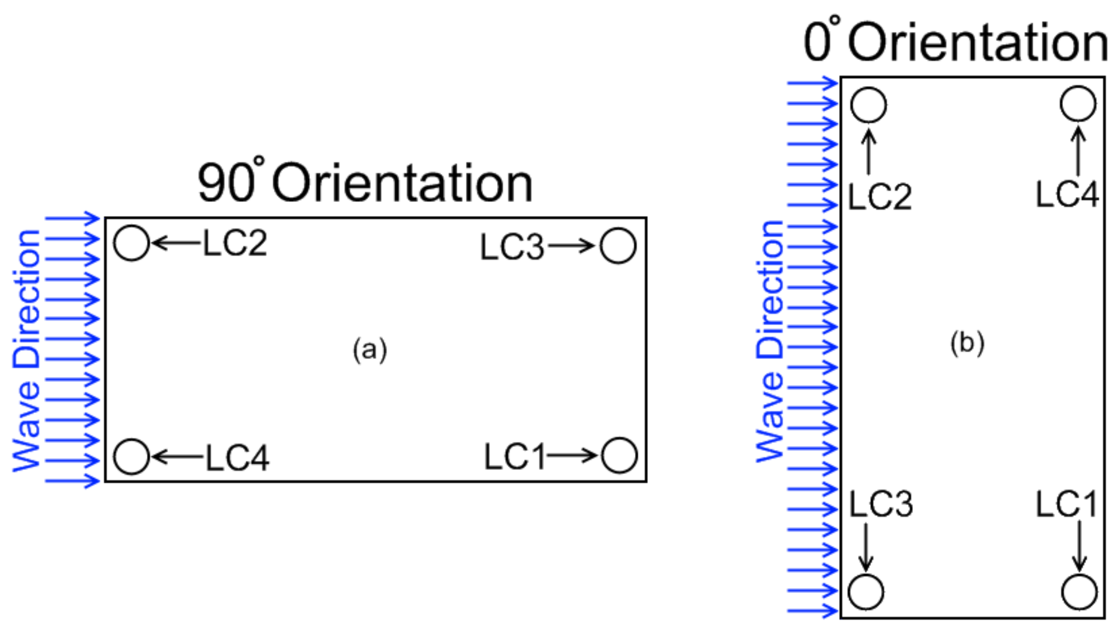

Figure 6: Orientation and load cell (LC) locations with respect to wave direction, (a) 90° (b) 0°

The structure had openings for windows and doors, which were covered in some trials by thin rigid plastic to simulate boarded windows. There was approximately a 4 cm gap beneath the steel plate necessitated by the placement of the load cells, which in some trials was covered by a thin gauge sheet metal flashing to prevent water intrusion beneath the plate. This was thought to model the presence of an open crawlspace versus a slab/stemwall foundation. In several trials the structure was raised an additional 5 cm through the use of rigid aluminum risers, to simulate the effects of a slightly elevated structure.

Throughout the following sections the abbreviations listed below are used to indicate the specific testing configuration:

90	= 90° Orientation
0	= 0° Orientation
1.0	= 1.0 m water depth
1.1	= 1.1 m water depth
WO	= Windows open
WC	= Windows closed
E	= Elevated structure (baseplate ~10 cm above concrete floor)
NE	= Non-Elevated Structure (baseplate 4 cm above concrete floor)

Example: 90-1.1-WC-F-NE indicates a test conducted in the 90° orientation, with the water level at 1.1 m, window and door coverings installed, baseplate flashed to prevent water intrusion, and the structure fixed to the foundation in a non-elevated position. The flooded condition is indicated by 1.1 m water depth (1.1) and a non-elevated structure (NE).

Data Acquisition

Force was measured using four uniaxial load cells (LC1-LC4) placed in each corner beneath the structure, effectively measuring the overturning moment generated by the surge impacting the structure. Deflection *(Δ_W)* was measured at the second story roofline using a Linear Variable Differential Transformer (LVDT). Acceleration was measured on the second story roof near the front face of the structure using an accelerometer. Free field wave height was measured using a resistive wave gauge, and wave velocity was measured using an Acoustic Doppler Velocimeter (ADV). Figure 7 shows the experimental setup. Raw voltages were sent from the instrumentation through an amplifier into a National Instruments data acquisition card. The amplified voltages were then sent through a PC and recorded as text files using LabView version 8.0.

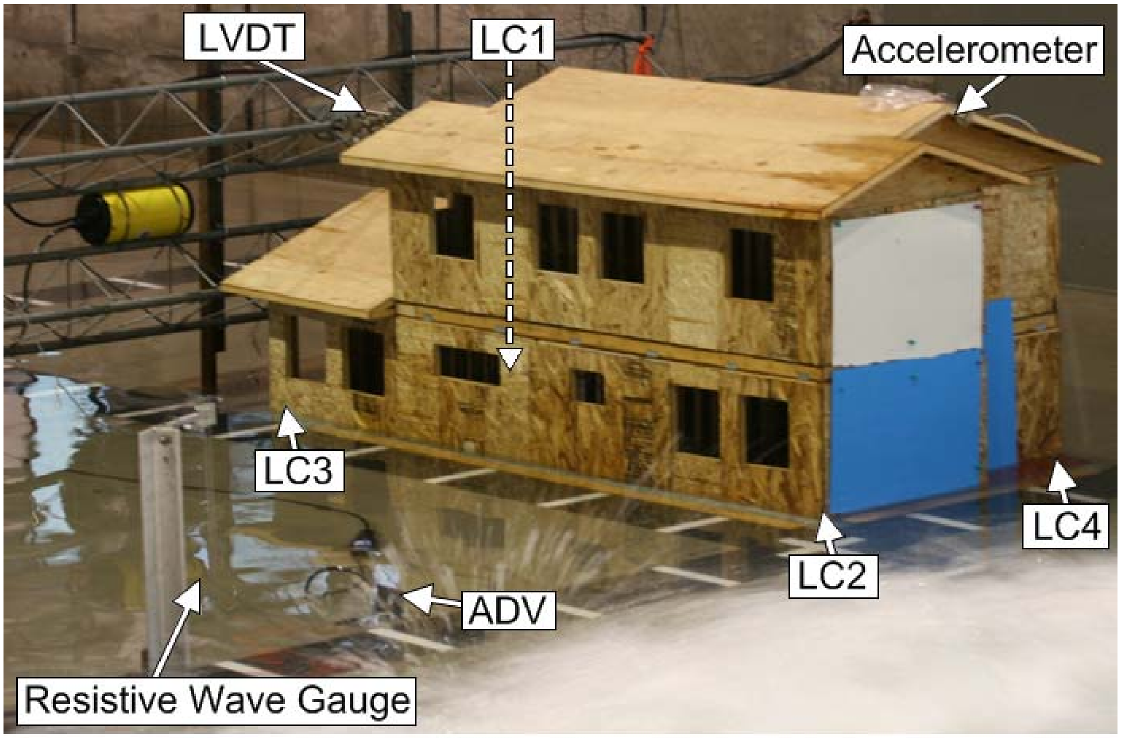

Figure 7: Instrumentation for testing at Tsunami Wave Basin

Data Analysis

The raw voltages were brought into Microsoft Excel and calibrated to metric units of force (N), deflection (mm), acceleration (g's), velocity (cm/s), and height (cm). Simple visual basic coding automated the task of importing and calibrating data, determining peak values, generating plots of load and deflection versus time and exporting the peak values and test information into a summary spreadsheet. The visual basic code required the user to visually indicate the range over which peak values would occur, ensuring an accurate time frame for peak loading as well as allowing the user to inspect plots of each data set.

Test Matrix

Testing at the TWB took place over nine days, comprising a total of 142 trials. There were 43 trials in the 0° orientation and 99 trials in the 90° orientation, as depicted in Tables 1 and 2.

Table 1: Test Matrix for Wave Lab Trials, 0° Orientation

Wave Ht. (cm)	*0-1.0-WC-F-NE*	*0-1.0-WO-F-NE*	*0-1.1-WC-F-NE*
10	2	0	2
20	2	4	4
30	2	0	2
40	4	3	4
50	2	0	2
60	3	5	2
Total →	*15*	*12*	*16*
		43 Total Trials	

Table 2: Test Matrix for Wave Lab Trials, 90° Orientation

Wave Ht. (cm)	*90-1.0-WC-F-NE*	*90-1.0-WO-NF-NE*	*90-1.1-WC-F-NE*	*90-1.1-WO-NF-E*	*90-1.1-WC-NF-E*
10	0	2	2	0	2
20	0	4	2	7	7
30	0	3	2	2	0
40	8	4	2	8	9
50	0	1	2	2	2
60	7	4	2	3	10
Other	0	0	2	0	0
Total →	*15*	*18*	*14*	*22*	*30*
			99 Total Trials		

Push Over Tests

Test Setup

The wave lab trials resulted in destruction of the first two models, thus a third model needed to be constructed for the push over tests. Although care was taken to follow the construction procedure identically, each structure could have had slight differences. For analysis these differences are assumed to be negligible. For the pushover tests the steel threaded rods were again used, this time welded to the steel strong floor in the structures testing bay. Anchorage was identical to the wave lab trials, i.e. nuts and washers above and below the load cells. A steel column was bolted to the floor 1.2 m from the face of the structure, to allow for the placement of a hydraulic cylinder. The hydraulic cylinder was pressurized with a hand pump, which although simple, didn't allow for regular rates of loading. The push over test setup is shown in Figure 8.

Force was applied as a distributed load, in both the 0° and 90° orientation, at several heights on the structures first floor wall. To create the distributed load a steel channel was placed between the structure and the hydraulic cylinder. For the 90° orientation loading was applied at 43 cm, 36 cm, 27 cm, and 18 cm. For the 0° orientation loading was applied at 43 cm, 38 cm, 26 cm, and 21 cm. The goal of moving the line load was to develop a relationship between the height of applied load (H_P), the input force (P_P) and the deflection (Δ_P). 43 cm is the height of the floor diaphragm between the first and second stories.

Throughout the following sections the abbreviations listed below are used to indicate the specific testing configuration:

90	= 90° Orientation
0	= 0° Orientation
DL	= Distributed Load
PLL	= Point Load Left
PLC	= Point Load Centered
PLR	= Point Load Right
43, 38, 36, etc.	= Height of loading, in cm
1, 2, 3	= LVDT Location, see Figure A10 in Appendix

Example: 0-DL-43-2 indicates a test conducted in the 0° orientation, with a distributed load applied at 43 cm, with the LVDT in location 2.

Data Acquisition

The hydraulic cylinder was installed with a uniaxial load cell on its face to measure the input force applied to the structure. Four uniaxial load cells were used in each corner beneath the structure, the same setup as for the wave lab trials. Deflection was measured at three locations on the second story roofline using an LVDT. Similar to the wave lab trials voltages were amplified, imported through National Instruments data acquisition hardware and recorded by LabView software.

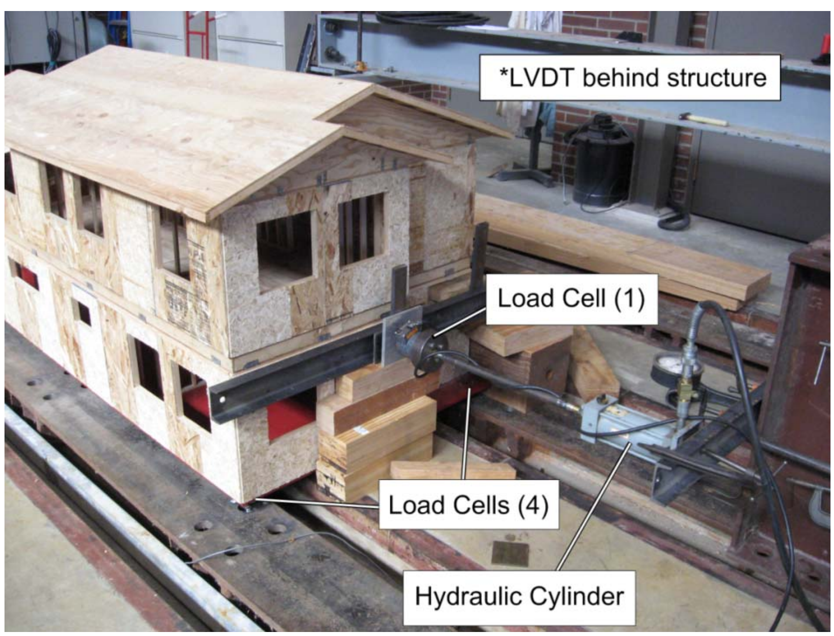

Figure 8: Instrumentation for pushover tests in Wood Engineering Structures Laboratory

Data Analysis

The raw voltages were brought into Microsoft Excel and calibrated to metric units of force (N) and deflection (mm). There were two main goals for the push over tests; first to find the relationship between the deflection (Δ_P) and the input loading (P_P) applied to the structure, the second was to determine the relationship between Δ_P and the change in the height of loading (H_P). Surge loading is assumed to apply a distributed load on the face of the structure, thus the only push over trials analyzed were those with distributed loading. The front two cells showed positive values of force and the rear cells had negative values of force. P_P and Δ_P were plotted for each trial to determine their relationship, which was found to be linear with a y-intercept of zero. The slope of this line was then found for each trial and averaged together amongst those with a similar test setup. Δ_P was then plotted against H_P to determine their relationship, which was best fit by an exponential. Once these relationships were determined, the deflection data from the wave lab (Δ_W) was input into the functions to determine wave input loading (P_W). The height variable used was the height of the bore (h).

Test Matrix

Testing in the WSE Structures Lab took place over four days, comprising a total of 93 trials. There were a total of 46 trials for the 0° orientation at four different heights of loading, as shown in Table 3. For the 90° orientation there were a total of 47 trials at five different heights of loading, as shown in Table 4. Since the focus of the push over tests was to replicate the wave loading, point loads were only applied for a few trials, thus the bulk of the testing had an applied distributed load.

Table 3: Test matrix for 0° orientation push over tests

Height of Load	43 cm				36 cm	27 cm	18 cm
Location	L	C	R	D	D	D	D
LVDT Location							
1	1	--	1	6	--	--	--
2	1	1	1	8	7	6	6
3	1	--	1	6	--	--	--
Totals →	*3*	*1*	*3*	*20*	*7*	*6*	*6*
	46 Total Trials						

L = Left, R = Right, C = Centered, D = Distributed

Table 4: Test matrix for 90° orientation push over tests

Height of Load	43 cm				38 cm	32 cm	26 cm	21 cm
Location	L	C	R	D	D	D	D	D
LVDT Location								
1	2	1	2	2	--	--	--	--
2	2	1	2	2	7	7	6	6
3	2	2	1	2	--	--	--	--
Totals →	*6*	*4*	*5*	*6*	*7*	*7*	*6*	*6*
	47 Total Trials							

L = Left, R = Right, C = Centered, D = Distributed

RESULTS AND DISCUSSION

During the wave lab trials several trends were expected from the data from the different loading conditions. It was expected to see an overturning moment generated by the wave loading putting the front two load cells in tension and the rear two load cells in compression, as depicted in Figure 9. To some extent it was expected to see uplift from water intrusion beneath the steel plate, especially in the elevated test condition. It was also expected that the force per unit width would be the same for the 0° and 90° orientation.

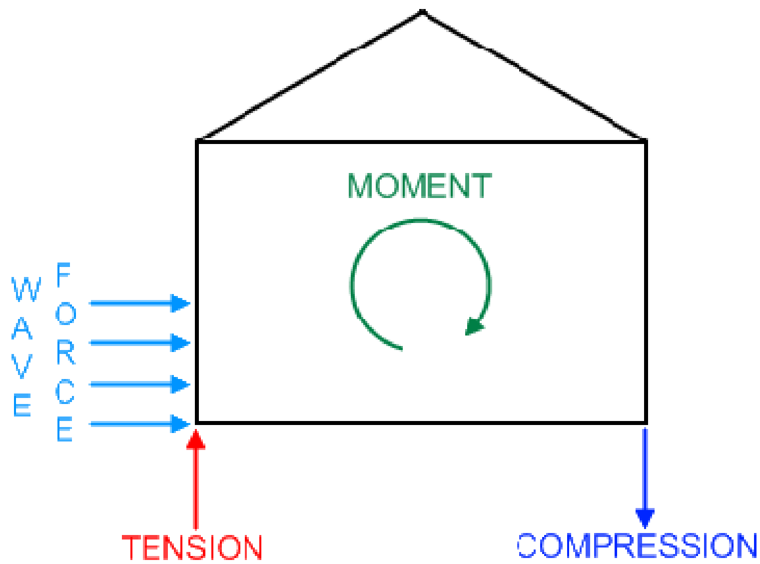

Figure 9: Forces and moment generated by the wave loading

Wave Lab Trials

Figure 10 shows an example of the data captured from a 40 cm high wave with a 0-1.0-WC-F-NE configuration. The black line indicates the time of maximum loading. Values for all of the instruments at the time of maximum loading were collected and exported from the individual files to a compiled summary sheet, as seen in Tables 5 and 6 (positive is tension negative is compression).

Complete test data and plots from the wave lab trials can be found in Appendix B. The testing at the HWRL was dictated by collaboration between several simultaneous research projects utilizing the TWB, and therefore it wasn't always possible to get consistent repetition of data sets. Additionally, the structure was wood framed and there is potential for change in the physical properties of the structure with further testing, e.g. moisture damage to the OSB sheathing as well as weakened connections through repeated loading. It was not within the scope of this study to quantify how the materials properties changed with each successive trial, and therefore the structural parameters of the model are assumed to be consistent throughout. Furthermore, this study does not seek to scale the force data collected from the 1/6th scale structure to the full-size structure. The study only seeks to relate force data to the model structure, i.e. to describe qualitatively the behavior of a small scale structure under wave loading.

The model has several structural irregularities, including a reentrant corner near the front door and a second story floor diaphragm that doesn't extend over the garage. During testing done in the 0° orientation the structure was expected to see higher loading from the impacting bore because of the increased surface area, while simultaneously it had the shortest shear walls to carry the loads. The opposite was true for the 90° orientation where loading was decreased and shear wall capacity was increased. The push over test results that follow this section help establish how differences in stiffness affected the load sharing between the load cells, and these results will be used to discuss the wave lab test data.

Tables 5 and 6 clearly show the captured force from a variety of testing configurations. The overturning moment can be seen as positive values for the front load cells (LC2 & LC4 for 90°, LC2 & LC3 for 0°) and negative values for the rear load cells (LC1 & LC3 for 90°, LC1 & LC4 for 0°). This is found in all of the 0° trials as well as the 90-1.0-WC-F-NE and 90-1.1-WC-F-NE, shown in Tables 5 and 6. Tables 5 and 6 also show where uplift is predominant, as all of the load cells have positive values indicating tension. This was found to be the case whenever the baseplate was not flashed.

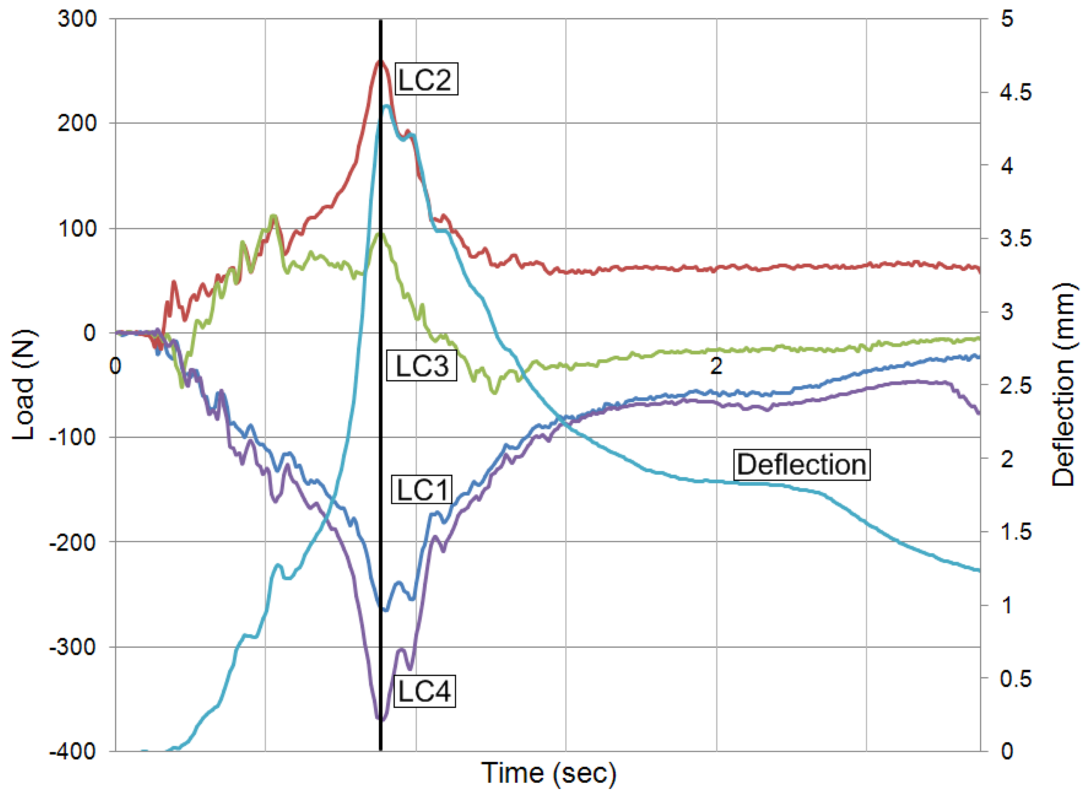

Figure 10: Example plot generated from 40 cm wave with 0-1.0-WC-F-NE configuration.

Typically, force values were found to increase with increasing solitary wave height (H_W), yet for 2 trials this was not the case. In these trials 0-1.1-WC-F-NE and 90-1.1-WC-F-NE, the force starts high, falls and then continues to rise again with increasing wave height. This was due to smaller waves breaking nearer the structure, which is discussed in greater detail later in this section. In Table 6 trial 90-1.1-WC-F-NE it can be seen that 2 additional wave heights were added, 12 cm and 15cm, this was in an attempt to see waves break directly on the structure. Δ_W in the 0-1.0-WC-F-NE and 0-1.1-WC-F-NE did not rise as expected between the 50 cm and 60 cm trials. This was because the LVDT used to measure deflections went overscale for these wave heights. Δ_W for the 90° orientation is much smaller than that in the 0° orientation. This is due to combined effects of reduced loading in the 90° orientation (less surface area for loading) and stiffer shearwalls (more than twice as long as the 0° orientation). The setup developed for the wave lab trials was successful at capturing the force from wave loads on the $1/6^{th}$ scale wood framed structure.

Table 5: Averaged Wave Lab Results, 0° Orientation

Trial	Wave Ht. (cm)	# of Trials	LC1 (N)	LC2 (N)	LC3 (N)	LC4 (N)	LC Sum (N)	Δ_{WAVE} (mm)
0-1.0-WO-F-NE	10	0	--	--	--	--	--	--
	20	4	-20	6	39	-20	85	0.0419
	30	0	--	--	--	--	--	--
	40	3	-85	81	177	-101	446	0.4518
	50	0	--	--	--	--	--	--
	60	5	-167	322	457	-182	1128	1.6233
0-1.0-WC-F-NE	10	2	-34	6	2	-40	82	0.1121
	20	2	-94	43	27	-103	267	0.6755
	30	2	-123	137	69	-245	574	2.9585
	40	4	-286	214	130	-343	974	3.9048
	50	2	-403	413	254	-542	1612	7.0111
	60	3	-602	418	554	-617	2192	4.6883
0-1.1-WC-F-NE	10	2	-413	936	828	-263	2440	3.7524
	20	4	-240	436	346	-234	1256	1.9093
	30	2	-497	735	590	-309	2132	4.6159
	40	4	-755	936	1025	-552	3268	9.5077
	50	2	-958	1169	1070	-606	3802	13.1918
	60	2	-761	1296	1376	-1012	4444	13.4318

Table 6: Averaged Wave Lab Results, 90° Orientation

Trial	Wave Ht. (cm)	# of Trials	LC1 (N)	LC2 (N)	LC3 (N)	LC4 (N)	LC Sum (N)	Δ_{WAVE} (mm)
90-1.1-WC-NF-E	10	2	297	359	316	385	1355	0.1501
	20	7	643	808	695	845	2991	0.0961
	30	0	--	--	--	--	--	--
	40	9	814	1064	847	1162	3887	0.5290
	50	2	941	1212	1025	1291	4469	1.3297
	60	10	1034	1329	1104	1410	4877	1.7930
90-1.1-WO-NF-E	10	0	--	--	--	--	--	--
	20	7	555	636	583	657	2431	0.0612
	30	2	671	988	752	886	3297	0.0939
	40	8	775	806	785	898	3265	0.2791
	50	2	680	839	716	919	3154	0.2375
	60	3	697	1014	765	1032	3509	0.6745
90-1.0-WC-F-NE	10	0	--	--	--	--	--	--
	20	0	--	--	--	--	--	--
	30	0	--	--	--	--	--	--
	40	8	-38	60	-72	31	200	0.0980
	50	0	--	--	--	--	--	--
	60	7	-77	188	-121	100	487	0.3021
90-1.0-WO-NF-NE	10	2	68	79	80	67	294	0.0833
	20	4	164	197	182	206	749	0.0712
	30	3	201	269	240	269	978	0.0767
	40	4	261	329	326	331	1247	0.1304
	50	1	282	337	336	349	1304	0.1967
	60	4	199	342	233	368	1142	0.2670
90-1.1-WC-F-NE	10	2	-117	405	-142	258	922	0.1969
	12	1	-105	411	-123	250	890	0.0860
	15	1	-127	442	-107	263	940	0.0961
	20	2	-55	287	-42	242	626	0.0615
	30	2	-78	289	-46	181	593	0.1376
	40	2	-78	364	-143	272	857	0.8626
	50	2	-184	511	-232	292	1219	1.1324
	60	2	-182	539	-273	360	1355	1.9882

Behavior of 1/6th Scale Structure

The results that follow include a depiction describing the test conditions for the trial being discussed overlaid with the plots for that trial. The wave direction can be seen in each representation, accompanied by a directional compass. Some Figures also have an x, y, z coordinate system to aid in the discussion that follows.

Elevated Structure: 90-1.1-WC-NF-E configuration

In this test setup there were 30 trials as seen in Table 2. The structure shown in the lower right corner of Figure 11 is elevated on aluminum risers and has the water depth set to 1.1 m with window coverings installed. With the water level at 1.1 m the structure would have been submerged during testing. As this was early in the testing of the model it was decided to raise the structure such that the water level was even with the steel baseplate to preserve the model for future testing as well as to examine the effects of having the model elevated. The elevated structure could be seen to model a structure built on piers or a house with an open crawlspace.

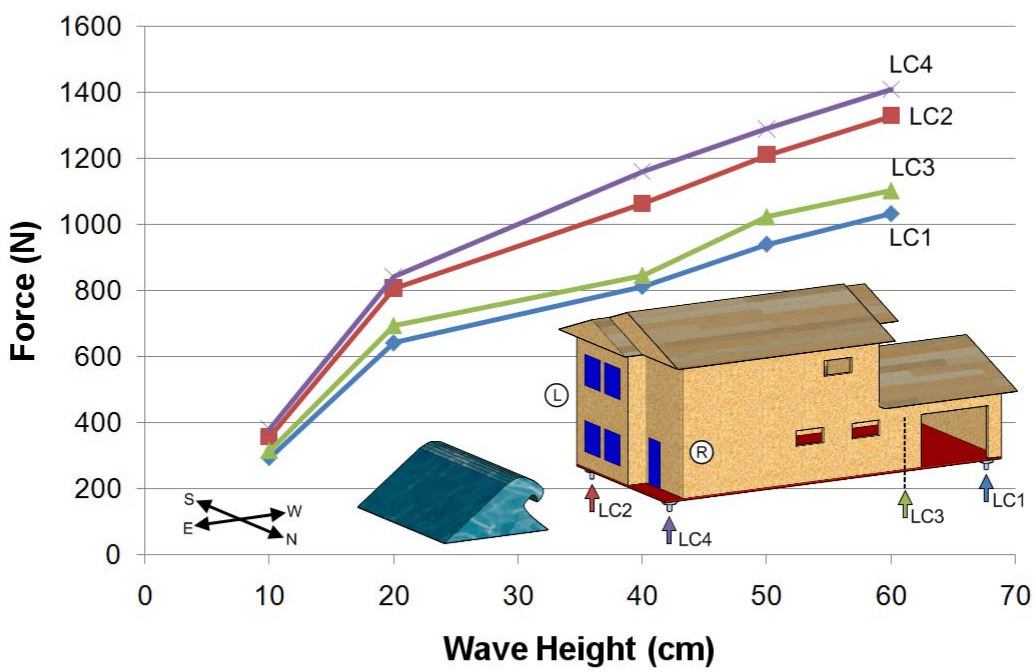

Figure 11: Load cell data and depiction of test configuration for 90-1.1-WC-NF-E

The load cell data were averaged over all of the trials with the same wave height for this configuration and are shown in Figure 11. Without an obstruction to water intrusion beneath the plate there are predominantly uplift forces generated, with all four load cells in tension. The uplift and overturning behavior can be seen as the difference in magnitude between the front and rear load cells. Furthermore, the differences between the two front load cells or two rear load cells can be seen to be differences in stiffness between the left (L) and right (R) side of the structure. Although push over tests, discussed later, confirmed that the left side of the structure had greater stiffness than the right, LC4 has higher loading than LC2. This could be due to leveling errors when installing the structure or effects from the wave action on the reentrant corner. For the 10 cm trial, the waves were not large enough to impact very high on the structure, with only uplift and smaller forces detected.

In a real world structure similar force trends would be found, indicating a need for special design considerations when examining this type of loading. Large uplift forces would necessitate stronger anchorage connections to keep the structure fixed to the foundation. It was seen in post Katrina damage that several homes were swept completely off their foundation from a combination of loading conditions, potentially including uplift of this nature. It should be noted that although the uplift forces are high, the horizontal impact loading on the structure would be reduced, as seen in Thusyanthan and Madabhushi (2008).

Elevated Structure: 90-1.1-WO-NF-E configuration

In this test setup there were 22 trials as seen in Table 2. The structure shown in Figure 12 is also elevated on aluminum risers and has the water depth of 1.1 m with the windows and doors open. Figure 12 also shows the averaged load cell data for this trial, where uplift forces are indicated by all load cells in tension, as well as the overturning behavior. The effect of removing the windows was to reduce the magnitude of the uplift forces, which could be seen as the combination of the effect of water applying a downward compressive force (once the water enters the structure through the windows) as well as less surface area on the front of the structure for loading. Window coverings in the model represent the situation where the home owner covered the windows with plywood, which is more likely with a hurricane where there is some advance warning of the storm. Absent window coverings would indicate a situation that required immediate evacuation more similar to a tsunami, but might reduce the loading enough to allow the structure to survive as seen in Thusyanthan and Madabhushi (2008).

With open windows the real structure would see smaller uplift forces since water flowing through the structure would apply a downward pressure. This can be seen by comparing Figures 11 and 12, where there is approximately a 25% reduction in force. This is not necessarily advantageous as the structure would face severe water damage, with interior non-structural elements like drywall and carpeting destroyed. In the short term if the reduction in forces allowed the structure to survive the initial impact it could protect immediate life safety and serve as shelter in the proceeding days. Also it is apparent that the force increases only slightly with increased wave height. It appears that larger waves send more water through the openings, which provides an increasing downward force with increasing wave height. Additionally, structures in coastal areas could be designed with interior elements in the lower stories to survive the water damage similar to areas with breakaway walls. It is clear that if a structure were designed to allow water intrusion beneath it the second story floor diaphragm should be as high as possible to prevent potential uplift and/or design proper anchorage.

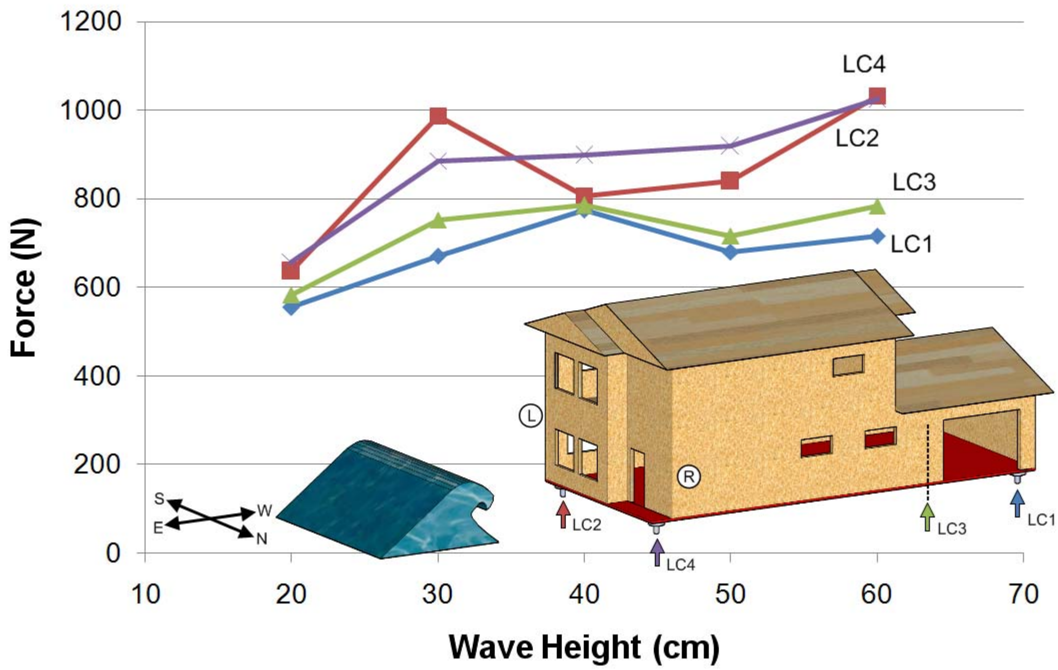

Figure 12: Load cell data and depiction of test configuration for 90-1.1-WO-NF-E

Non-Elevated Structure: 90-1.0-WC-F-NE configuration

In this test setup there were 15 trials as seen in Table 2. The configuration depicted in the lower left corner of Figure 13 is aligned with the short face to the oncoming waves, has window coverings installed, as well as flashing installed which prevents water intrusion beneath the structure. This could be seen to model a slab on grade foundation or stem wall with no openings on the loaded face. Figure 13, shows the averaged load cell data. Due to problems with instrumentation and scheduling data was collected for only the 40 cm and 60 cm wave heights.

The overturning moment is seen here as expected, with the front load cells in tension and the rear load cells in compression. Effects from the asymmetrical structural stiffness and reentrant corner can be seen as the difference in magnitude between the two front load cells and the two rear load cells. LC2 has a higher magnitude throughout the trials, which as discussed earlier was found to be due to the difference in stiffness from the left side to the right side of the structure. The left side is stiffer due to the longer second floor diaphragm on that side, combined with the large opening for the garage door on the right side, which reduces the stiffness on that side. Stiffness attracts load, thus it follows that the left side takes a higher portion of the loading. Data from the push over tests, discussed later, indicate a similar trend.

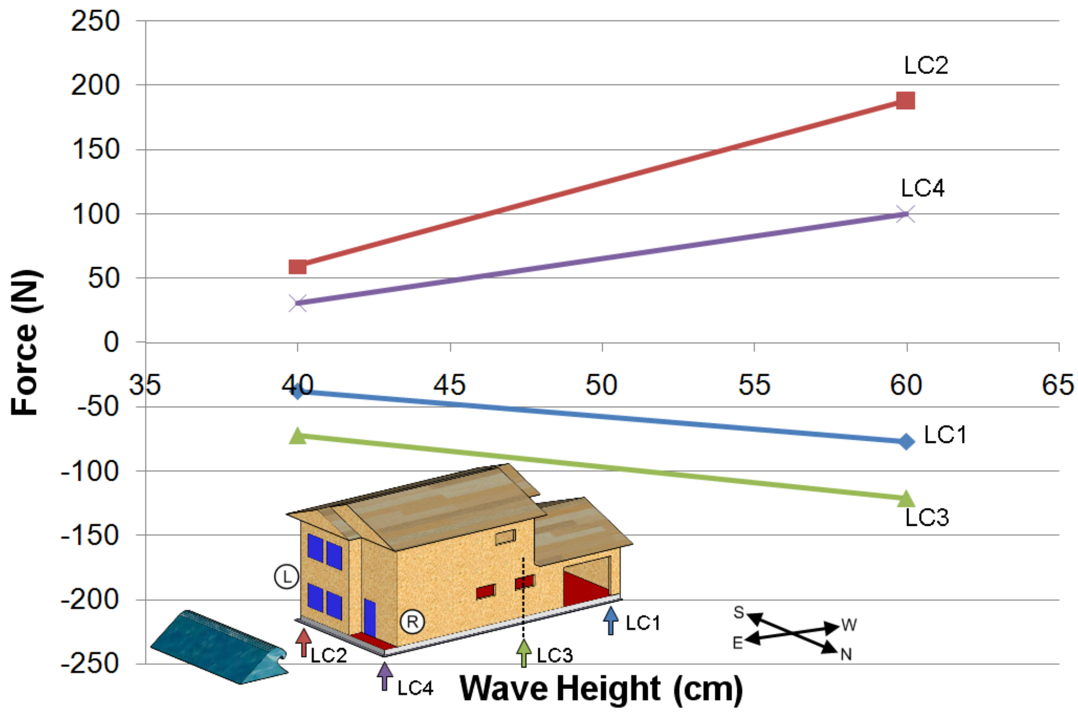

Figure 13: Load cell data and depiction of test configuration for 90-1.0-WC-F-NE

This type of loading shows that the anchorage connections would be most vital on the side of the structure facing the oncoming waves. It is also clear that preventing water intrusion beneath the structure helps to reduce the uplift forces and thus the overall magnitude of the tensile forces are reduced. Typically when working with a flexible diaphragm (such as found in wood framed buildings) it is assumed that the load is carried equally in each shearwall, this is not the case in this model. This is most likely due to a much stiffer floor diaphragm than would be seen in the full scale structure, yet clearly the shearwalls do not equally carry loads between them. If this is not an artifact from scaling the model, there would be a need to examine the loading found in the stiffest shear wall and design for that load.

Non-Elevated Structure: 90-1.0-WO-NF-NE configuration

In this test setup there were 18 trials as seen in Table 2. This structural configuration is aligned with the short face to the oncoming waves, has no window coverings and has an open "crawl space", as depicted in the lower right corner of Figure 14. The averaged load cell data for this trial can also be seen in Figure 14, which shows predominantly uplift forces. The overturning behavior is not obvious in this trial. For the 10 cm and 20 cm wave heights the bore height reached just above the steel plate, generating only uplift due to the water running under the plate. For larger wave heights some difference in magnitude is seen between the front and rear load cells, but not until the 60 cm wave does this difference clearly indicate the overturning moment expected. Smaller waves have access to the full width of the structure for loading, but as the waves get higher the windows effectively halve the surface area available. The 60 cm wave was seen to overtop the first story window and door openings, thus having the full width of the structure for loading in that region. This is thought to be why LC1 and LC3 decrease, showing the overturning moment more clearly with the largest wave.

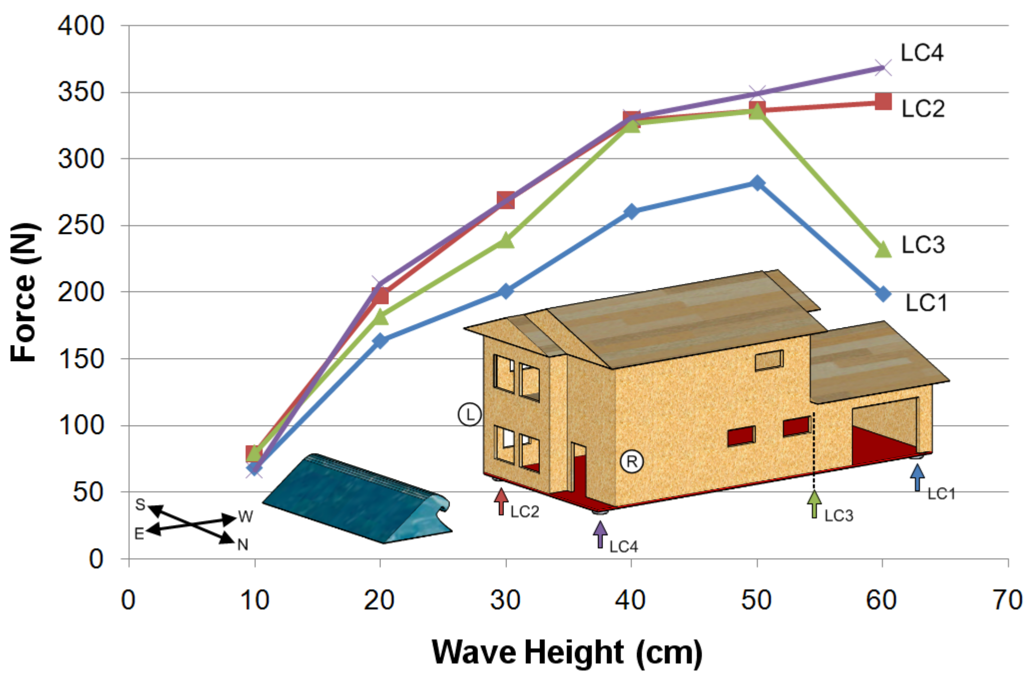

Figure 14: Load cell data and depiction of test configuration for 90-1.0-WO-NF-NE

This wave trial is difficult to analyze due to the many changing variables. As water moves beneath the plate uplift of the plate occurs, yet with openings in the structure water can also travel across the top of the plate potentially reducing this force. Furthermore, the window openings give different surface areas for loading depending on the height of the bore. Clearly uplift is the dominant portion of the loading. Windows open with a flashed baseplate wasn't tested, which would have allowed further isolation of these variables from the uplift forces for analysis. As was stated in earlier discussion, if water is allowed beneath the structure the horizontal surge loading would be reduced, as was found in Thusyanthan and Madabhushi (2008). Additionally, the openings in the structure would further reduce this loading, as there is less surface area for loading. Again special design of anchorage would need to be considered.

Non-Elevated Structure: 0-1.0-WC-F-NE configuration

In this test setup there were 15 trials as seen in Table 1. The structure tested is depicted in the lower left corner of Figure 15. This structure is oriented with the long face to the oncoming waves, has window coverings, and flashing around the plate to prevent water intrusion. Here the overturning moment is prominent, and as expected rising force follows rising wave height. One exception is with LC2 during the 60 cm wave trials, which has no increase in loading between the 50 cm and 60 cm trials. The smallest wave, 10 cm, was only high enough to strike the flashing beneath the steel plate and thus provided little loading for the actual structure.

As indicated by push over tests the right side has greater stiffness than the left side, and therefore attracts a higher portion of the loading. It would then be expected that LC2 and LC4 would have a higher magnitude of loading than LC1 and LC3. Yet in the largest wave LC2 drops in magnitude. This was found to be due to the first story overhang above the garage. The largest waves were applying an upward vertical force to this eave, evident not only from observation, but also in the loosening of the plywood roofing on this side. This would indicate strong uplift forces applied on the front left corner above LC3. This upward force at the left side of the structure would cause an additional overturning moment, rotating the structure in the y-z plane as indicated by the coordinate axis in Figure 15. This additional moment would cause the front right load cell (LC2) to decrease in magnitude and the front left (LC3) to increase in magnitude, which is what the data indicates.

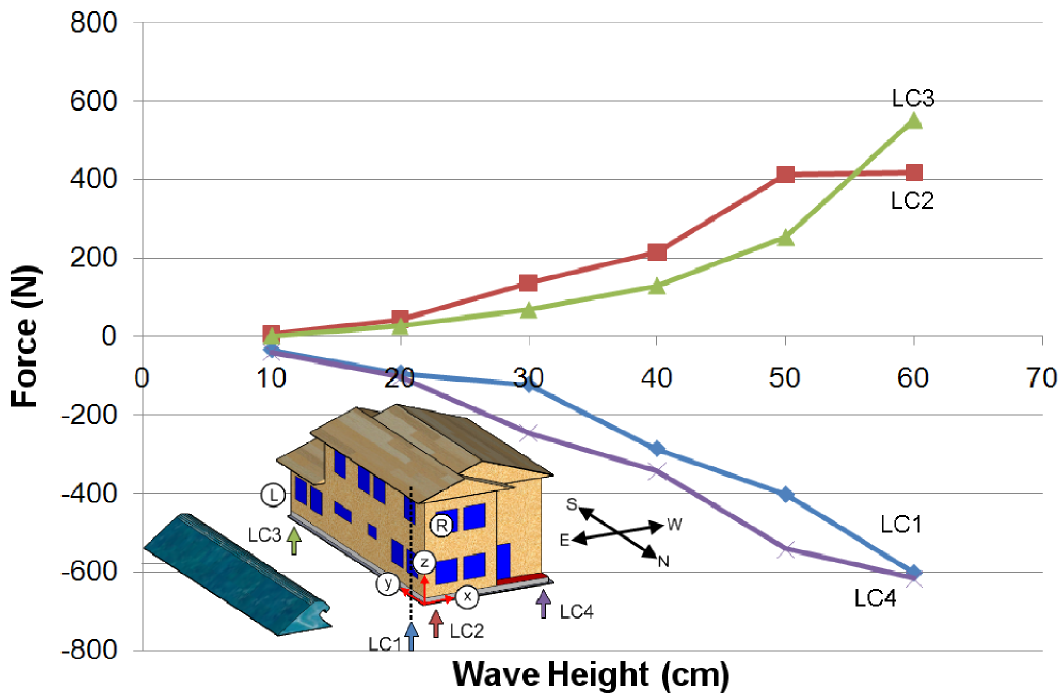

Figure 15: Load cell data and depiction of test configuration for 0-1.0-WC-F-NE

Non-Elevated Structure: 0-1.0-WO-F-NE configuration

In this test setup there were 12 trials as seen in Table 1. The configuration depicted in the upper left corner of Figure 16 is aligned with the long face to the oncoming waves, has no window coverings installed and has flashing installed to prevent water intrusion beneath the structure. Figure 16 also shows the averaged load cell data, where the overturning moment is indicated as expected. There are fewer wave heights for this trial, e.g. only 20 cm, 40 cm, and 60 cm, yet each wave height had higher repetition than many of configurations, with at least 3 trials each.

Given that the right side of the structure is stiffer than the left, it is not clear why LC3 would have a greater magnitude of force than LC2. The previous trial clearly indicated the opposite trend, and the only variable changed was the opening of the windows, so the answer must lie with water intrusion through the openings. There are two additional windows on the front right corner (on the narrow face of the structure) where water was seen to enter during testing. It is likely that more water enters at the right side lowering the tensile forces on that side. Further testing would be necessary to fully isolate the effects of changing window coverings, but it is clear from test data that the magnitude of the forces are decreased disproportionately to the reduction in surface area.

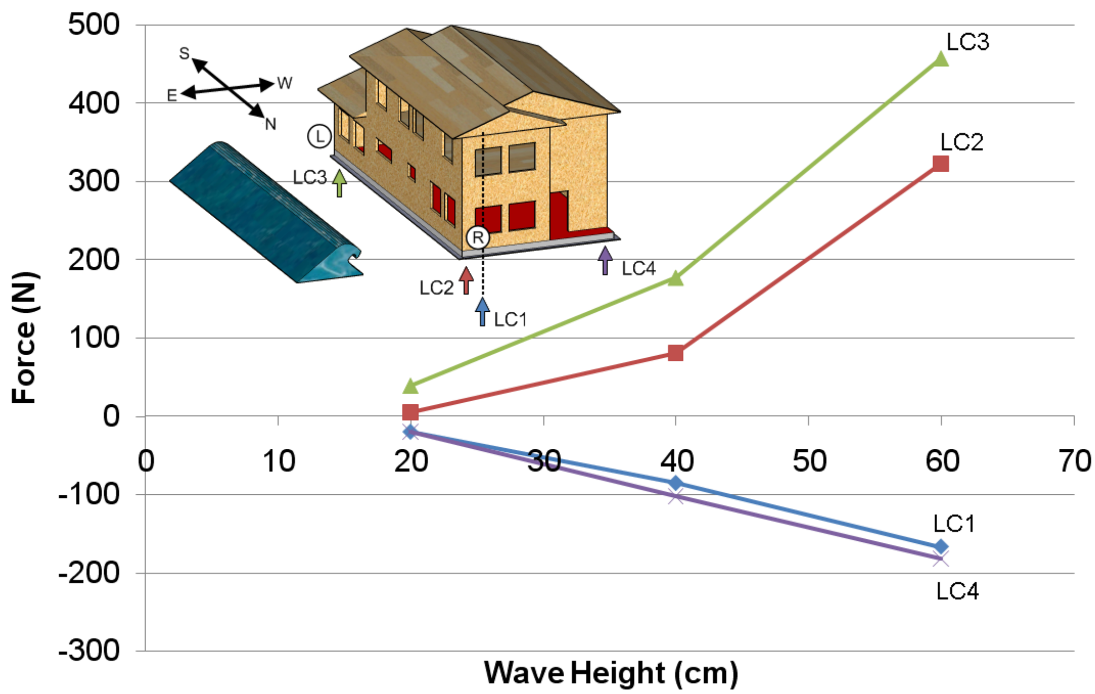

Figure 16: Load cell data and depiction of test configuration for 0-1.0-WO-F-NE

Submerged Structure: 90-1.1-WC-F-NE configuration

In this test setup there were 14 trials as seen in Table 2, including 2 unique tests at 12 cm and 15 cm. This configuration has the same setup as that depicted in Figure 17, yet has the water level raised to 1.1 m leaving the structure partially submerged. The collected load cell data shown in Figure 17 indicates an increase in loading for the waves around 10-15 cm in height. This was followed by a decrease in loading when the wave height was increased.

It was found that the smaller waves were breaking on or very near the structure. To this end, 12 cm and 15 cm trials were added to investigate waves breaking directly on the structure. Since waves lose energy when they break, a breaking wave on the structure would impart higher loading. As the wave heights increased the waves broke further off shore and this explains the reduced loading. Once the waves had broken offshore the force increases with increasing wave height as expected. Trends found in the 90-1.0-WC-F-NE trial are repeated here with higher loading values due to the increased water depth. Again the overturning moment is generated, and again the front right load cell (LC4) sees a decrease in loading, which would be an indicator of increased structural stiffness on the right side.

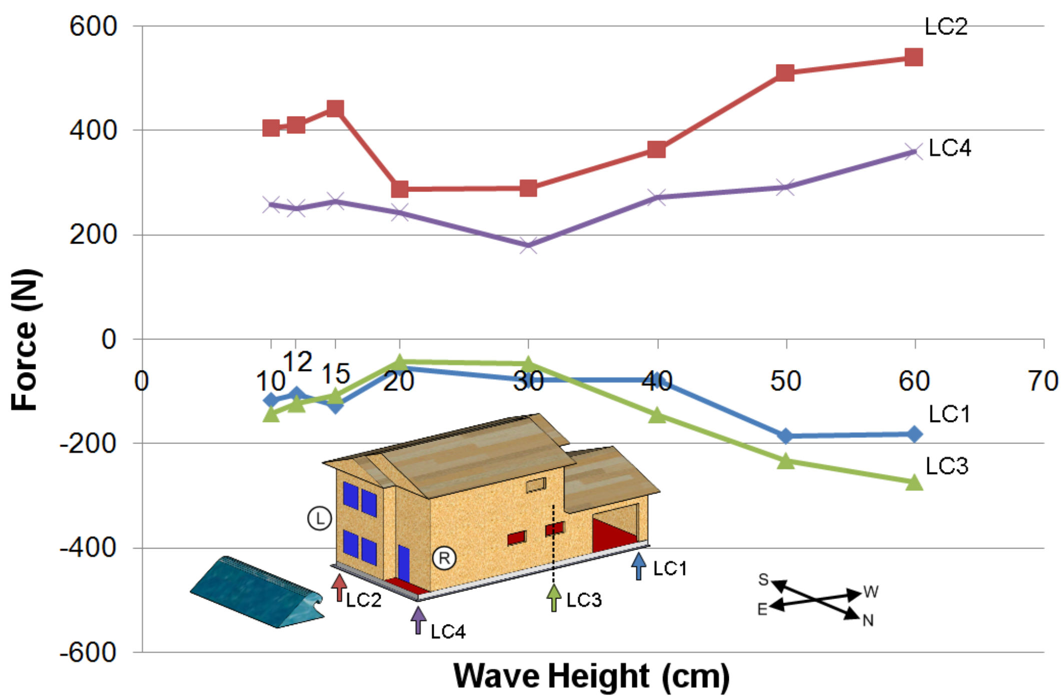

Figure 17: Load cell data and depiction of test configuration for 90-1.1-WC-F-NE
**additional 12 and 15 cm trials included to determine wave breaking point

Submerged Structure: 0-1.1-WC-F-NE configuration

In this test setup there were 16 trials as seen in Table 1. This configuration (Figure 18) is identical to that found in Figure 15, with an increase in water depth to 1.1 m. Correspondingly there are higher forces in these trials, seen by comparing Figure 15 with Figure 18. The load cell values are shown in Figure 18, where again higher loading is caused by the breaking waves in the 10 cm waves. As before, when the waves cease breaking on the structure the loading increases with increasing wave height.

This is the structural configuration that ultimately failed the structure, as shown in Figure 19. Loading was highest in these trials since the water depth was increased and the structure was oriented with its largest face to the oncoming waves. Trends found in the 0-1.0-WC-F-NE trial are repeated here, with higher loading values due to the increased water depth. The overturning moment is clearly indicated, as well as differences in magnitude between load cells due stiffness irregularities. The 60 cm trial again shows a decrease in loading on the right side, indicative of the loading applied to the eaves on the left side of the structure.

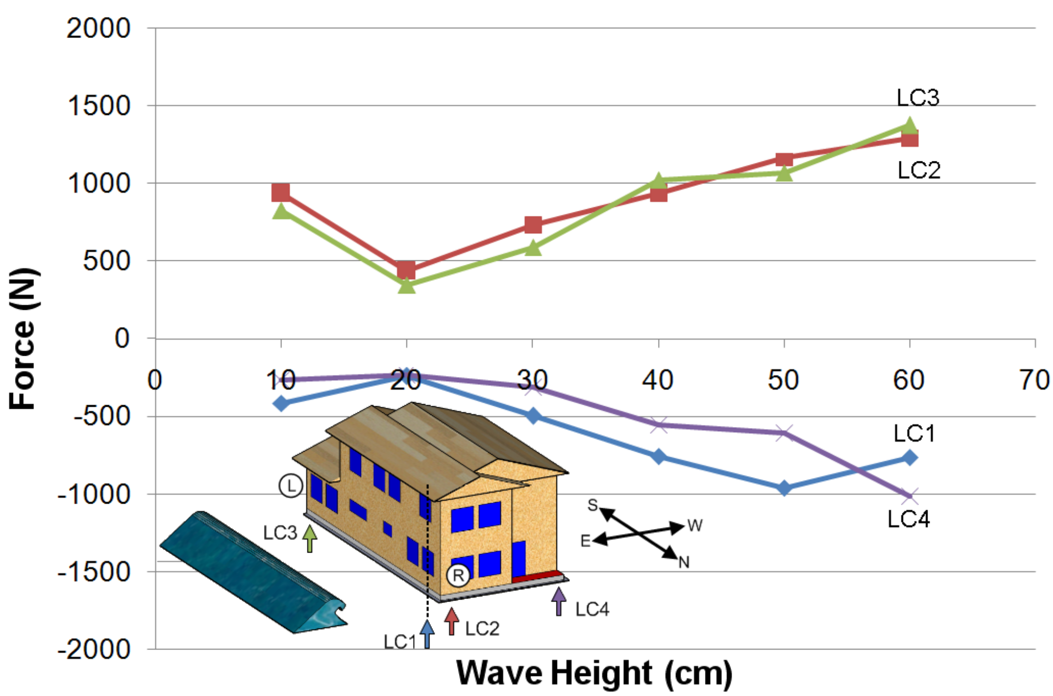

Figure 18: Load cell data and depiction of test configuration for 0-1.1-WC-F-NE

Figure 19: Lower story shear failure after a 60 cm, 0-1.1-WC-F-NE

0° versus 90°

In comparing the 0° and 90° orientation the most regular structural configuration is examined, i.e. windows closed, flashed baseplate and a non-elevated condition. Figure 20 shows a comparison between the 0° orientation and the 90° orientation, in both 1 m and 1.1 m water depth. For these plots the four load cell values were summed as absolute values, as an indication of the total force at a given time. As expected, the 0° orientation has larger total force when compared to the 90° orientation. However, when total load is normalized by the width of the structure it is still higher for the 0° orientation compared to the 90° orientation. The aspect ratio of the structure is approximately 2:1, yet the difference in load is approximately 3:1 from the 0° to the 90° orientation in both water levels. There are a variety of forces during wave loading, including buoyant, surge, drag, and hydrostatic forces. It is probable that other loading effects are causing the discrepancy in loading between the 0° and 90° orientations.

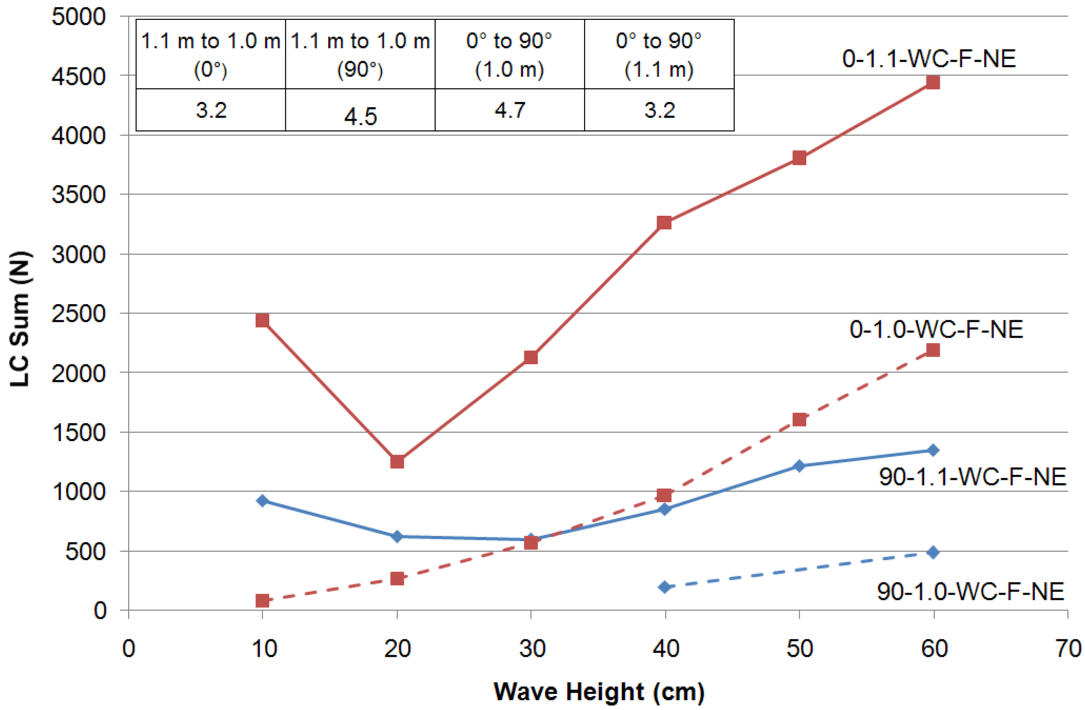

Figure 20: Force plotted as LC Sum comparing wave height and orientation

Open Windows versus Closed Windows

To examine the effects of open windows versus closed windows more closely LC Sum was plotted against the wave height (H_W) for the 0-1.0-WC-F-NE and 0-1.0-WO-F-NE trials, as seen in Figure 21. With windows closed, water travels through the structure adding a compessive force as well as reducing the available surface area for loading. The ratio of force from the windows closed condition to the windows open condition is about 2.5:1. Although the surface area for loading is different depending on the runup for a given wave, the windows account for ~25% of the first story surface area in the 0° orientation. This reduction in loading is significant, and could mean the survival of a structure as seen in the paper by Thusyanthan and Madabhushi (2008).

Flooded versus Non-Flooded

Testing took place with a water level of 1.0 m and 1.1 m. To compare these two conditions the combined load cell data is examined over varying wave heights for the 0-1.1-WC-F-NE and 0-1.0-WC-F-NE trials, as seen in Figure 21. The wave data below 20 cm is eliminated in this case to avoid the breaking wave condition present only during the 1.1 m water level. The addition of 10 cm of water provides a significant addition of force and represents a flooded condition similar to that seen during hurricanes. The ratio of force from the flooded to the non-flooded trials was approximately 3:1 in the 0° orientation. It is interesting that as H_W increases the difference between the forces also increases, as seen in Figures 20 and 21. Equations for theoretically determining the wave force (discussed in detail in a later section) relate the surge force to the square of the bore height, which might explain this trend.

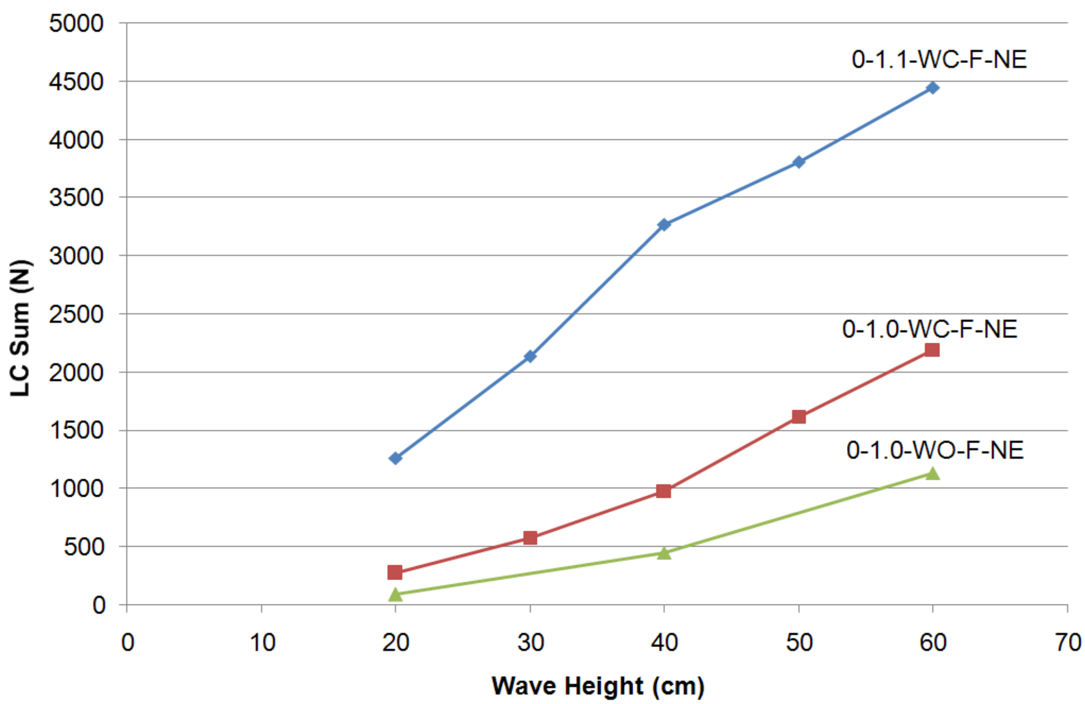

Figure 21: Force plotted between the 0-1.1-WC-F-NE, 0-1.0-WC-F-NE, 0-1.0-WO-F-NE configurations

Push Over Tests

As discussed in previous sections the push over tests were conducted at the OSU Wood Science and Engineering Structures Laboratory. Tests were conducted in both the 0° and 90° orientations. Loading was applied at a variety of heights to determine the relationships between input loading (P_P), deflection (Δ_P) and height of applied load (H_P). For the purposes of interpreting the wave lab data the trials discussed in this section are the distributed load push over tests, as these most closely represent wave loading. Each test was conducted up to an average maximum load of 1400 N for the 0° orientation and 2200 N for the 90° orientation. This load was determined based on test observation while loading the structure, keeping the deflection within the linear range.

0° Orientation

In this test setup there were a total of 43 trials, of which the 39 distributed load trials were analyzed, as seen in Table 3. Loads were applied as both point loads and distributed loads at varying heights and the LVDT's position was moved between three positions as shown in Figure A10. For this study it was assumed that the wave forces were most closely modeled as a distributed force, and the LVDT location needed to match the location used in the wave lab trials. Given these conditions, the only trials used in these results were the 27 trials with a distributed load. Figure 22 below shows the load cell distribution from one of the push over trials, which represents a distributed load applied at 43 cm in the 0° orientation. As discussed in the wave lab results section the load cells did not equally share load from side to side, instead differences in stiffness determined how the load was distributed throughout the structure.

Figure 22 clearly shows the overturning moment seen in Figure 10, where LC2 and LC4 see a higher magnitude of force based on differences in structural stiffness. From the push over tests in this orientation the relationship between P_P and Δ_P was found to be linear, as shown in Figure 23. This linear fit was used up to the maximum applied load, and neglects the unloading period. The slope was found for each trial and averaged for a given H_P, as shown in Table 7.

Table 7: Linear fit between input loading and deflection at the given height of loading

H_P (cm)	# of Trials	P_P / Δ_P
43	20	168
36	7	186
27	6	263
18	6	415

When comparing the relationship between P_P / Δ_P and H_P the relationship was best fit by an exponential, as shown in Figure 24. The exponential equation (1) shown on Figure 24 will provide the relationship between P_P and Δ_P for any given height, H_P.

$$P_P = \Delta_P \cdot 746 \cdot \exp^{-0.03648 \cdot H_P} \qquad (1)$$

Where, P_P is the input loading, Δ_P is the combined load cell output, and H_P is the height of applied loading.

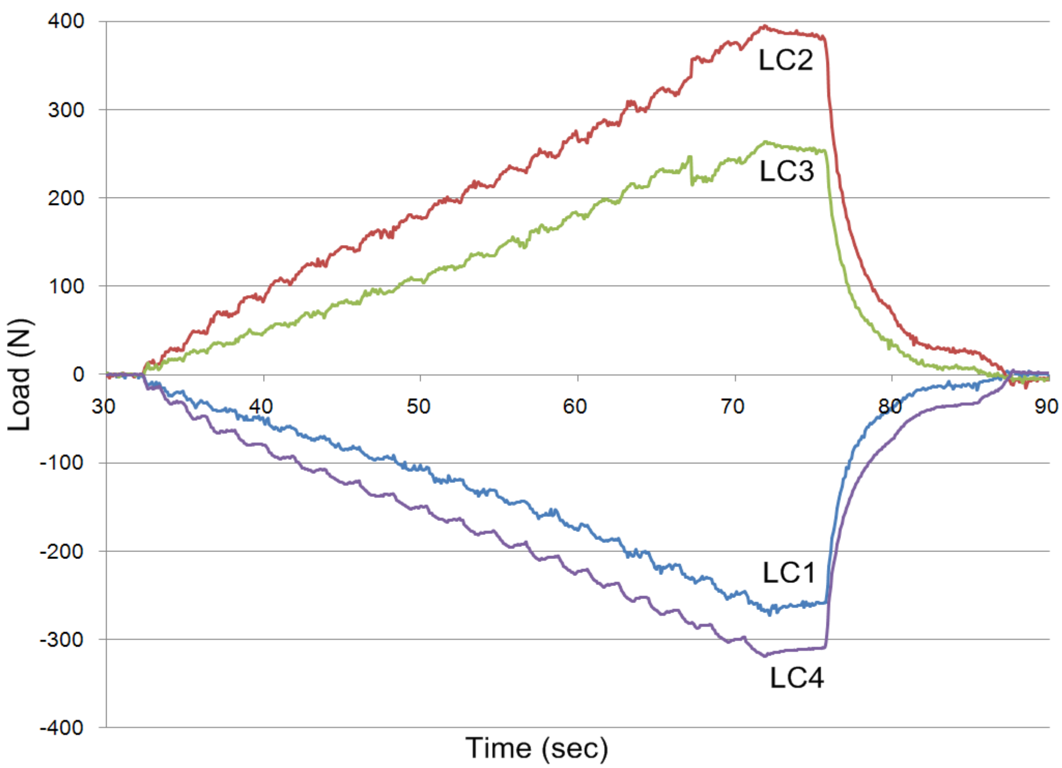

Figure 22: Load cell data from 0-DL-43-2 push over test

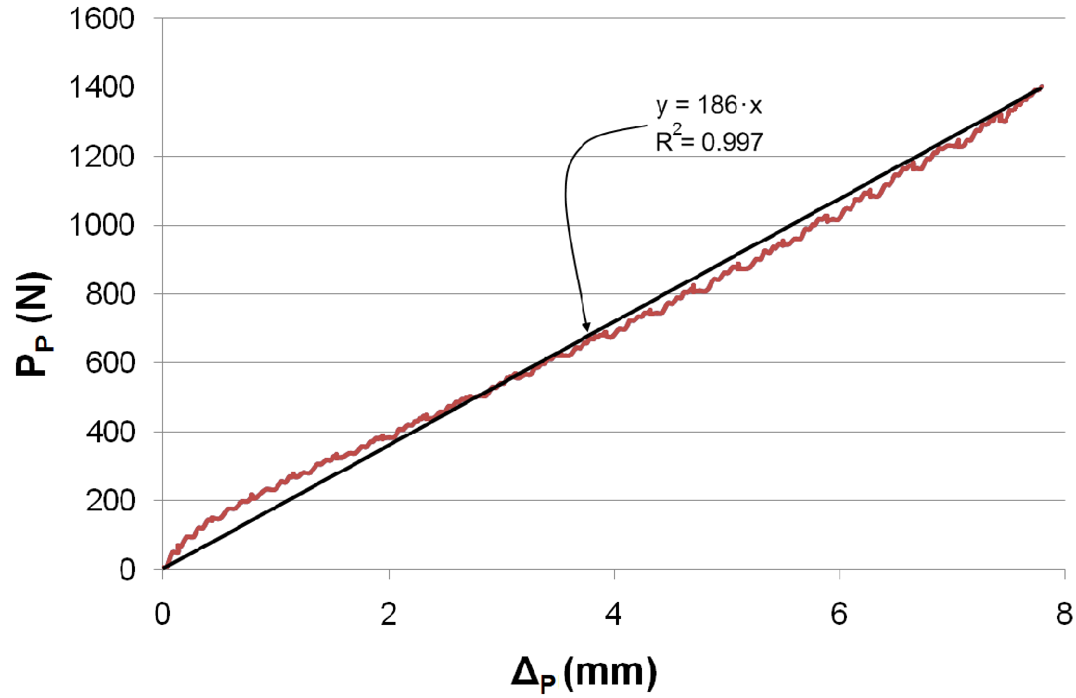

Figure 23: Linear relationship between P_P and Δ_P, 0-DL-43-2

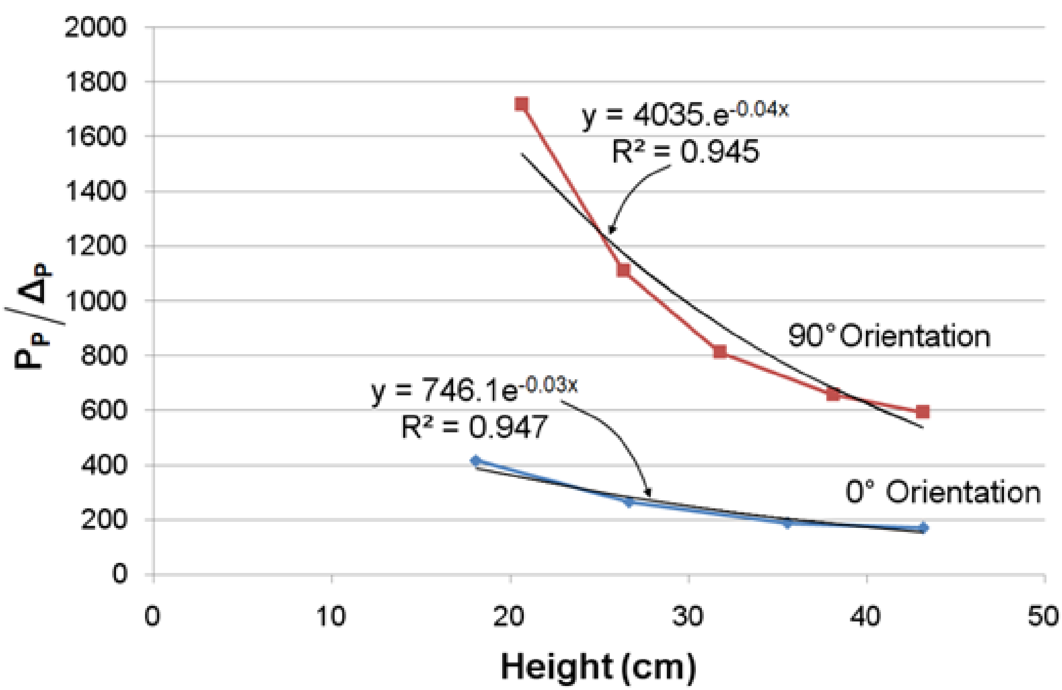

Figure 24: Exponential relationship between H_P and P_P / Δ_P, 0° and 90° orientation

This relationship can now be used to interpret the wave lab data to determine the input loading generated by the wave, P_W. In reality the height is the location of the resultant of the wave force, in the bore height is used in these equations. This is the same method as indicated by the City and County of Honolulu Building Code (HBC). Determining the exact location of the resultant of the wave force experimentally is challenging without more elaborate instrumentation to find the pressure distribution on the face of the structure. This would be an interesting and useful process if it could be validated with future experimental results.

Deflection for the 0° orientation was found to go over scale for the 50 cm and 60 cm trials. Deflection data for the 10 cm – 40 cm trials was plotted and a quadratic was found to be the best fit of the data, as shown in Figure 25. This quadratic relationship was used to estimate the deflection in the 50 cm and 60 cm trials, as shown in column 3 of Table 8.

Table 8: Quadratic fit to deflection data in 0-1.0-WC-F-NE

0-1.0-WC-F-NE		
H_W (cm)	Δ_W (mm)	Δ_W from Quadratic (mm)
10	0.112	0.048
20	0.675	0.866
30	2.364	2.173
40	3.905	3.968
50	*Overscale*	6.252
60	*Overscale*	9.025
Quadratic Fit		
A_0	A_1	A_2
0.0024	0.0085	-0.2808

90° Orientation

In this test setup there were 47 trials as seen in Table 4. The test setup was the same as that described in the 0° orientation section. Again, only the 28 trials which had applied distributed loads and LVDT location 2 were used for this study. Similar to the 0° orientation, Figure 26 below shows the load cell distribution from one of the push over trials, which represents a distributed load applied at 43 cm in the 0° Orientation. Linear fits were again applied to P_P versus Δ_P and averaged together for a given H_P as shown in Table 9. The exponential relationship between the ratio of P_P / Δ_P and H_P, equation (2), is shown in Figure 26.

$$P_P = \Delta_P \cdot 4036 \cdot \exp^{-0.04677 \cdot H_P} \qquad (2)$$

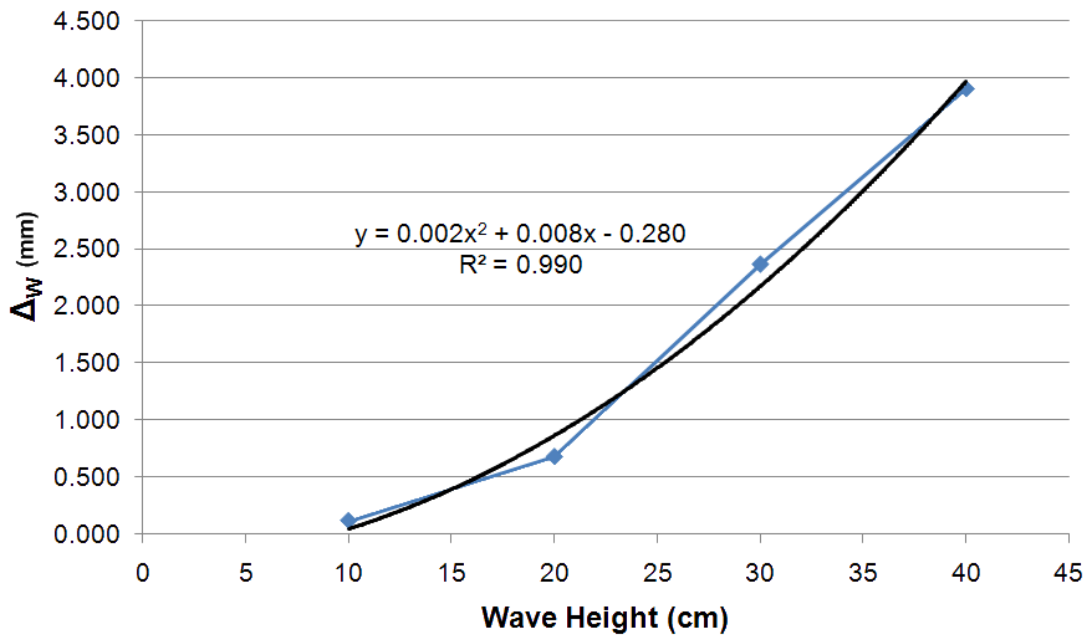

Figure 25: Quadratic fit to deflection data for the 0-1.0-WC-F-NE trial

Table 9: Linear fit between input P_P, Δ_P and H_P

H_P (cm)	# of Trials	P_P / Δ_P
43	6	592
38	7	656
32	7	812
26	6	1109
21	6	1719

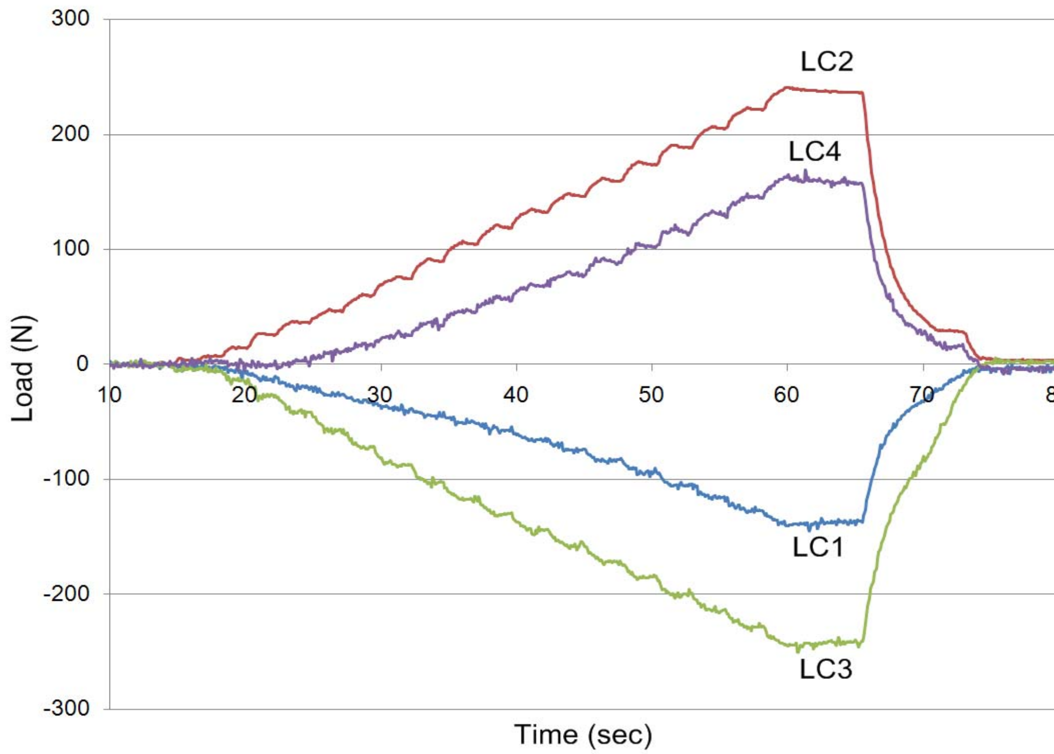

Figure 26: Load cell data from, 90-DL-43-2

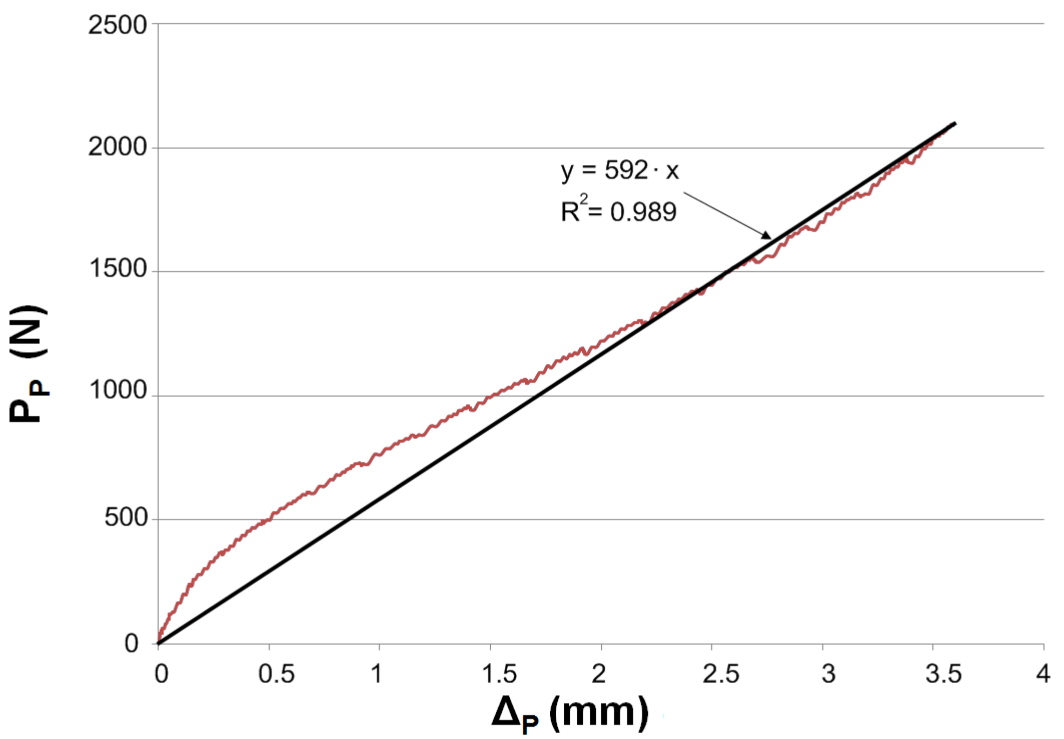

Figure 27: Linear relationship between P_P and Δ_P, 90-DL-43-2

Relating Push Over Tests to the Wave Lab Tests

As wave lab testing is complicated and expensive it would be valuable to be able to apply wave type forces in a dry land testing condition. This could be used as the first phase in structural testing prior to moving into the wave lab for testing. Of course, this type of simulation testing would not exactly replicate the myriad of forces and conditions developed during wave loading, but it may be able to mimic the reactions developed from surge loading. To this extent the combined load cell values from the wave lab trials were matched with similar combined load cell values in the push over tests to determine if the reactions matched, as depicted in Figures 28 and 29.

To compare the load cell values (reactions) between the wave lab trials and the push over tests averaged load cell contributions were compiled, as shown in Table 10. There were four wave lab trials, each aligned in the 0-1.0-WC-F-NE orientation with a 40 cm wave height. There were 20 trials from the push over tests which were also aligned in the 0° orientation with loading applied at a height of 43 cm.

Table 10: Averaged Load Cell Values from Wave Lab and Push Over Trials

	LC1 (N)	LC2 (N)	LC3 (N)	LC4 (N)
Push Over Trials	-205	303	216	-250
Wave Lab Trials	-286	214	130	-343
% Difference	39.8%	29.4%	39.7%	37.3%

As can be seen in Table 10 there are differences between individual load cells, but the overall trends are the same. As the push over tests applied controlled, distributed loading, it would follow that the wave loading had more complexity, which is not easily replicated. It is well known that there are multiple aspects to wave loading, and it is likely that the effects of hydrostatic and drag loads add additional variability to individual load cells that doesn't fit with the distributed loading assumed by the push over tests. It is also reasonable to assume that differences between structural models used for wave lab trials and push over trials may account for some of these differences.

Although the complexity of wave loading and its distribution throughout the structure is not identically replicated, the overall loading and behavior of the structure was simulated. Using (1) and (2) a prediction for P_W can be developed using Δ_W as input, which was recorded during the wave lab trials. The bore height and velocity data collected was found to be unreliable, and therefore data in Table 11 from Robertson et al (2008) was used as input for (1) and (2). The data in Table 11 was collected as part of a larger project at the TWB, which had a similar reef configuration. Figure 30 shows plots of P_W versus solitary wave height using equations (1) and (2), h, and Δ_W data from the wave lab trials. P_W has been normalized per unit width (N/m) for comparison.

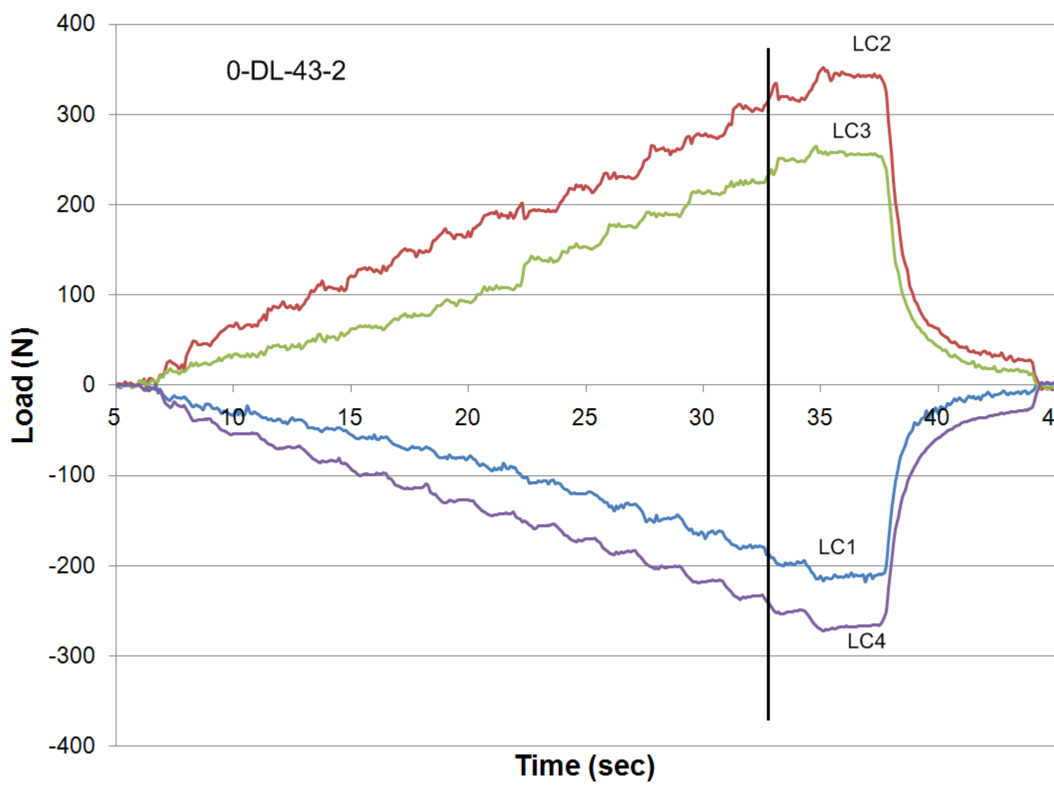

Figure 28: Point in time where combined load cells are at the correspondingly maximum value in the push over trial shown in Figure 29

Similar to what was discussed in an earlier section Figure 30 demonstrates that, unlike pure surge loading, forces found in this study do not scale per unit width. This again indicates that other loads are clearly present, for example the drag and hydrostatic forces as given in the

HBC. One example of a structural difference that might change the loading between orientations is the reentrant corner and front porch area present in the 90° orientation, which would significantly alter the flow around the structure altering the drag forces.

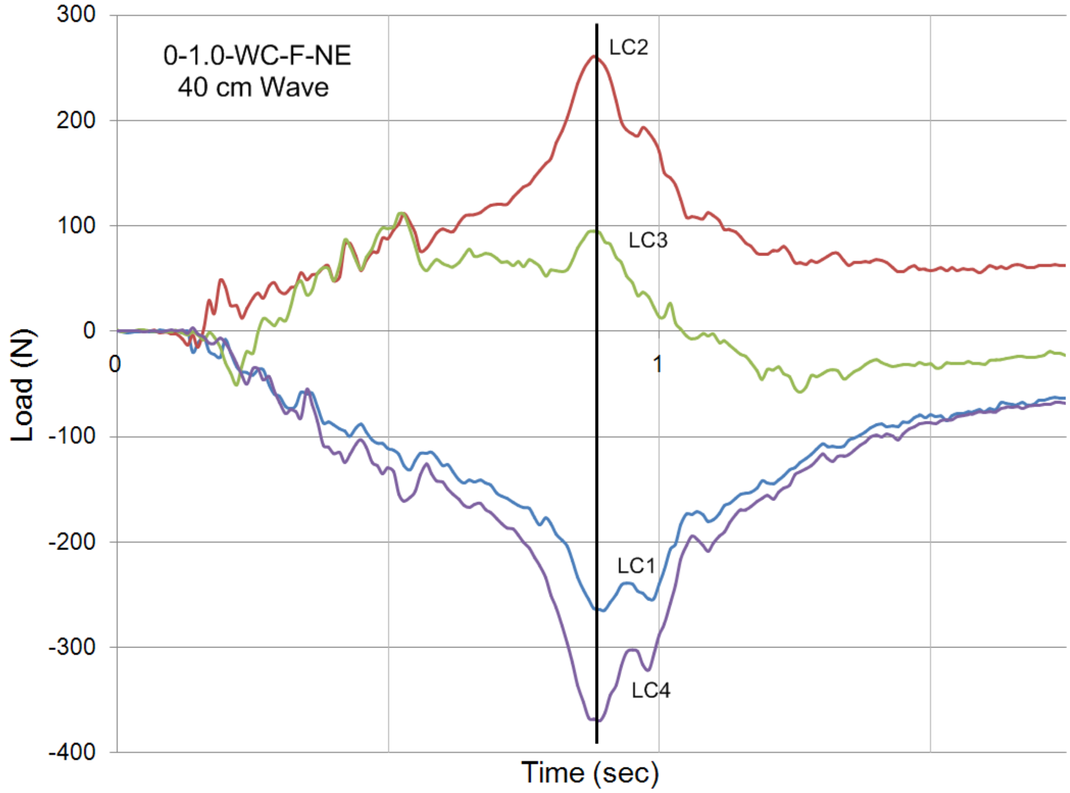

Figure 29: Point in time where combined load cells are at a maximum value in wave lab trial

One of the goals of this study was to compare these results to the HBC, which can be accomplished by working with the wave lab and push over data using total combined load. The HBC provides equation (3) for surge loading where ρ is the density of water, g is acceleration due to gravity, and h is the height of the surge.

$$F_S = 4.5 \cdot \rho \cdot g \cdot h^2 \qquad (3)$$

This equation gives force per unit width (F_S). In metric units ρ = 1000kg/m^3, g = 9.81 m/s^2, and h is in meters, which gives units of N/m. In Imperial units ρ = 1.94 lbf-s^2/ft^4, g = 32.2 ft/s^2, and h is in ft, which gives units of lbf/ft. Equation (3) is the reduced form of the original equation, which is derived from a combination of the hydrostatic force and the change in momentum of the surge front, (Dames and Moore, 1980). Equation (3) assumes a linear pressure distribution and runup height of $3 \cdot h$, and is thus invalid for structures higher than $3 \cdot h$. The original equation is shown in (4).

$$F_S = \tfrac{1}{2} \cdot \rho \cdot g \cdot h^2 + \rho \cdot u^2 \cdot h \qquad (4)$$

The additional term u is the velocity of the surge. As u is difficult to determine, it is estimated as $u = 2\sqrt{g \cdot h}$, (Bretschneider, 1974). This assumption was developed assuming a bore-like wave form. This substitution reduces equation (4) to that shown in (3).

The bore height *(h)* and velocity *(u)* in Table 11 (Robertson et al, 2008) are used as inputs to (1) and (2) to calculate the forces shown in Tables 12 and 13. Also presented in Tables 12 and 13 is force computed using (3) and (4). These table values have been computed for each configuration, but only include values for the 1 m water depth, due to uncertainty in how the HBC deals with flood condition wave loading. The reef configuration is similar, yet not identical to that in this study, nor is the location of the measurements in the same precise location.

Table 11: Input data for equations 1-4 for calculations in Tables 12 and 13

Trial	H_W (cm)	Δ_W (mm)	h (cm)	u (cm/s)
0-1.0-WC-F-NE	20	0.675	6.0	191
	40	3.905	13.1	310
	60	9.030	16.6	375
90-1.0-WC-F-NE	40	0.098	13.1	310
	60	0.302	16.6	375

Table 12: Force comparison between lab test results and calculated results for the 0° orientation

Wave Ht. (cm)	P_W/b (1), (N/m)	Eqn. 3, (N/m)	Over-Estimate	Eqn. 4, (N/m)	Over-Estimate
20	166	159	1.0	237	1.4
40	741	758	1.0	1343	1.8
60	1508	1216	0.8	2470	1.6

Table 13: Force comparison between lab test results and calculated results for the 90° orientation

Wave Ht. (cm)	P_W/b (2), (N/m)	Eqn. 3, (N/m)	Over-Estimate	Eqn. 4, (N/m)	Over-Estimate
40	188	758	4.0	1343	7.2
60	491	1216	2.5	2470	5.0

It is contrary to theory that (4) should provide more accurate results than (3), as the addition of velocity data should improve upon the assumption of $u=2\sqrt{g\cdot h}$. For comparison Arnason and Ramsden's data have been used to similarly calculate the force in (3) and (4), and is compared with their directly measured force in Appendix Tables D1 and D2. Arnason's results indicate an average over-prediction by ~1.5 from (4) over the measured values. This fits closely with the measurements from the 0° orientation ("box-like" structure); the square column used in Arnason's study was also "box-like". It is difficult to draw many conclusions from Ramsden and Arnason's work, since they used a small range of wave heights and regular "box-like" structures.

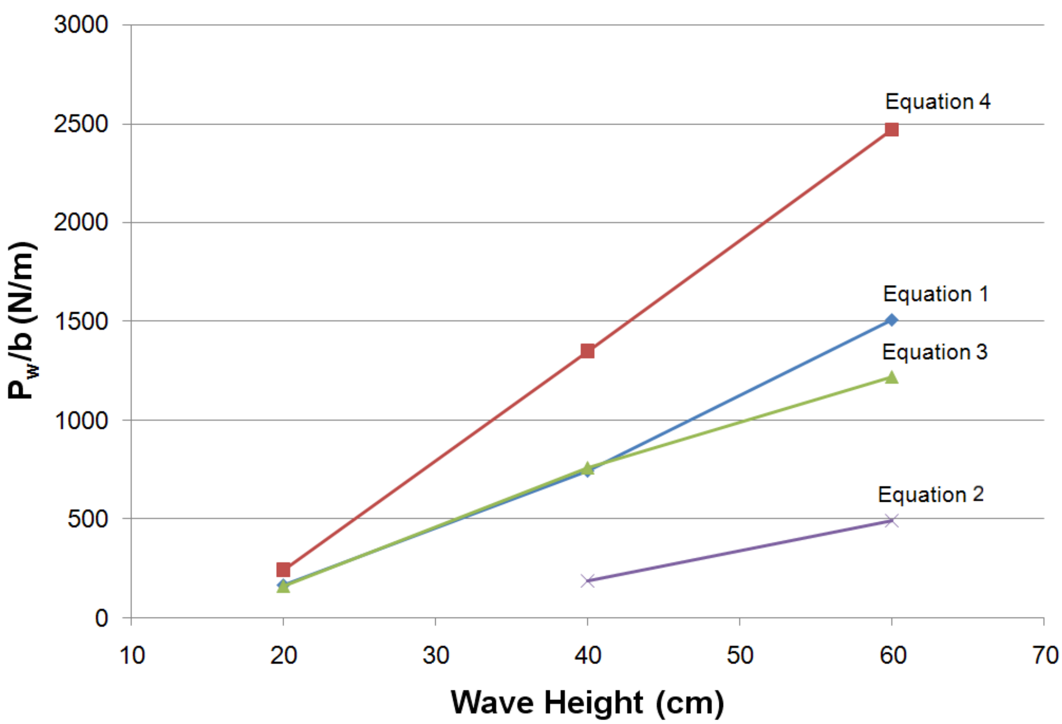

Figure 31: Comparison of force calculated using (1), (2), (3), and (4)

Water as a natural force is no less complex than wind; both are fluids that apply force to structures as a pressure. From the series of different configurations tested in this study, and the varied results from each, it is clear that care must be taken to not over simplify the design of structures in coastal regions. Coastal structures, especially residential structures, show a great deal of architectural variety, if only one parameter is examined (i.e. the width of the structure) it is unlikely good engineering design will follow. As discussed earlier, there are ~60 pages detailing wind loading in ASCE 07-05and only 2 pages on wave loading, there is clearly a need to further detail the complexity of wave loading.

CONCLUSIONS

The study was successful both in meeting its objectives as well as preparing methodology and guidelines for future studies. As there is little research done in this area, one of the major accomplishments was to successfully setup an experiment to capture force and deflection data from wave loading. The loading behavior found was mostly overturning moments and uplift forces.

To prepare for future studies this project qualitatively examined the structural response to many different testing conditions. This qualitative approach showed that: (1) differences in structural stiffness throughout the structure will cause a different load distribution on the output reactions, (2) architectural features, e.g. overhanging eaves above the garage and reentrant corners, can provide unanticipated loading conditions, (3) if water travels beneath the structure, uplift becomes the predominant component of loading, and (4) the effect of waves breaking on or near the structure greatly increases the loading.

By comparing configuration changes in the different trials it was found that the difference in loading from the 0° to 90° orientation averages ~4:1. Since the aspect ratio of the structure is approximately 2:1, this is at odds with surge loading equations, which assume a uniform force per unit width. The ratio of force from the windows closed condition to the windows open condition is ~2.5:1. The ratio of force from the 1.1 m water depth to the 1.0 m water depth averages ~3.8:1. There are a variety of forces during wave loading, including buoyant, surge, drag, and hydrostatic forces, which are likely causing the discrepancy in loading between the different trial orientations.

Through the push over tests relationships were developed between resultant height, input loading and deflection, shown in equations (1) and (2). These equations, combined with bore height data (*h)* allowed estimation of P_W from the deflection data Δ_W.

$$P_W = \Delta_W \cdot 746 \cdot exp^{-0.03648 \cdot h} \qquad (1)$$

$$P_W = \Delta_W \cdot 4036 \cdot exp^{-0.04677 \cdot h} \qquad (2)$$

These equations can be used on this model to determine P_W for a given h and Δ_W, which both can be determined experimentally. This technique would be useful to compare against input force determined theoretically as well as that calculated from pressure sensors.

Equation (3) predicts force on a per unit width basis, and seems well suited to estimating force if the structure is regular in shape or “box-like.” Comparing measured force data with the theoretical values from (3) there is large differences between different wave heights and structural configurations. There were also differences found between flooded and non-flooded conditions. Residential coastal structures vary in architectural design, thus it is important to develop methods for determining wave loads taking into consideration the shape of the structure. It was found that opening the windows and doors reduced loading by 40%. This indicates a need to research special designs for coastal structures to reduce wave loading, similar to work done by Thusyanthan and Madabhushi (2008). Wave loading is complex and large differences can be seen with small changes in structural configuration and coastal conditions, this clearly necessitates further research to develop accurate and reliable engineering design guidelines.

Recommendations for Future Studies

As a preliminary study, one of the main goals was to develop methodology for successive studies. The results of this study have generated the following recommendations:

1. Further tests with simplified structures to enable isolation of single variables to analyze.
2. Future structures should be placed further from the breaking waves to allow for fully developed, regular bores.
3. Additional load cells to directly measure the force in the direction of wave loading, either triaxial cells or two sets of uniaxial load cells.
4. More accurate and repeatable measurements for bore and runup height as well as bore velocity, laser imaging of the water surface is most likely the best option.
5. Consolidated data acquisition between wave height/velocity measurements and load cell/deflection measurements to correlate time between instruments.
6. Higher repetition of individual trials for statistical certainty in results.
7. Method of determining effects of wave loading and water damage on the structural stiffness after individual trials.

BIBLIOGRAPHY

American Forest and Paper Association (AFPA). (2006). “Guide to Wood Construction in High Wind Areas for One- and Two-Family Dwellings - 130 mph Exposure B Wind Zone.” Washington, D.C.

Arnason, H. (2005). “Interactions between an Incident Bore and a Free-Standing Coastal Structure.” Ph.D. Thesis, University of Washington, Seattle, WA.

ASCE. (2005). “Minimum design loads for buildings and other structures.” ASCE 7-05, Reston, VA.

C. L. Bretschneider. (1974). “Development of Structural Standards in Flood and Tsunami Areas for the Island of Hawaii,” Ocean Engineering Consultants, Inc., Honolulu, Hawaii.

Clinton, W.J. (2006). “Lessons Learned from Tsunami Recovery: Key Propositions for Building Back Better.” United Nations Secretary-General's Special Envoy for Tsunami Recovery, United Nations, New York.

Dahdouh-Guebas, F. (2006). “Mangrove forests and tsunami protection”. McGraw-Hill Yearbook of Science & Technology, McGraw-Hill Professional, New York, USA, pp. 187-191.

Dames & Moore. (1980). “Design and Construction Standards for Residential Construction in Tsunami-Prone Areas in Hawaii.” Prepared for the Federal Emergency Management Agency, Contract H-4842.

HBC. (2000). Department of Planning and Permitting of Honolulu Hawai'i. City and County of Honolulu Building Code, Chapter 16, Article 11. July.

FEMA. (2005). “Coastal Construction Manual: Principles and Practices of Planning, Siting, Designing, Constructing, and Maintaining Buildings in Coastal Areas.” FEMA 55, Edition 3, Federal Emergency Management Agency, Washington, DC.

Garcia, Rachel. (2008). “Wave and Surge Loading On Light-Frame Wood Structures.” Master’s thesis, Colorado State University, Fort Collins, CO.

Gerstner, FJ von. (1802). “Theorie der Wellen.” Abhand. Kön. Böhmischen Gesel. Wiss, Prague.

GESAMP (IMO/FAO/UNESCO-IOC/WMO/WHO/IAEA/UN/UNEP, Joint Group of Experts on the Scientific Aspects of Marine Environmental Protection). (2001). “Protecting the oceans from land-based activities - Land-based sources and activities affecting the quality and uses of the marine, coastal and associated freshwater environment.” Rep. Stud. GESAMP No. 71, 162 pp.

Goring, N.D. (1979). “Tsunamis - The Propagation of Long Waves onto a Shelf.” Report No. KH-R-38, W.M. Keck Laboratory, California Institute of Technology, Pasadena, CA.

Knabb, R.D., J.R. Rhome, and D.P. Brown. (2005). “Tropical Cyclone Report - Hurricane Katrina.” National Hurricane Center.

National Weather Service. (2005). “Hurricane Katrina, A Climatological Perspective.” Technical report 2005-01. National Oceanic and Atmospheric Administration, National Weather Service, Silver Spring, MD.

NOAA. (2004). “Population Trends Along the Coastal United States: 1980-2008.” Coastal Trends Report Series. National Oceanic and Atmospheric Administration, National Ocean Service, Silver Spring, MD.

Nirupama, N., Murty, T. S., Nistor, I. and Rao, A. D.(2006). “Energetics of the Tsunami of 26 December 2004 in the Indian Ocean: A Brief Review.” Marine Geodesy, Volume 29, Issue 1, pp. 39-47.

Pielke, Jr., R.A., Gratz, J., Landsea, C.W., Collins, D., Saunders, M., and Musulin, R. (2007). “Normalized Hurricane Damages in the United States: 1900-2005.” Natural Hazards Review. Volume 9, Issue 1, pp. 29-42.

Ramsden, J.D. (1993). “Tsunamis: Forces on a Vertical Wall Caused by Long Waves, Bores, and Surges on a Dry Bed.” Report No. KH-R-54, W.M. Keck Laboratory, California Institute of Technology, Pasadena, CA.

Robertson, I.N., Riggs, H.R., Mohammed, A. (2008). “Experimental results of tsunami bore forces on structures.” Proc., 27th International Offshore Mechanics and Arctic Engineering Conference, paper OMAE2008-57525, 9 pp.

Su, C.H. and Mirie, Rida M. (1980). “On Head-on Collisions Between Two Solitary Waves.” Journal of Fluid Mechanics, Vol. 98, Issue 3, 509-525.

Thusyanthan, N. I. and Madabhushi, S. P. Gopal. (2008). “Tsunami Wave Loading on Coastal Houses: A Model Approach.” New Civil Engineer International, Volume 161, Issue 2, 77-86.

van de Lindt, John W., Graettinger, Andrew, Gupta, Rakesh, Skaggs, Thomas, Pryor, Stephen, Fridley, Kenneth J. (2007). “Performance of Wood-Frame Structures during Hurricane Katrina.” ASCE Journal of Performance of Constructed Facilities, Vol. 21, No. 2, March/April 2007, pp. 108-116.

Yeh, Harry, Robertson, Ian, Preuss, Jane. (2005). “Development of Design Guidelines for Structures that Serve as Tsunami Vertical Evacuation Sites.” National Tsunami Hazard Mitigation Program (NTHMP), Seattle, WA.

Wydajewski, Kenneth J. (1998). “Response of Breakaway Walls to Hydrodynamic Wave Loading.” Master’s thesis, Oregon State University, Corvallis, OR.

APPENDICES

Appendix A – Model Construction & Setup

Model Construction

The model structure was assembled from pre-built wall panels constructed at Colorado State University. The 1st floor was composed of six wall panels, and the 2nd floor had 8 wall panels. The first floor wall panels are shown assembled in Figure A1.

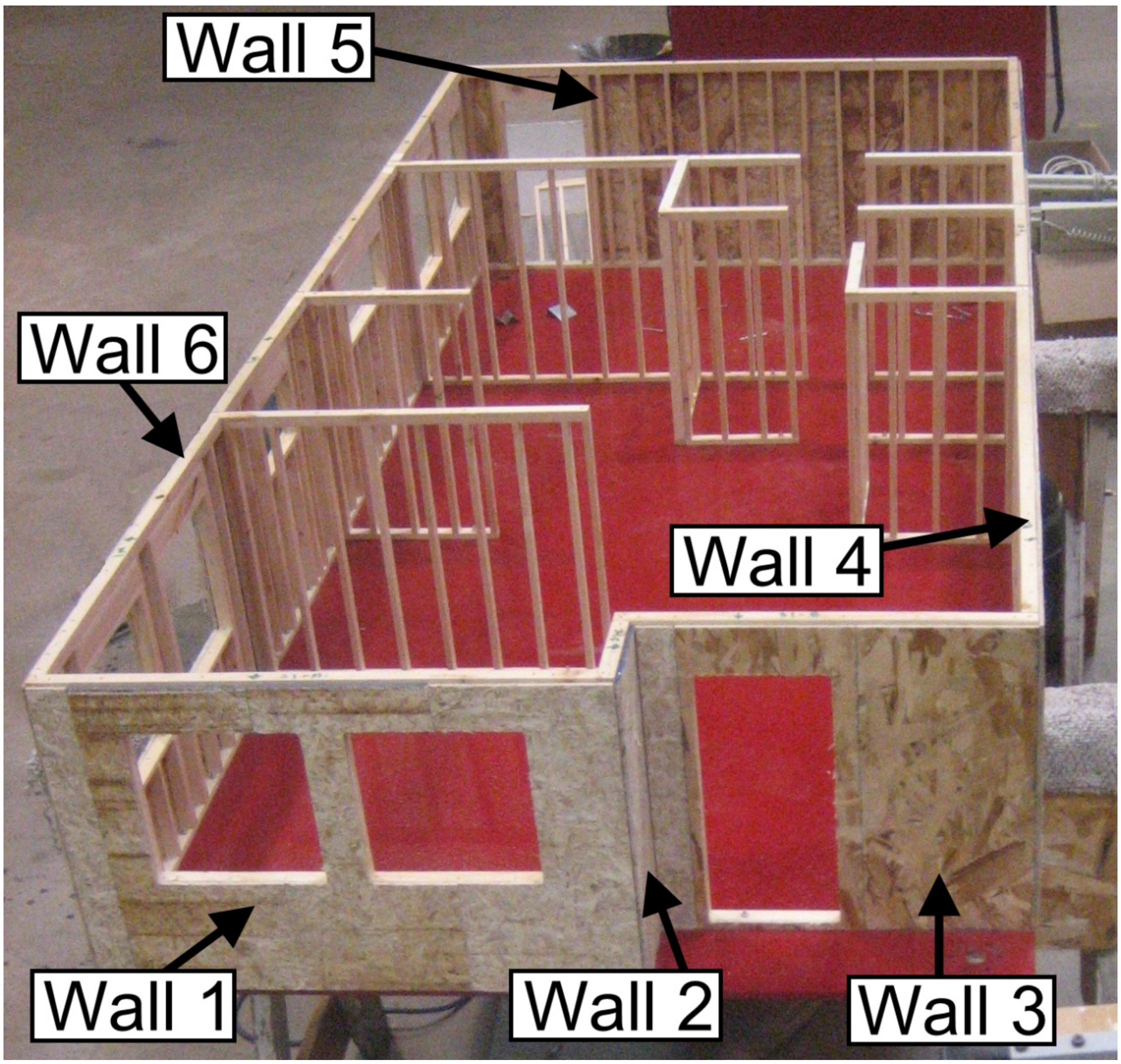

Figure A1: First floor walls assembled on steel baseplate.

Figure A2 shows the steel plate hole layout, with 3.8 mm holes drilled for the anchor bolts, 6.75 mm holes for the load cell mounting bolts, and 25.4 mm clearance holes for anchoring the load cells to the wave basin concrete floor. This was the prescribed spacing for 209 km/hour (130 mph) prescriptive code (AFPA, 2006). The wall panels were then clamped to the steel baseplate, which was used as a template for drilling holes into the bottom plate of the wall panels at the appropriate locations. The bottom plate of the wall panels was then attached to the steel baseplate with 3.18 mm stainless steel anchor bolts with nuts and washers.

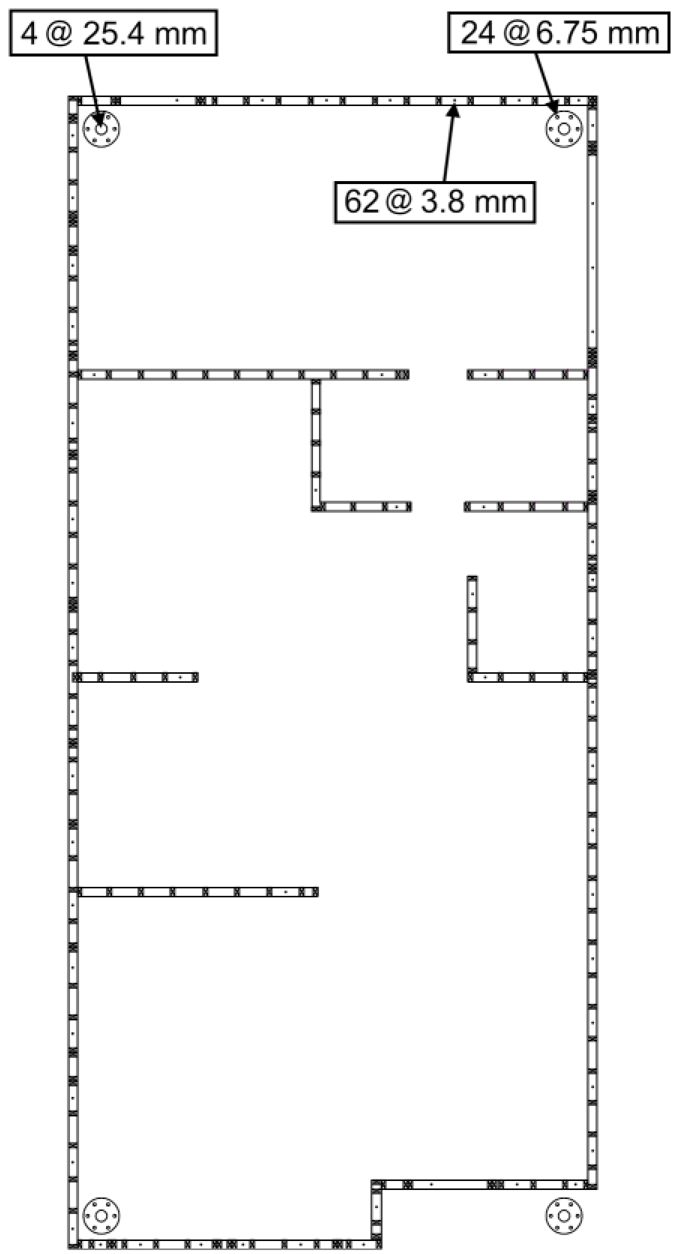

Figure A2: Anchorage and load cell bolt patterns on the steel baseplate

The 2nd story was similarly built upon the 2nd floor diaphragm using 1 mm x 25.4 mm staples. To connect the 2nd story floor diaphragm and wall assemblage to the 1st story top plate thin galvanized sheet metal plates were used, as shown in Figure A3. These plate were installed every ~ 30 cm, using 5 staples on each vertical face of the connector, indicated by an x on the right of Figure A3.

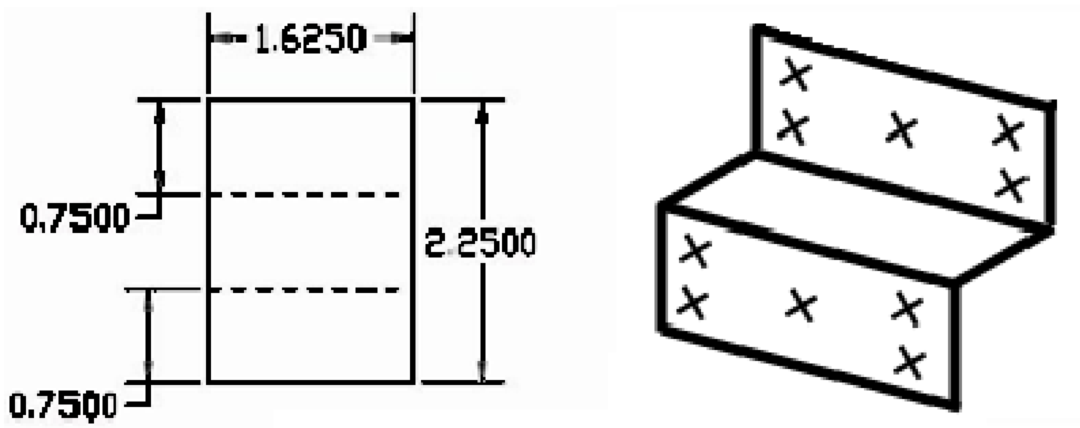

Figure A3: Sheet metal plates used to connect 1st and 2nd story, with bends made along dotted long as shown at right.

The roof diaphragm was then attached using thin gauge sheet metal joist hangers, as shown in Figure A4. The metal straps were placed over the roof joists and were connected to the 2nd story top plate using 4 - 1 mm x 25.4 mm staples, as indicated by an x on the right of Figure A4.

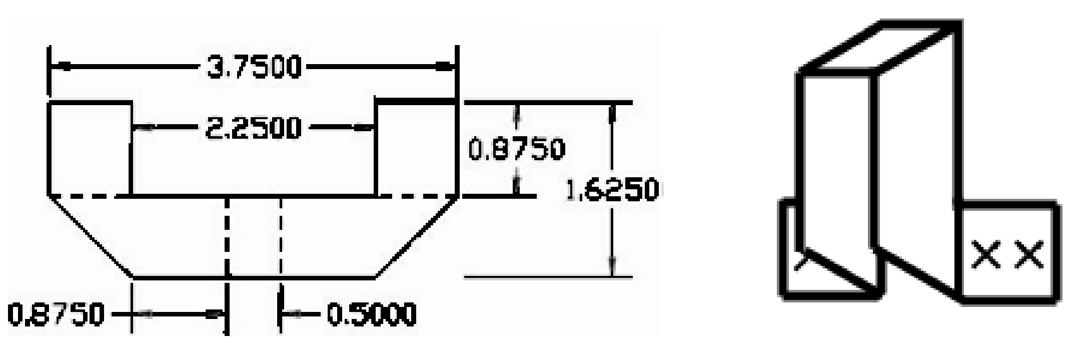

Figure A4: Sheet metal roof connection, with bends made along the dotted lines.

The fully assembled structure was then mounted to the concrete floor of the tsunami wave basin. A concrete drill was used to make 12.7 mm holes in the concrete floor of the tsunami wave basin. Stainless steel threaded rods, measuring 0.635 cm x 15.24 cm (1/4-20 thread pitch, were then anchored into the floor with epoxy using the steel plate as a template, as shown in Figure A5. A nut and washer was used above and below each load cell for leveling the structure, and balancing the load cells.

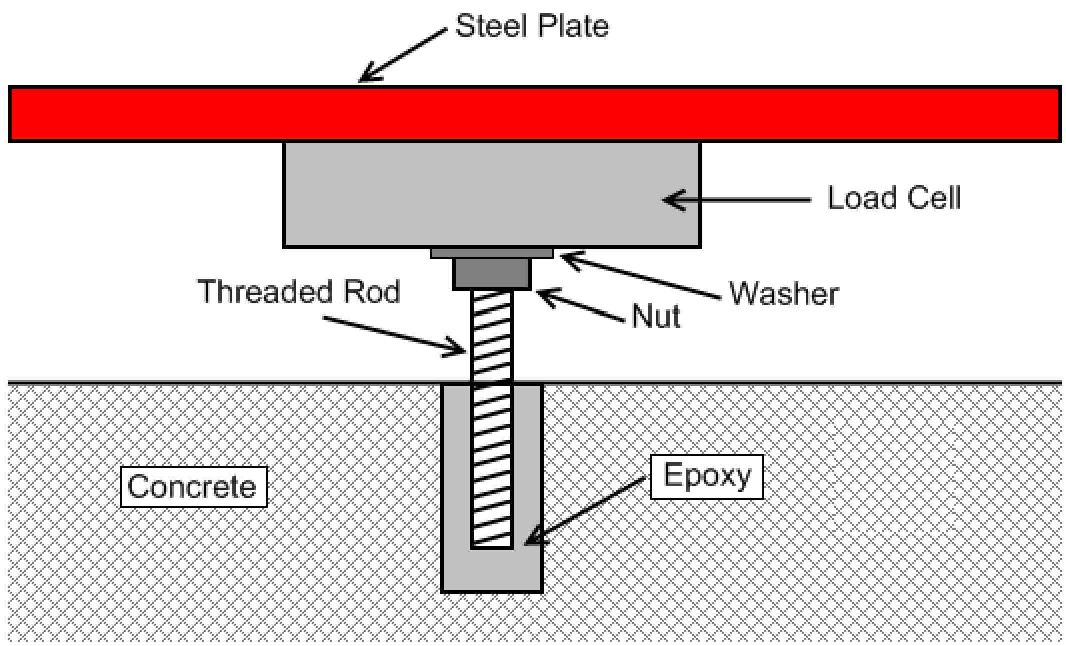

Figure A5: Anchorage to concrete floor in Tsunami Wave Basin

Wave Lab Setup

The TWB utilizes a piston type, electrically driven wave maker composed of 29 waveboards each measuring 2 m high. The wave basin measures 48.8 m long x 26.5 m wide x 2.1 m deep, as shown in Figure A6. Figure A6 also shows the concrete slope poured which starts 10 m from the wave maker at a 1:15 slope, followed by a 1:30 slope starting 17.5m from the wavemaker, ending in a flat plane starting 32.5 m from the wave maker effectively raising the testing area 1 m above the basin bottom. The location of the model structure can also be seen in Figure A6, being positioned ~ 10 cm back from the start of the flat region.

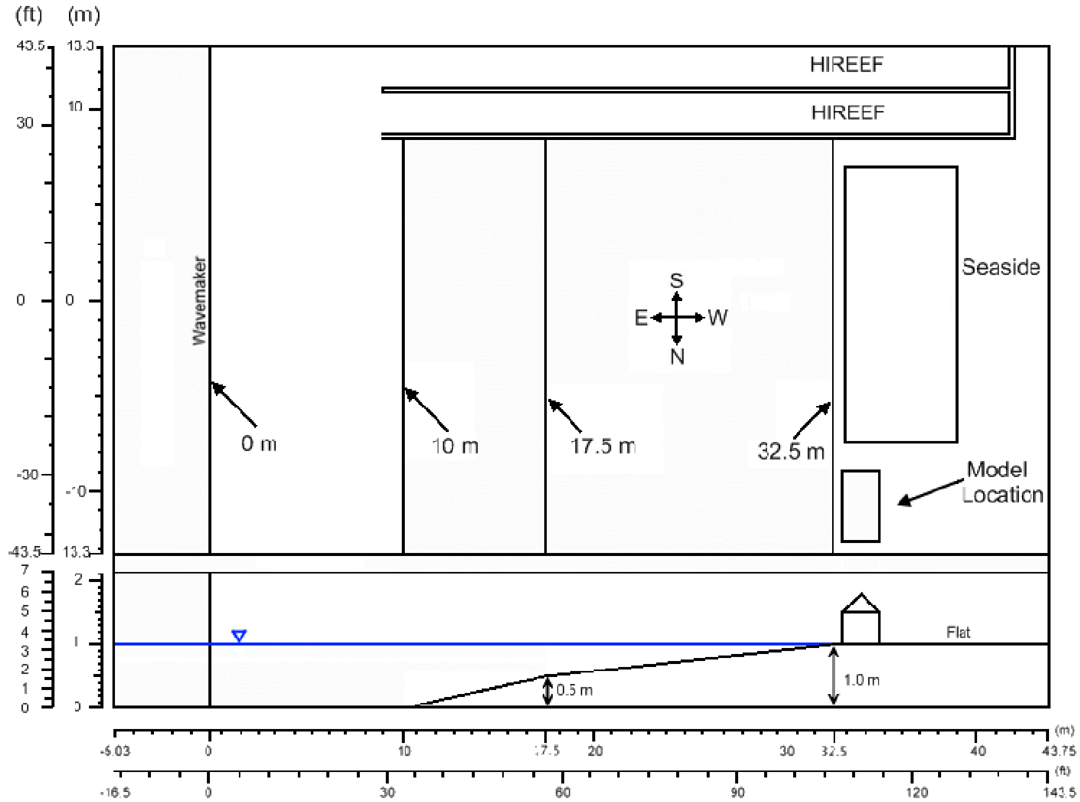

Figure A6: Elevation and profile view of testing area at Tsunami Wave Basin

A rigid testing frame was bolted to the concrete floor behind the structure for mounting instrumentation and wiring, as shown in Figure A7.

Figure A7: Testing frame for mounting instrumentation

Figure A8 shows a detail of the flashing used to prevent water intrusion beneath the baseplate, and Figure A9 shows a detail of the aluminum risers used to elevate the structure.

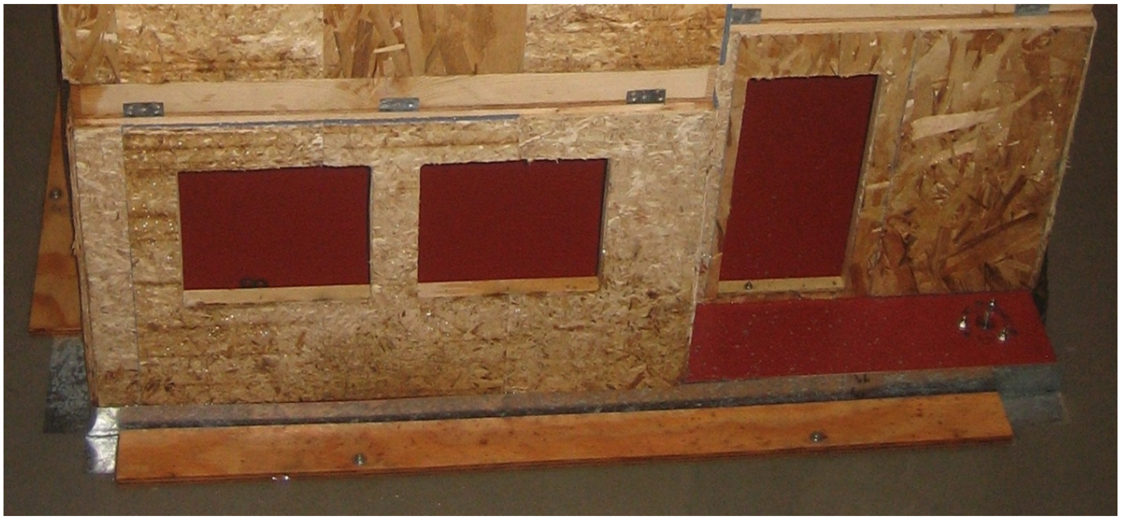

Figure A8: Flashing detail

Figure A9: Aluminum riser used to elevate steel plate and model structure

Push Over Test Setup

Figure A10 depicts the numbering scheme for the LVDT locations during the push over tests. LVDT position 2 was used for most trials, but additional testing was done in case additional data was required or insightful. Figure A11 shows a detail of the LVDT mounting frame.

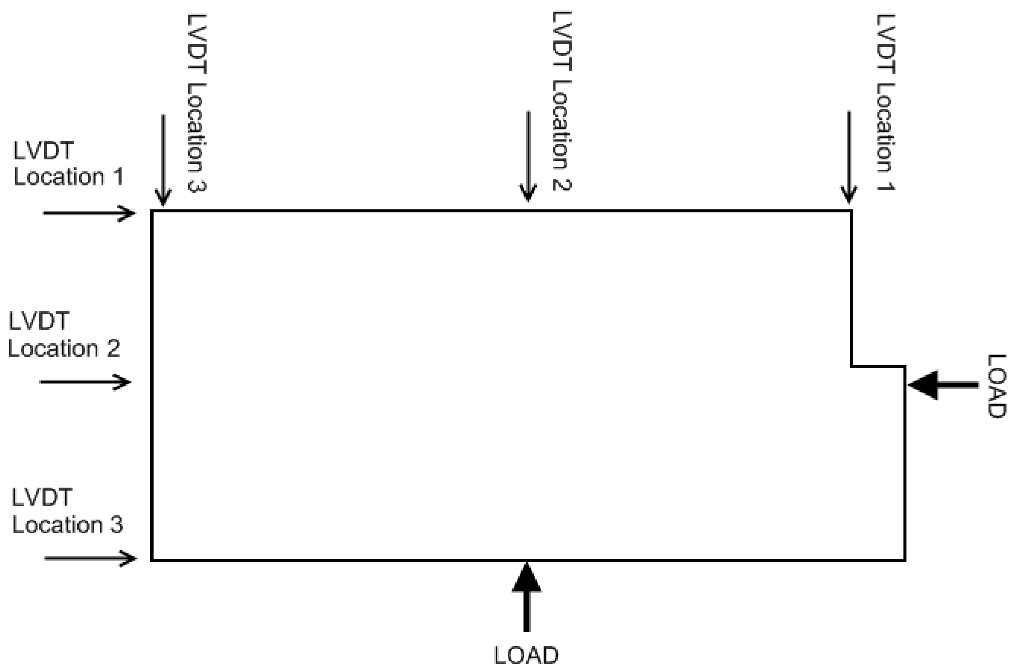

Figure A10: LVDT locations for push over tests

Figure A11: LVDT mounting detail for push over tests

Instrument Calibration

The calibration factors in Table A1 were used to convert raw voltages into the units indicated.

Table A1: Calibration coefficients

LC1 (N/Volt)	LC2 (N/Volt)	LC3 (N/Volt)	LC4 (N/Volt)	Accelerometer (g/Volt)	LVDT (mm/Volt)	Wave Height (cm/Volt)
675.7	676.1	685.0	400.3	1.000	1.837	6.350

Appendix B – Wave Lab Trials

Table B1: Summarized values for elevated wave lab tests, 90-1.1-WC-NF-E

Trial	Wave Ht. (cm)	LC1 (N)	LC2 (N)	LC3 (N)	LC4 (N)	Defl. (mm)	Acc. (g's)
16Nov_07_10	10	457	575	481	578	0.318	0.949
16Nov_08_10	10	137	142	150	191	-0.018	0.179
	Average	**297**	**359**	**316**	**385**	**0.150**	**0.564**
	C.O.V.	**76.3%**	**85.4%**	**74.0%**	**71.1%**	**158.4%**	**96.5%**
16Nov_09_20	20	633	828	686	908	0.104	0.517
16Nov_10_20	20	659	780	700	824	0.038	0.295
16Nov_25_20	20	653	832	706	859	0.162	0.376
19Nov_14_20	20	627	784	676	832	0.148	0.303
19Nov_15_20	20	641	796	687	822	0.045	0.138
19Nov_19_20	20	636	796	697	823	0.086	1.322
19Nov_21_20	20	653	837	713	846	0.089	0.962
	Average	**643**	**808**	**695**	**845**	**0.096**	**0.559**
	C.O.V.	**1.8%**	**3.0%**	**1.8%**	**3.7%**	**49.0%**	**76.3%**
16Nov_11_40	40	851	1146	923	1299	0.728	2.331
16Nov_12_40	40	862	1128	874	1227	0.285	2.628
16Nov_28_40	40	872	1191	926	1276	0.164	2.990
19Nov_08_40	40	894	1157	902	1208	0.417	5.144
19Nov_09_40	40	894	1209	934	1280	0.557	5.142
19Nov_16_40	40	872	1091	923	1209	0.813	1.542
19Nov_17_40	40	900	1080	907	1233	0.392	4.538
19Nov_22_40	40	914	1263	967	1332	1.203	2.478
19Nov_23_40	40	266	314	270	390	0.201	0.118
	Average	**814**	**1064**	**847**	**1162**	**0.529**	**2.990**
	C.O.V.	**25.4%**	**27.0%**	**25.7%**	**25.2%**	**63.7%**	**56.5%**
16Nov_24_50	50	903	1224	1002	1283	1.475	4.306
19Nov_10_50	50	980	1200	1049	1298	1.185	4.504
	Average	**941**	**1212**	**1025**	**1291**	**1.330**	**4.405**
	C.O.V.	**5.8%**	**1.4%**	**3.3%**	**0.8%**	**15.4%**	**3.2%**

Table B2: Summarized values for elevated wave lab tests, 90-1.1-WC-NF-E

Trial	Wave Ht. (cm)	LC1 (N)	LC2 (N)	LC3 (N)	LC4 (N)	Defl. (mm)	Acc. (g's)
16Nov_05_60	60	1039	1354	1103	1420	2.672	4.227
16Nov_06_60	60	1092	1347	1134	1511	1.171	2.753
16Nov_13_60	60	925	1327	1054	1316	1.356	1.865
16Nov_14_60	60	856	1165	959	1206	0.778	2.715
16Nov_21_60	60	1088	1398	1156	1465	1.544	4.120
16Nov_29_60	60	1042	1331	1087	1453	1.794	1.505
19Nov_13_60	60	1076	1288	1189	1316	1.792	5.138
19Nov_18_60	60	1056	1325	1100	1482	1.528	2.691
19Nov_24_60	60	1074	1340	1117	1384	1.882	3.776
19Nov_25_60	60	1089	1419	1146	1549	3.413	2.875
	Average	**1034**	**1329**	**1104**	**1410**	**1.793**	**3.167**
	C.O.V.	**7.7%**	**5.2%**	**5.8%**	**7.5%**	**42.2%**	**35.6%**

Table B3: Summarized values for elevated wave lab tests,90-1.1-WO-NF-E

Trial	Wave Ht. (cm)	LC1 (N)	LC2 (N)	LC3 (N)	LC4 (N)	Defl. (mm)	Acc. (g's)
16Nov_01_20	20	526	601	546	632	0.089	0.481
16Nov_02_20	20	554	602	568	620	0.059	0.759
16Nov_17_20	20	590	742	644	710	0.006	0.537
16Nov_18_20	20	616	663	631	774	0.020	0.292
16Nov_26_20	20	538	657	566	624	0.068	0.263
19Nov_26_20	20	525	609	559	642	0.089	0.224
19Nov_27_20	20	535	577	568	598	0.097	0.352
	Average	**555**	**636**	**583**	**657**	**0.061**	**0.415**
	C.O.V.	**6.3%**	**8.9%**	**6.5%**	**9.4%**	**58.1%**	**45.7%**
16Nov_15_30	30	675	967	770	870	0.180	0.299
16Nov_16_30	30	667	1008	735	903	0.008	0.248
	Average	**671**	**988**	**752**	**886**	**0.094**	**0.274**
	C.O.V.	**0.9%**	**3.0%**	**3.2%**	**2.6%**	**129.2%**	**13.1%**

Table B4: Summarized values for elevated wave lab tests,90-1.1-WO-NF-E

Trial	Wave Ht.	LC1 (N)	LC2 (N)	LC3 (N)	LC4 (N)	Defl. (mm)	Acc. (g's)
16Nov_03_40	40	751	825	816	895	0.193	1.965
16Nov_04_40	40	809	770	797	953	0.112	0.558
16Nov_19_40	40	862	806	839	976	0.755	1.658
16Nov_20_40	40	830	823	837	1097	0.395	1.971
16Nov_27_40	40	754	875	757	824	0.049	2.948
19Nov_07_40	40	648	738	688	695	0.004	0.356
19Nov_28_40	40	738	774	752	809	0.372	3.405
19Nov_29_40	40	813	838	796	936	0.354	0.827
	Average	**775**	**806**	**785**	**898**	**0.279**	**1.711**
	C.O.V.	**8.7%**	**5.4%**	**6.5%**	**13.6%**	**87.5%**	**64.3%**
16Nov_23_50	50	670	848	712	916	0.169	3.148
19Nov_11_50	50	690	830	720	921	0.306	4.768
	Average	**680**	**839**	**716**	**919**	**0.238**	**3.958**
	C.O.V.	**2.1%**	**1.5%**	**0.8%**	**0.4%**	**40.6%**	**29.0%**
16Nov_22_60	60	755	1068	823	1009	0.636	1.553
19Nov_12_60	60	738	985	733	1082	0.353	5.139
19Nov_30_60	60	657	1042	797	982	0.996	1.149
	Average	**697**	**1014**	**765**	**1032**	**0.674**	**3.144**
	C.O.V.	**7.5%**	**4.2%**	**6.1%**	**5.0%**	**47.8%**	**69.9%**

Table B5: Summarized values for non- elevated wave lab tests, 90-1.0-WC-F-NE

Trial	Wave Ht. (cm)	LC1 (N)	LC2 (N)	LC3 (N)	LC4 (N)	Defl. (mm)	Acc. (g's)
10Dec_02_40	40	-35	55	-72	30	0.088	0.140
10Dec_03_40	40	-45	49	-72	26	0.103	0.162
10Dec_04_40	40	-37	73	-70	75	0.113	0.278
10Dec_05_40	40	-36	62	-76	41	0.099	0.131
10Dec_10_40	40	-36	61	-71	33	0.080	0.100
10Dec_11_40	40	-42	74	-71	19	0.097	0.247
10Dec_14_40	40	-36	59	-71	15	0.097	0.163
10Dec_15_40	40	-35	47	-72	6	0.106	0.191
	Average	**-38**	**60**	**-72**	**31**	**0.098**	**0.177**
	C.O.V.	**-9.4%**	**16.6%**	**-2.5%**	**68.1%**	**10.7%**	**33.9%**

Table B6: Summarized values for non- elevated wave lab tests, 90-1.0-WC-F-NE

Trial	Wave Ht. (cm)	LC1 (N)	LC2 (N)	LC3 (N)	LC4 (N)	Defl. (mm)	Acc. (g's)
10Dec_06_60	60	-80	178	-118	137	0.244	5.006
10Dec_07_60	60	-95	224	-129	94	0.571	2.367
10Dec_08_60	60	-69	104	-116	74	0.231	0.763
10Dec_09_60	60	-74	231	-126	75	0.337	2.921
10Dec_12_60	60	-69	253	-112	110	0.239	0.402
10Dec_13_60	60	-71	143	-124	100	0.240	0.732
10Dec_16_60	60	-81	185	-124	113	0.253	1.468
	Average	**-77**	**188**	**-121**	**100**	**0.302**	**1.951**
	C.O.V.	**-12.1%**	**28.0%**	**-5.0%**	**22.4%**	**41.1%**	**83.6%**

Table B7: Summarized values for non-elevated wave lab tests, 90-1.0-WO-NF-NE

Trial	Wave Ht.	LC1 (N)	LC2 (N)	LC3 (N)	LC4 (N)	Defl. (mm)	Acc. (g's)
14Nov_01_10	10	50	81	65	63	0.100	0.164
14Nov_02_10	10	86	77	94	71	0.066	0.156
	Average	**68**	**79**	**80**	**67**	**0.083**	**0.160**
	C.O.V.	**37.4%**	**4.1%**	**25.0%**	**7.9%**	**28.9%**	**3.7%**
14Nov_03_20	20	164	194	173	214	0.070	0.717
14Nov_04_20	20	193	214	208	232	0.047	0.153
14Nov_14_20	20	136	184	160	166	0.127	0.172
14Nov_15_20	20	162	198	187	212	0.041	0.201
	Average	**164**	**197**	**182**	**206**	**0.071**	**0.311**
	C.O.V.	**14.4%**	**6.4%**	**11.4%**	**13.7%**	**55.4%**	**87.4%**
14Nov_05_30	30	180	239	239	243	0.077	0.316
14Nov_06_30	30	218	290	241	310	0.080	0.181
14Nov_07_30	30	205	278	239	253	0.073	0.285
	Average	**201**	**269**	**240**	**269**	**0.077**	**0.261**
	C.O.V.	**9.5%**	**9.9%**	**0.6%**	**13.5%**	**4.7%**	**27.1%**
14Nov_08_40	40	252	354	334	364	0.166	0.364
14Nov_09_40	40	236	358	312	328	0.137	0.567
14Nov_16_40	40	290	343	350	338	0.100	0.377
14Nov_17_40	40	265	261	309	293	0.119	0.657
	Average	**261**	**329**	**326**	**331**	**0.130**	**0.491**
	C.O.V.	**8.8%**	**13.9%**	**5.9%**	**8.9%**	**21.6%**	**29.4%**

Table B8: Summarized values for non-elevated wave lab tests, 90-1.0-WO-NF-NE

Trial	Wave Ht.	LC1 (N)	LC2 (N)	LC3 (N)	LC4 (N)	Defl. (mm)	Acc. (g's)
14Nov_13_50	**50**	**282**	**337**	**336**	**349**	**0.197**	**0.825**
14Nov_10_60	60	206	314	297	360	0.280	0.782
14Nov_11_60	60	119	312	127	280	0.249	1.269
14Nov_18_60	60	328	395	337	483	0.275	1.488
14Nov_19_60	60	143	349	170	350	0.265	0.624
	Average	**199**	**342**	**233**	**368**	**0.267**	**1.041**
	C.O.V.	**47.0%**	**11.3%**	**43.0%**	**23.0%**	**5.1%**	**38.9%**

Table B9: Summarized values for non-elevated wave lab tests, 0-1.0-WO-F-NE

Trial	Wave Ht. (cm)	LC1 (N)	LC2 (N)	LC3 (N)	LC4 (N)	Defl. (mm)	Acc. (g's)
05Dec_18_20	20	-117	15	38	-159	0.318	0.193
05Dec_19_20	20	-120	6	44	-147	0.260	0.137
05Dec_23_20	20	-129	8	48	-172	0.290	0.304
05Dec_24_20	20	-122	7	28	-154	0.274	0.159
	Average	**-122**	**9**	**39**	**-158**	**0.285**	**0.198**
	C.O.V.	**-4.3%**	**48.2%**	**21.7%**	**-6.6%**	**8.7%**	**37.3%**
05Dec_20_40	40	-458	67	153	-617	1.773	0.312
05Dec_25_40	40	-500	100	184	-652	1.852	0.470
05Dec_26_40	40	-492	115	195	-625	1.663	0.355
	Average	**-483**	**94**	**177**	**-631**	**1.763**	**0.379**
	C.O.V.	**-4.6%**	**26.2%**	**12.0%**	**-2.9%**	**5.4%**	**21.6%**
05Dec_17_60	60	-985	418	490	-1164	4.401	1.592
05Dec_21_60	60	-1207	448	486	-1170	3.836	2.037
05Dec_22_60	60	-896	317	457	-1093	3.608	1.091
05Dec_27_60	60	-1023	366	513	-1077	3.503	1.265
05Dec_28_60	60	-982	229	342	-1006	3.378	0.487
	Average	**-1018**	**356**	**457**	**-1102**	**3.745**	**1.294**
	C.O.V.	**-11.3%**	**24.4%**	**14.8%**	**-6.1%**	**10.8%**	**44.6%**

Table B10: Summarized values for non-elevated wave lab tests, 0-1.0-WC-F-NE

0-1.0-WC-F-NE							
Trial	**Wave Ht. (cm)**	**LC1 (N)**	**LC2 (N)**	**LC3 (N)**	**LC4 (N)**	**Defl. (mm)**	**Acc. (g's)**
05Dec_05_10	10	-36	9	2	-43	0.129	0.176
05Dec_06_10	10	-33	2	1	-37	0.095	0.083
	Average	**-34**	**6**	**2**	**-40**	**0.112**	**0.130**
	C.O.V.	**-4.8%**	**82.5%**	**28.9%**	**-9.9%**	**21.2%**	**50.9%**
05Dec_08_20	20	-91	43	27	-99	0.685	0.274
05Dec_09_20	20	-96	43	27	-106	0.666	0.286
	Average	**-94**	**43**	**27**	**-103**	**0.675**	**0.280**
	C.O.V.	**-4.0%**	**0.6%**	**0.4%**	**-5.0%**	**1.9%**	**3.0%**
05Dec_01_30	30	-107	165	56	-265	3.553	0.328
05Dec_02_30	30	-140	108	82	-226	2.364	0.328
	Average	**-123**	**137**	**69**	**-245**	**2.959**	**0.328**
	C.O.V.	**-19.0%**	**29.2%**	**27.3%**	**-11.1%**	**28.4%**	**0.1%**
05Dec_10_40	40	-265	260	111	-370	4.407	0.321
05Dec_11_40	40	-282	223	125	-330	3.790	0.321
05Dec_14_40	40	-294	185	134	-337	3.879	0.209
05Dec_15_40	40	-304	188	150	-337	3.542	0.269
	Average	**-286**	**214**	**130**	**-343**	**3.905**	**0.280**
	C.O.V.	**-5.9%**	**16.6%**	**12.6%**	**-5.2%**	**9.3%**	**19.0%**
05Dec_03_50	50	-373	405	233	-555	7.775	0.366
05Dec_04_50	50	-432	422	274	-530	6.247	0.604
	Average	**-403**	**413**	**254**	**-542**	**7.011**	**0.485**
	C.O.V.	**-10.4%**	**2.9%**	**11.3%**	**-3.4%**	**15.4%**	**34.8%**
05Dec_12_60	60	-602	429	586	-621	5.082	2.204
05Dec_13_60	60	-632	435	599	-650	4.805	2.253
05Dec_16_60	60	-572	391	477	-581	4.179	1.586
	Average	**-602**	**418**	**554**	**-617**	**4.688**	**2.014**
	C.O.V.	**-4.9%**	**5.6%**	**12.1%**	**-5.6%**	**9.9%**	**18.5%**

Table B11: Summarized values for submerged wave lab tests, 90-1.1-WC-F-NE

90-1.1-WC-F-NE							
Trial	**Wave Ht. (cm)**	**LC1 (N)**	**LC2 (N)**	**LC3 (N)**	**LC4 (N)**	**Defl. (mm)**	**Acc. (g's)**
10Dec_17_10	10	-171	435	-169	286	0.177	1.730
10Dec_18_10	10	-63	374	-116	230	0.217	2.160
	Average	**-117**	**405**	**-142**	**258**	**0.197**	**1.945**
	C.O.V.	**-65.6%**	**10.6%**	**-26.4%**	**15.6%**	**14.4%**	**15.6%**
10Dec_30_12	**12**	**-105**	**411**	**-123**	**250**	**0.086**	**0.368**
10Dec_29_15	**15**	**-127**	**442**	**-107**	**263**	**0.096**	**0.254**
10Dec_23_20	20	-41	281	-30	236	0.072	0.154
10Dec_24_20	20	-68	293	-54	249	0.051	0.217
	Average	**-55**	**287**	**-42**	**242**	**0.062**	**0.186**
	C.O.V.	**-34.6%**	**3.1%**	**-40.6%**	**3.7%**	**23.2%**	**23.9%**
10Dec_19_30	30	-87	275	-52	158	0.132	0.360
10Dec_20_30	30	-68	304	-39	203	0.143	0.466
	Average	**-78**	**289**	**-46**	**181**	**0.138**	**0.413**
	C.O.V.	**-16.9%**	**7.1%**	**-19.7%**	**17.8%**	**5.4%**	**18.1%**
10Dec_25_40	40	-90	354	-133	282	0.866	1.649
10Dec_26_40	40	-66	373	-154	262	0.860	2.807
	Average	**-78**	**364**	**-143**	**272**	**0.863**	**2.228**
	C.O.V.	**-21.6%**	**3.7%**	**-10.0%**	**5.2%**	**0.5%**	**36.8%**
10Dec_21_50	50	-132	409	-162	245	1.152	2.865
10Dec_22_50	50	-236	612	-303	338	1.112	1.995
	Average	**-184**	**511**	**-232**	**292**	**1.132**	**2.430**
	C.O.V.	**-39.8%**	**28.1%**	**-43.0%**	**22.6%**	**2.5%**	**25.3%**
10Dec_27_60	60	-198	525	-295	357	2.124	4.364
10Dec_28_60	60	-167	552	-251	363	1.853	2.067
	Average	**-182**	**539**	**-273**	**360**	**1.988**	**3.216**
	C.O.V.	**-11.9%**	**3.5%**	**-11.4%**	**1.2%**	**9.7%**	**50.5%**

Table B12: Summarized values for submerged wave lab tests, 0-1.1-WC-F-NE

0-1.1-WC-F-NE							
Trial	**Wave Ht. (cm)**	**LC1 (N)**	**LC2 (N)**	**LC3 (N)**	**LC4 (N)**	**Defl. (mm)**	**Acc. (g's)**
12Dec_01_10	10	-492	1324	1236	-269	3.910	0.015
12Dec_02_10	10	-334	548	421	-257	3.595	4.147
	Average	**-413**	**936**	**828**	**-263**	**3.752**	**2.081**
	C.O.V.	**-27.1%**	**58.6%**	**69.6%**	**-3.2%**	**5.9%**	**140.4%**
11Dec_01_20	20	-176	351	354	-316	2.268	0.529
11Dec_02_20	20	-198	395	460	-271	2.112	0.366
12Dec_03_20	20	-303	503	270	-196	1.735	0.383
12Dec_04_20	20	-282	496	301	-152	1.523	0.456
	Average	**-240**	**436**	**346**	**-234**	**1.909**	**0.434**
	C.O.V.	**-25.9%**	**17.2%**	**24.1%**	**-31.4%**	**17.9%**	**17.3%**
12Dec_05_30	30	-497	790	556	-299	4.942	2.258
12Dec_06_30	30	-498	681	625	-319	4.290	1.884
	Average	**-497**	**735**	**590**	**-309**	**4.616**	**2.071**
	C.O.V.	**-0.2%**	**10.4%**	**8.2%**	**-4.6%**	**10.0%**	**12.8%**
11Dec_03_40	40	-636	773	1133	-644	9.393	2.325
11Dec_04_40	40	-647	821	1189	-738	8.246	2.603
12Dec_07_40	40	-824	1107	835	-418	8.754	4.145
12Dec_08_40	40	-913	1044	944	-409	11.638	4.143
	Average	**-755**	**936**	**1025**	**-552**	**9.508**	**3.304**
	C.O.V.	**-18.0%**	**17.5%**	**16.0%**	**-29.8%**	**15.7%**	**29.6%**
12Dec_09_50	50	-1044	1208	1147	-604	14.099	2.167
12Dec_10_50	50	-872	1130	993	-608	12.285	3.167
	Average	**-958**	**1169**	**1070**	**-606**	**13.192**	**2.667**
	C.O.V.	**-12.6%**	**4.7%**	**10.2%**	**-0.5%**	**9.7%**	**26.5%**
11Dec_05_60	60	-913	1248	1285	-923	11.236	5.601
12Dec_11_60	60	-608	1344	1467	-1100	15.627	4.164
	Average	**-761**	**1296**	**1376**	**-1012**	**13.432**	**4.882**
	C.O.V.	**-28.3%**	**5.2%**	**9.4%**	**-12.4%**	**23.1%**	**20.8%**

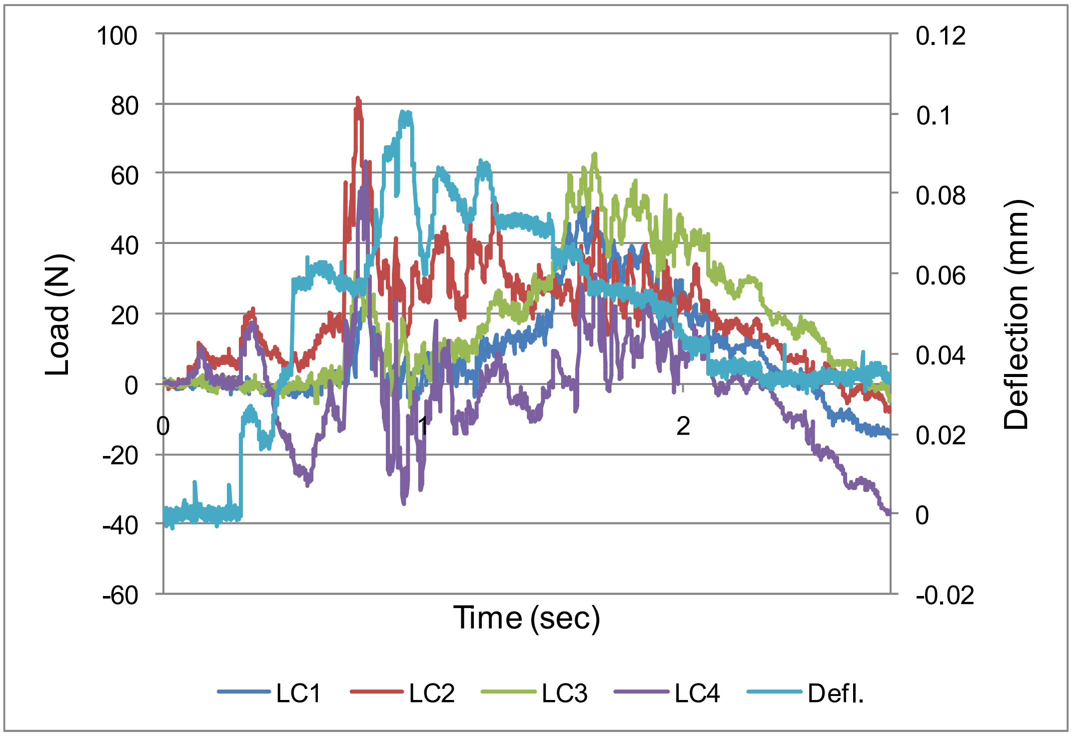

Figure B1: Load and deflection versus time for 10 cm wave lab trial, 90-1.0-WO-NF-NE

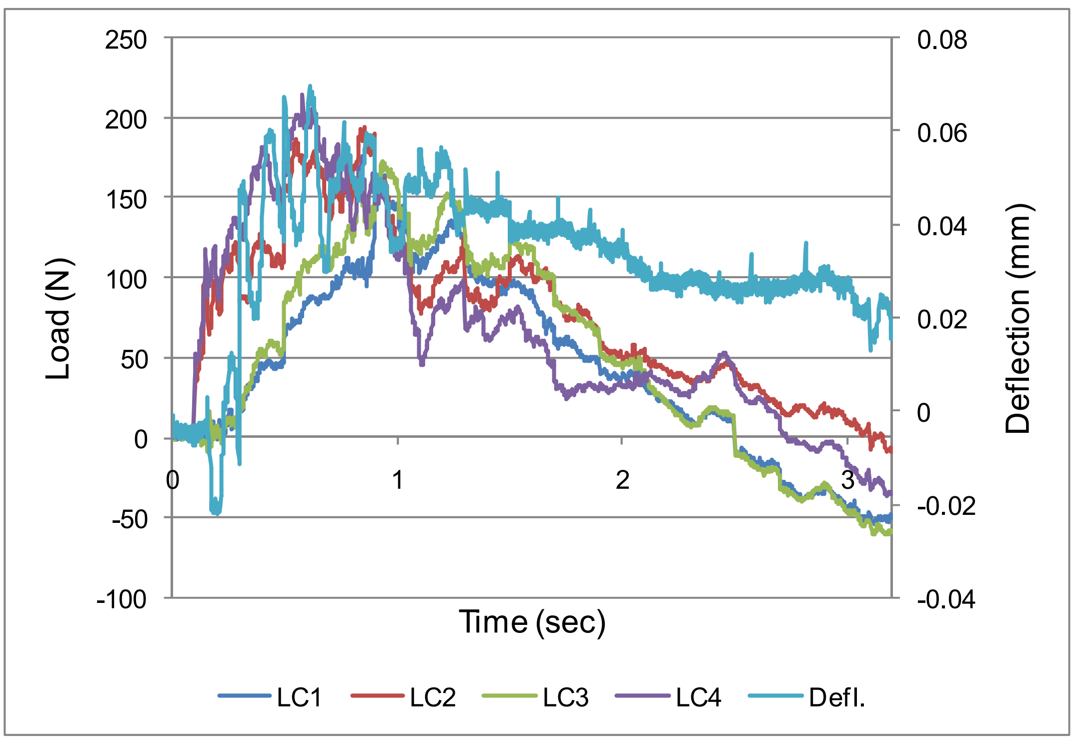

Figure B2: Load and deflection versus time for 20 cm wave lab trial, 90-1.0-WO-NF-NE

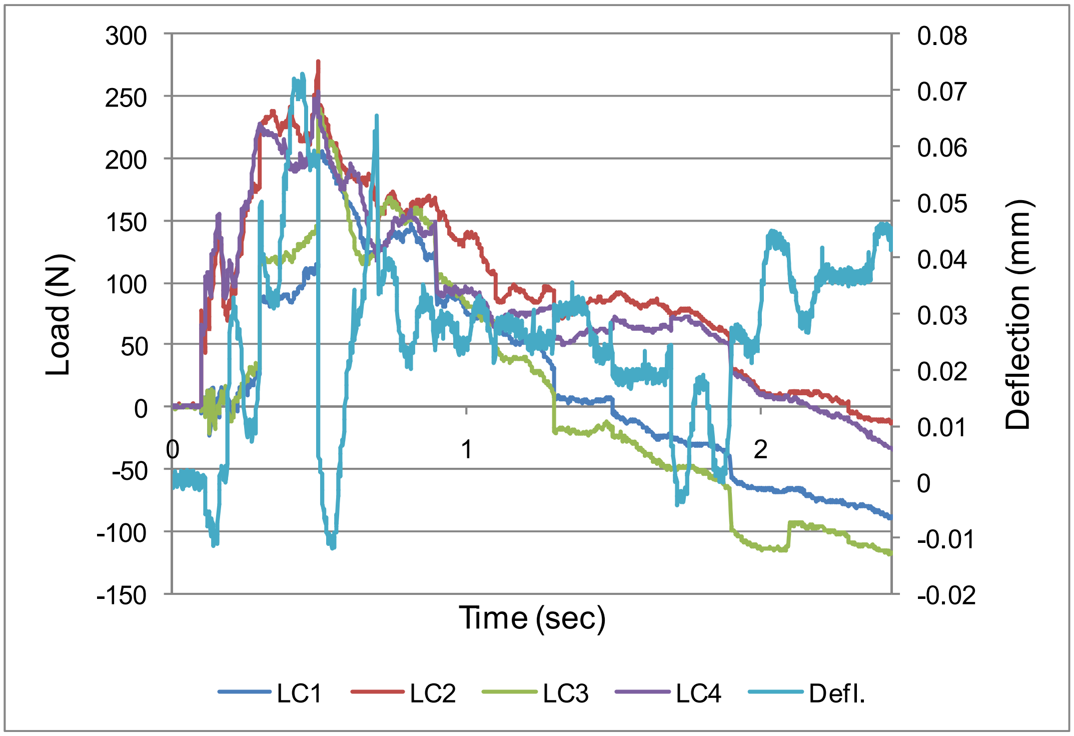

Figure B3: Load and deflection versus time for 30 cm wave lab trial, 90-1.0-WO-NF-NE

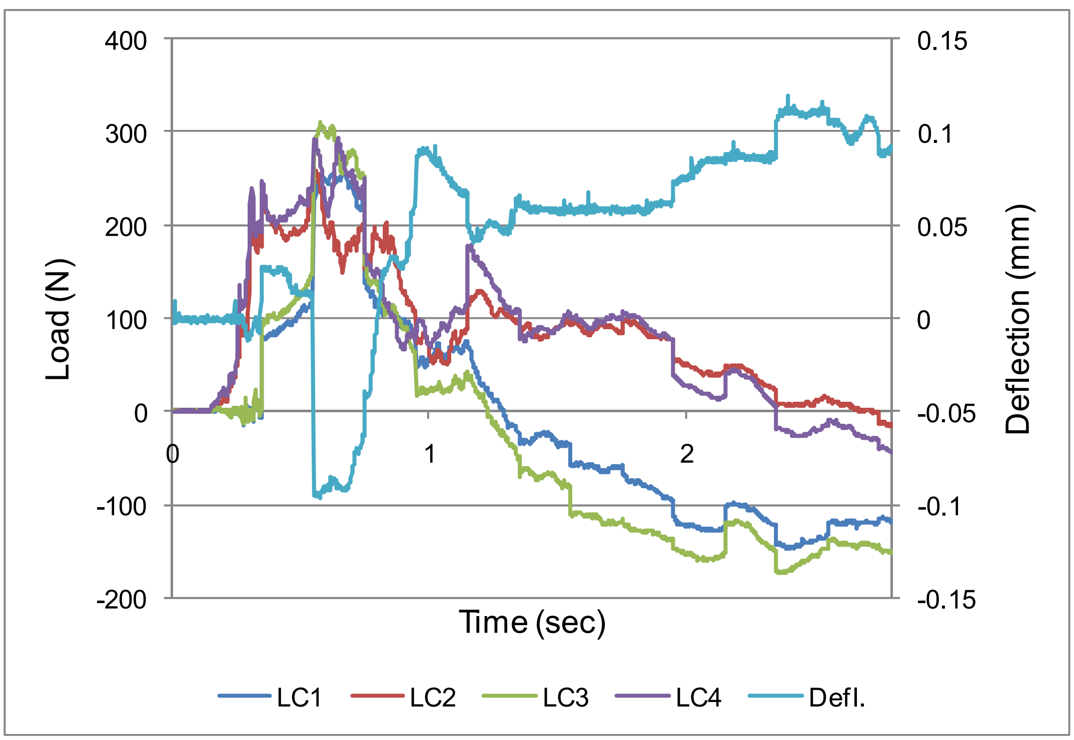

Figure B4: Load and deflection versus time for 40 cm wave lab trial, 90-1.0-WO-NF-NE

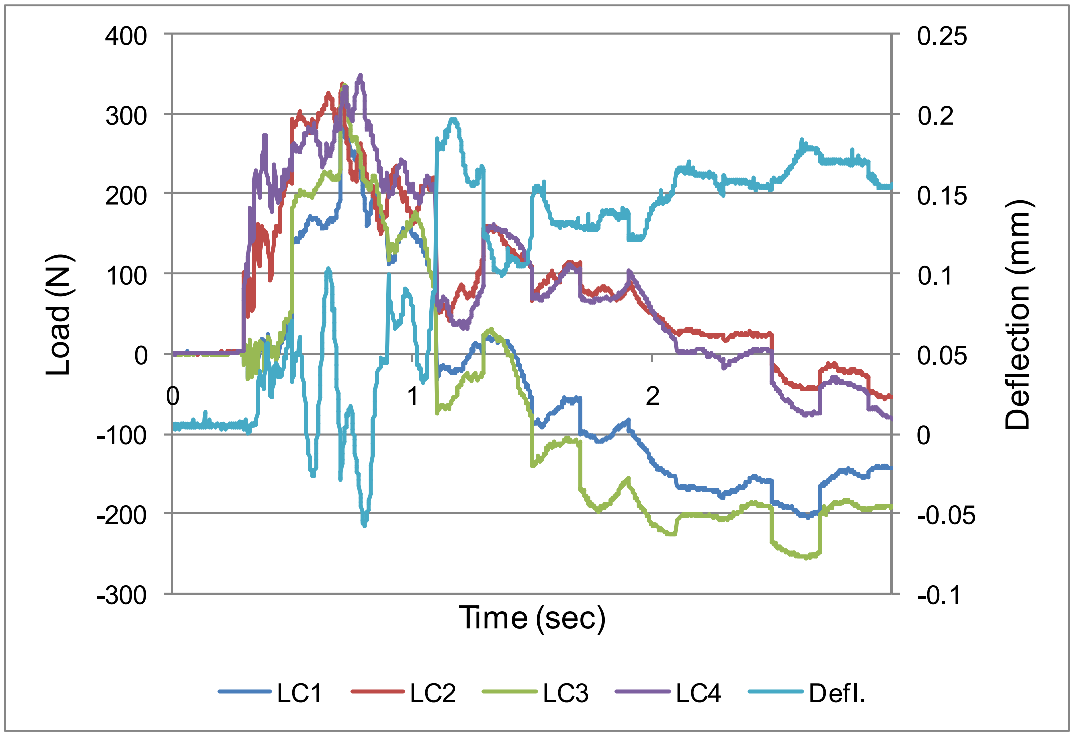

Figure B5: Load and deflection versus time for 50 cm wave lab trial, 90-1.0-WO-NF-NE

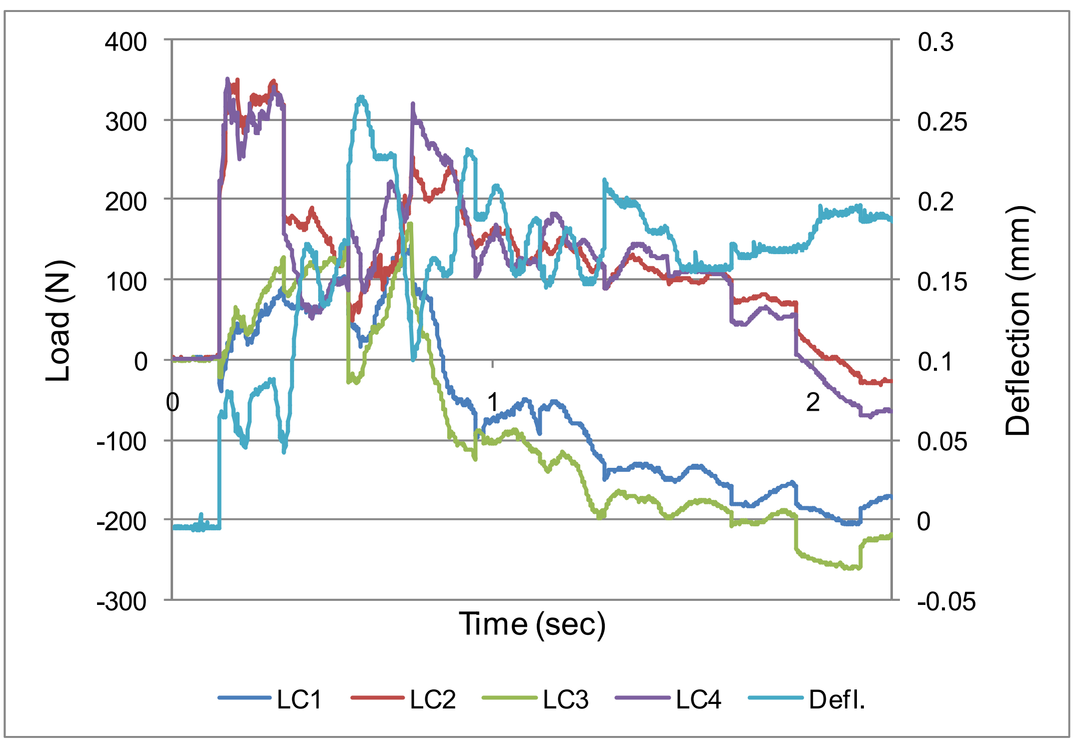

Figure B6: Load and deflection versus time for 60 cm wave lab trial, 90-1.0-WO-NF-NE

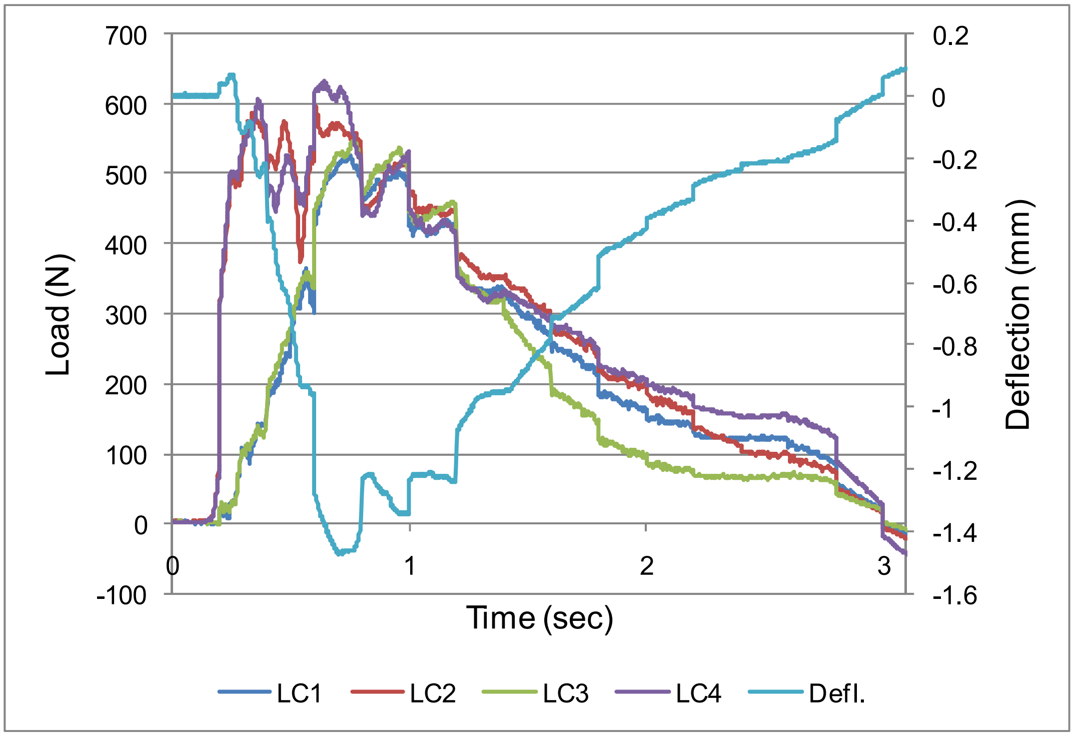

Figure B7: Load and deflection versus time for 20 cm wave lab trial, 90-1.1-WO-NF-E

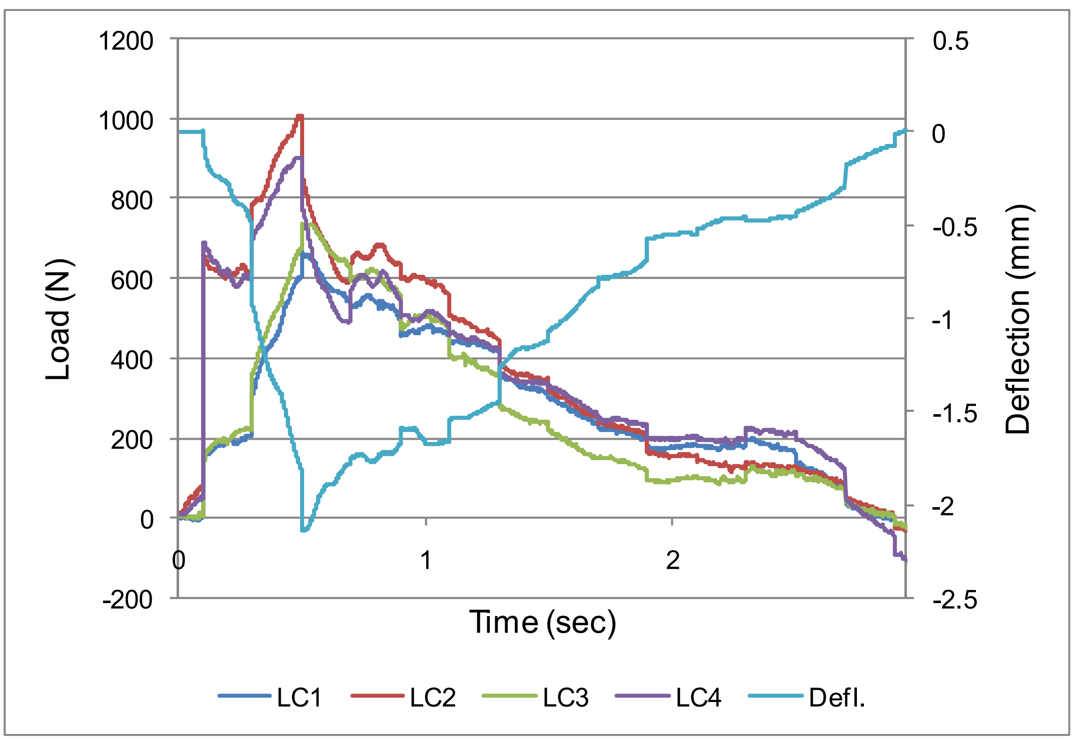

Figure B8: Load and deflection versus time for 30 cm wave lab trial, 90-1.1-WO-NF-E

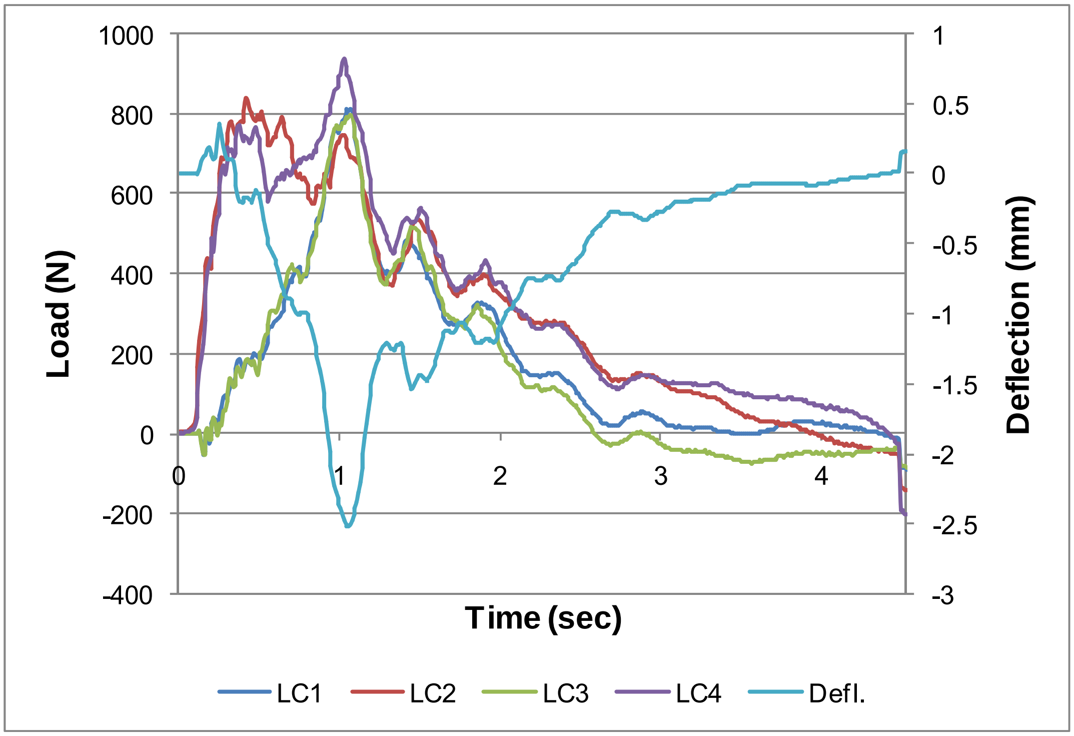

Figure B9: Load and deflection versus time for 40 cm wave lab trial, 90-1.1-WO-NF-E

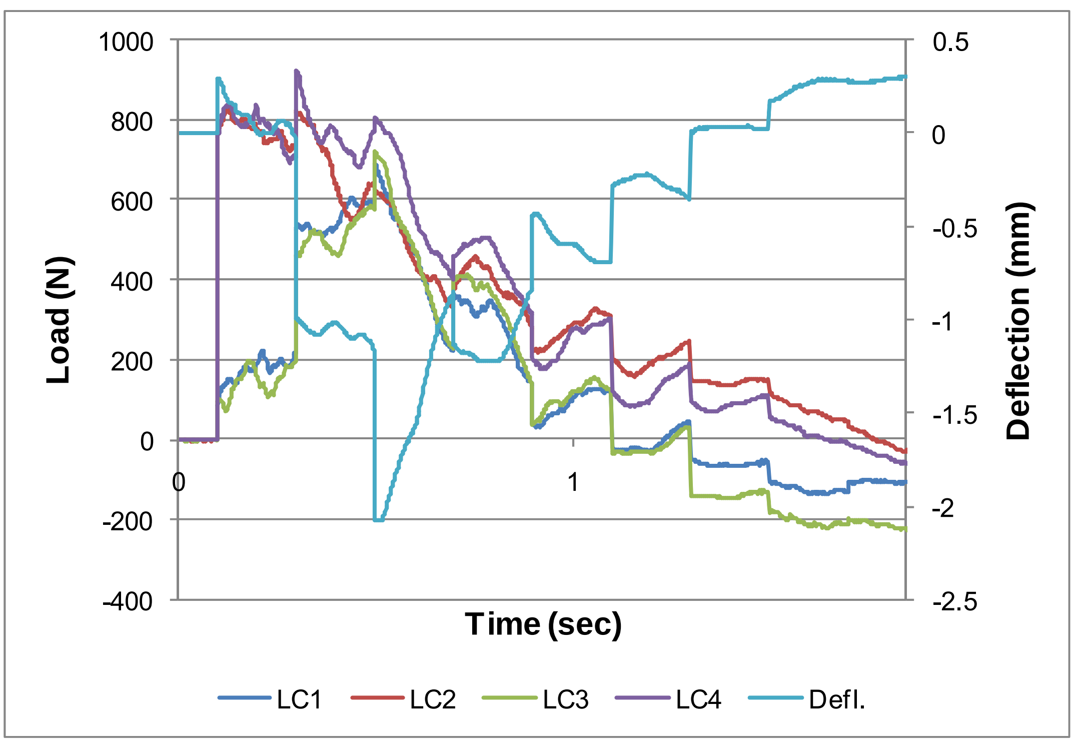

Figure B10: Load and deflection versus time for 50 cm wave lab trial, 90-1.1-WO-NF-E

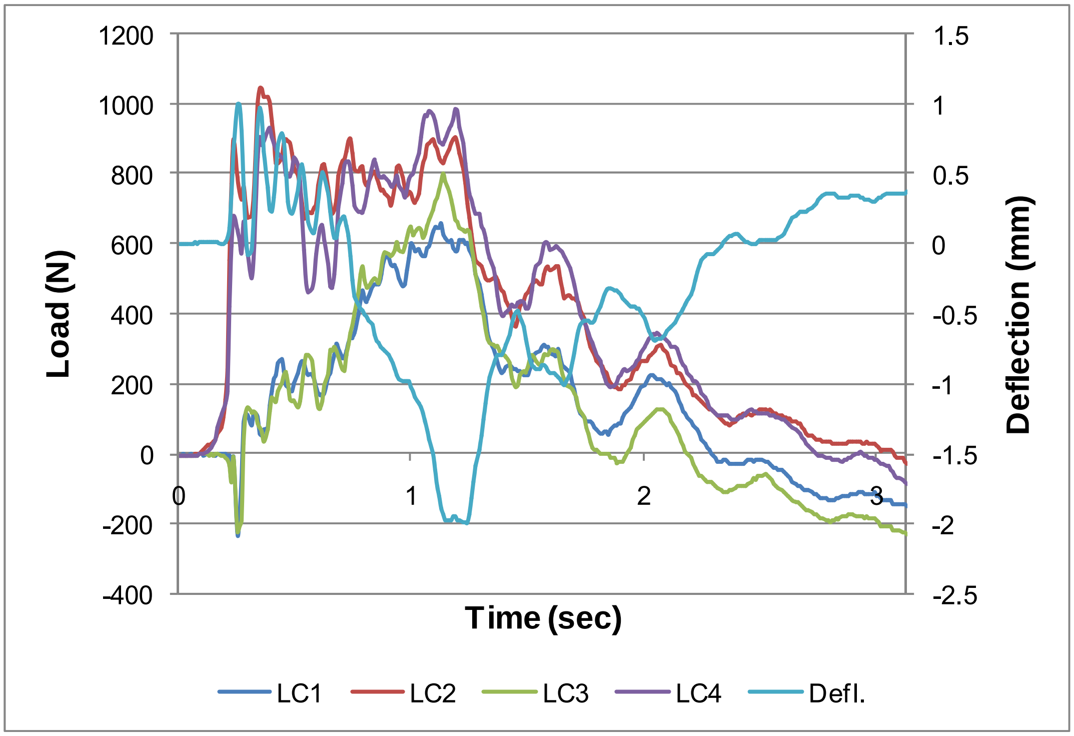

Figure B11: Load and deflection versus time for 60 cm wave lab trial, 90-1.1-WO-NF-E

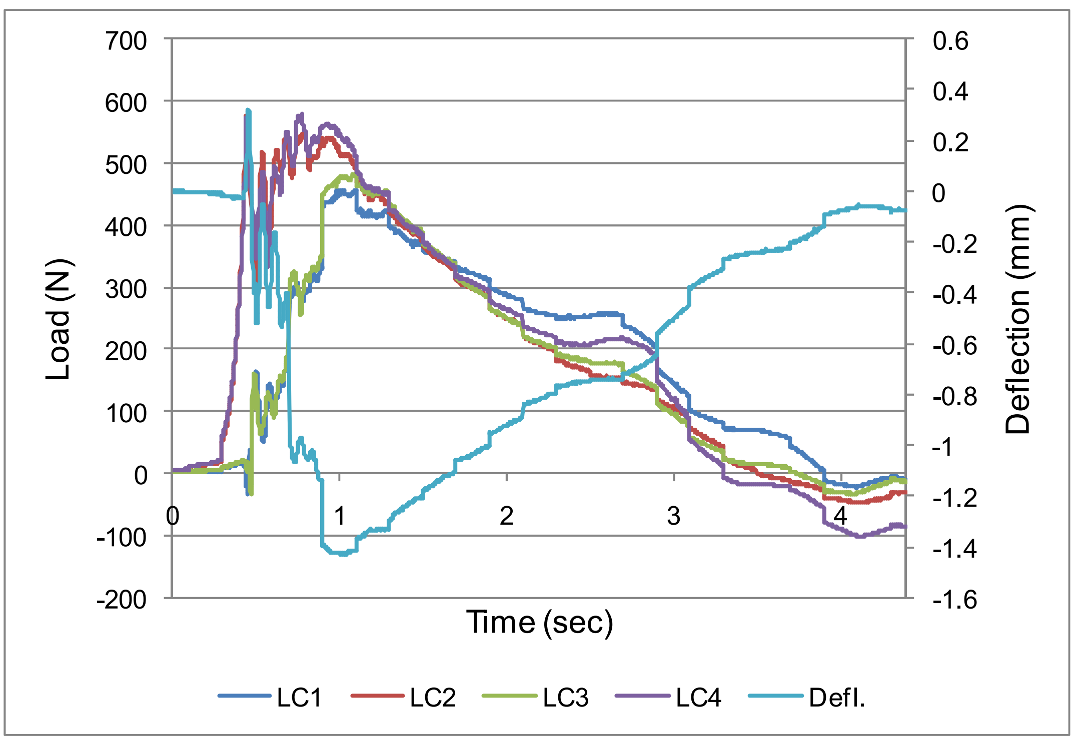

Figure B12: Load and deflection versus time for 10 cm wave lab trial, 90-1.1-WC-NF-E

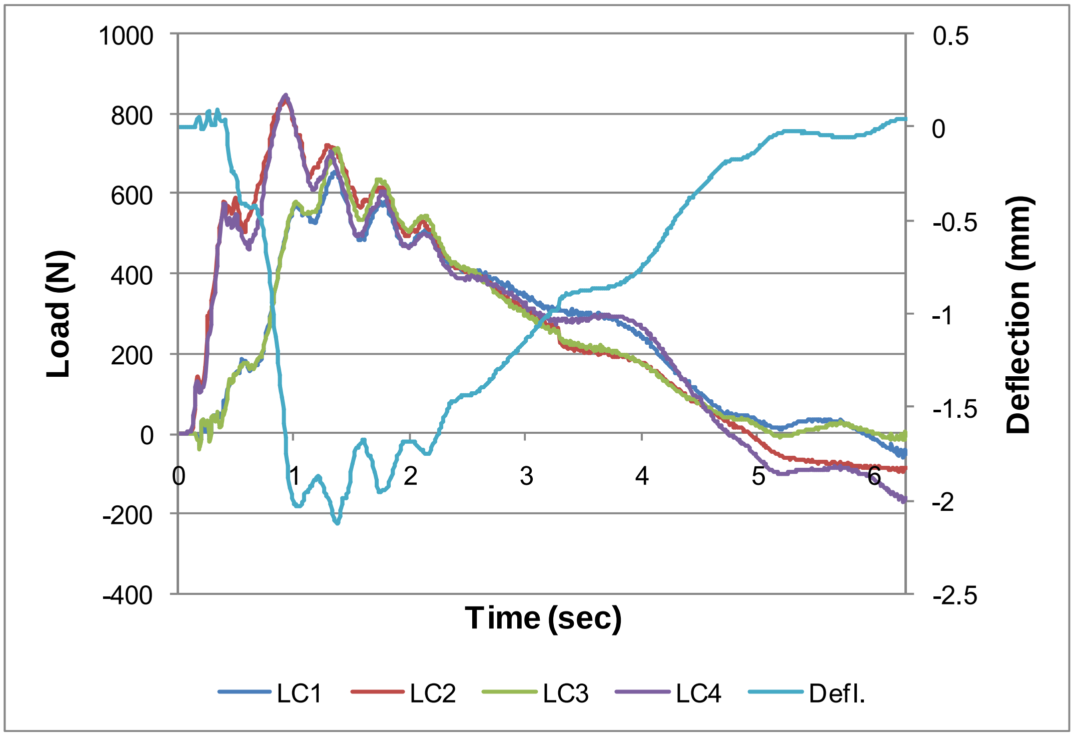

Figure B13: Load and deflection versus time for 20 cm wave lab trial, 90-1.1-WC-NF-E

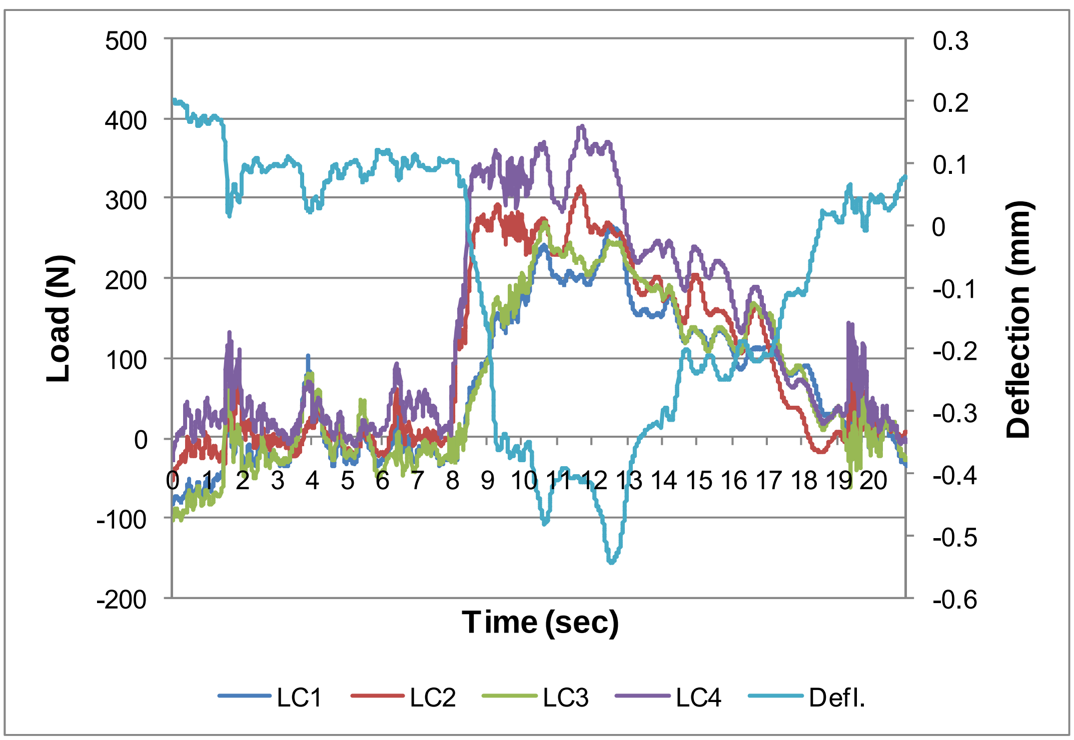

Figure B14: Load and deflection versus time for 40 cm wave lab trial, 90-1.1-WC-NF-E

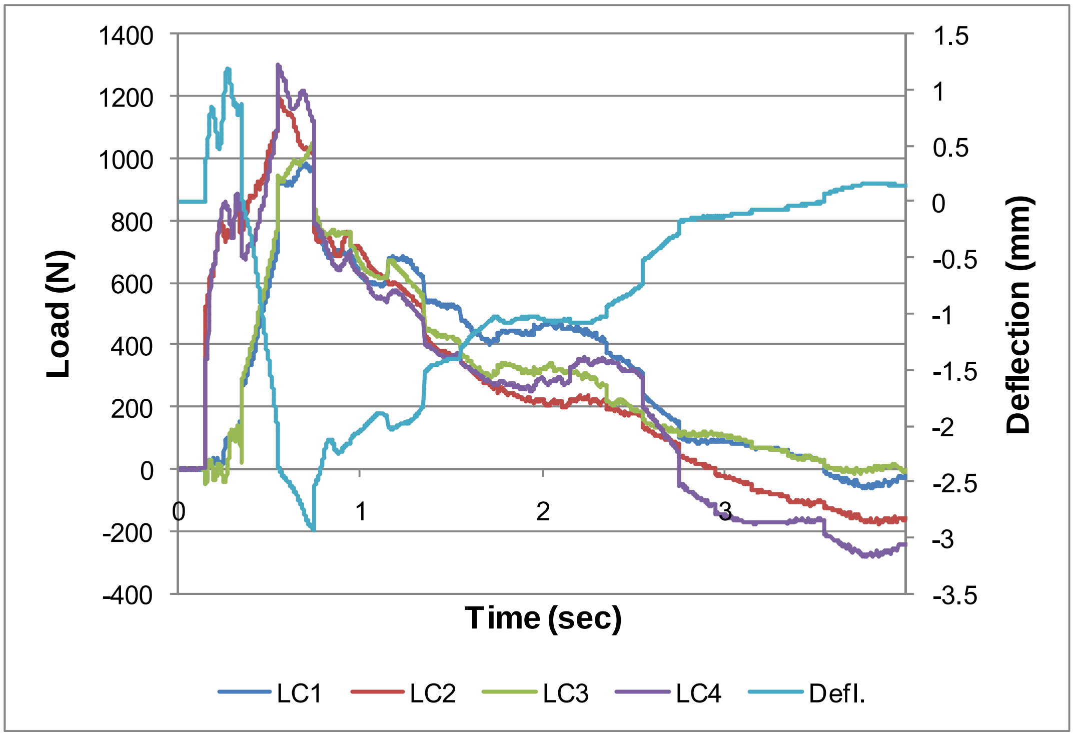

Figure B15: Load and deflection versus time for 50 cm wave lab trial, 90-1.1-WC-NF-E

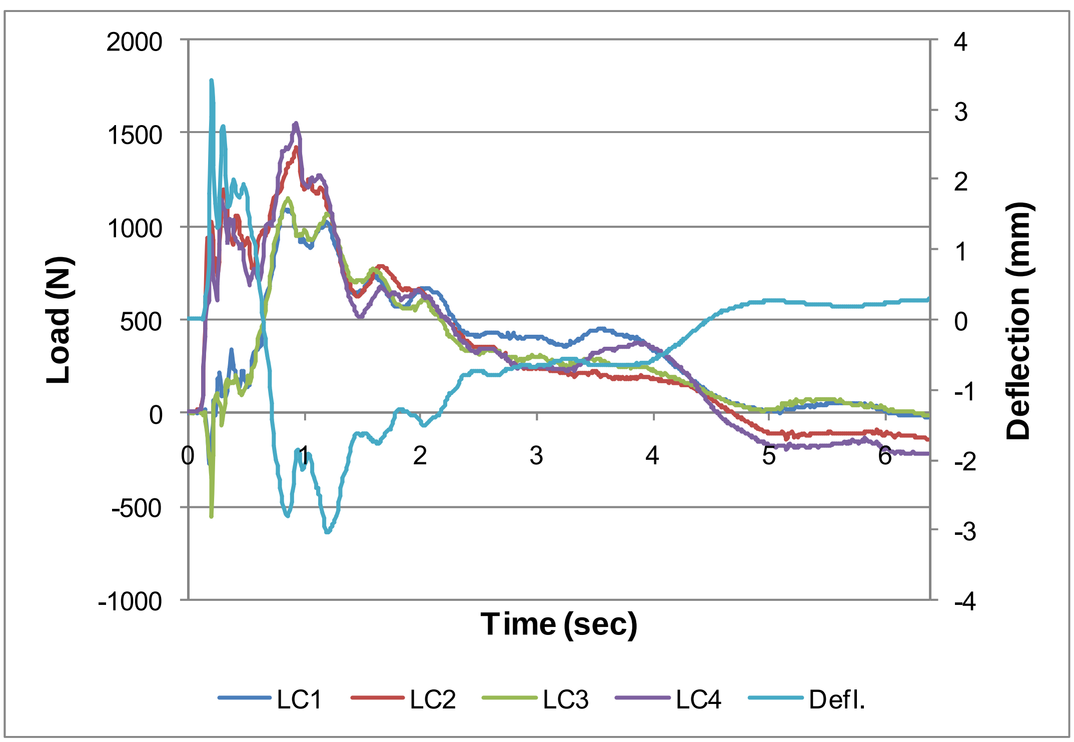

Figure B16: Load and deflection versus time for 60 cm wave lab trial, 90-1.1-WC-NF-E

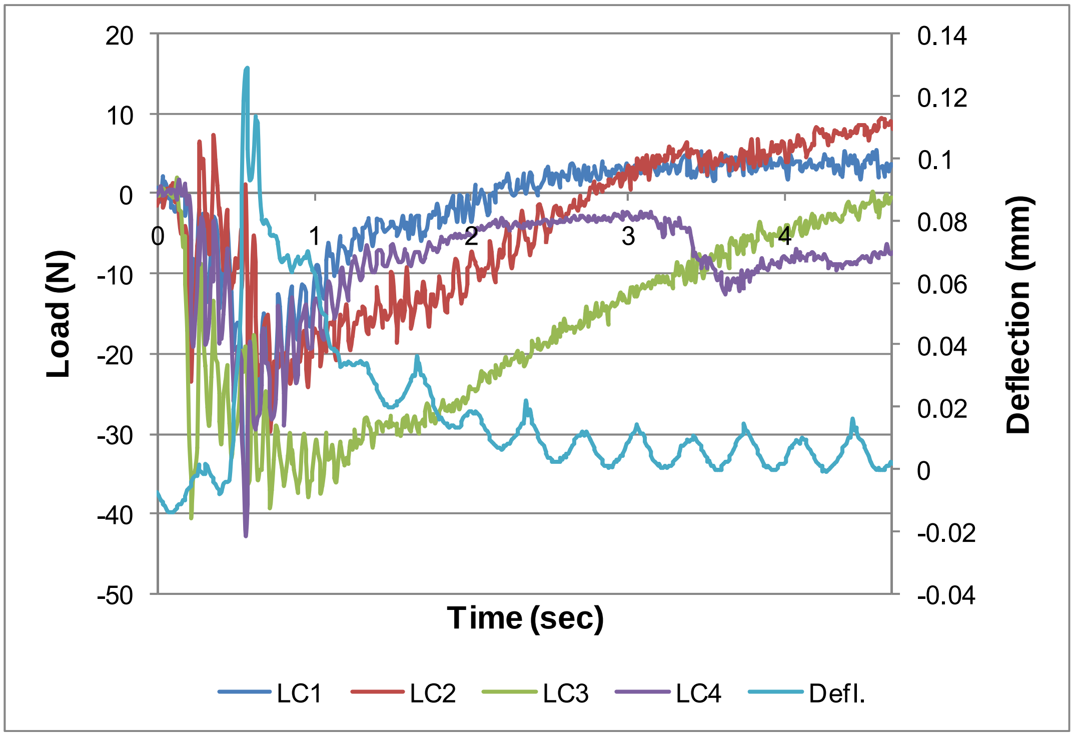

Figure B17: Load and deflection versus time for 10 cm wave lab trial, 0-1.0-WC-F-NE

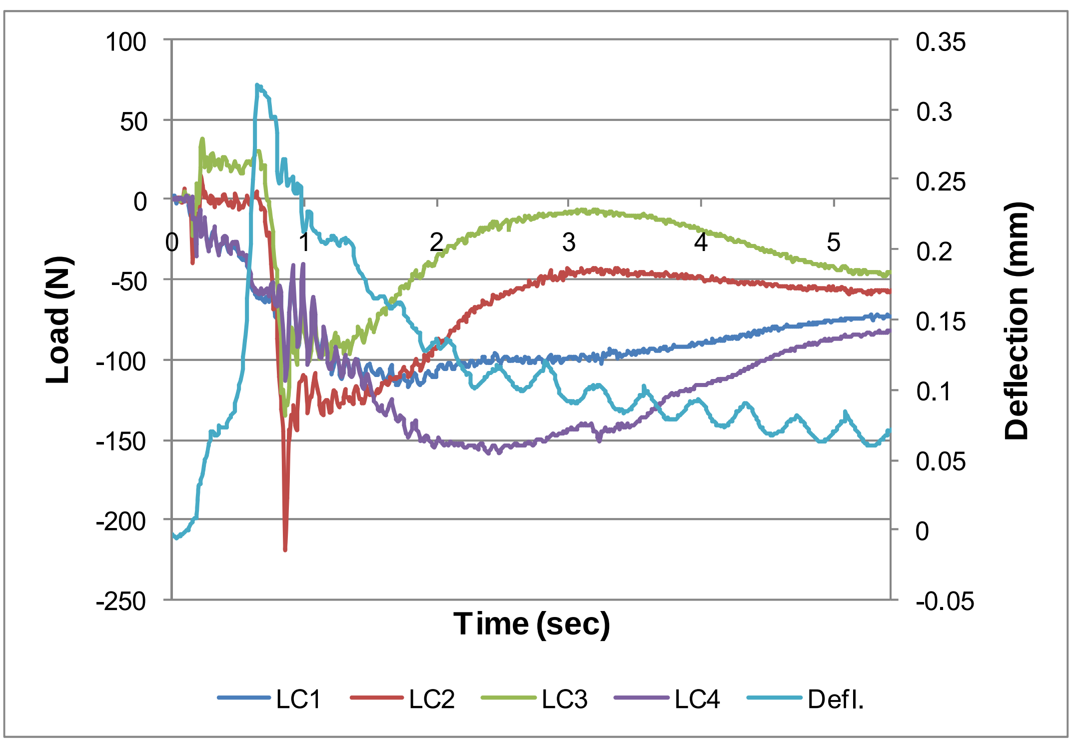

Figure B18: Load and deflection versus time for 20 cm wave lab trial, 0-1.0-WO-F-NE

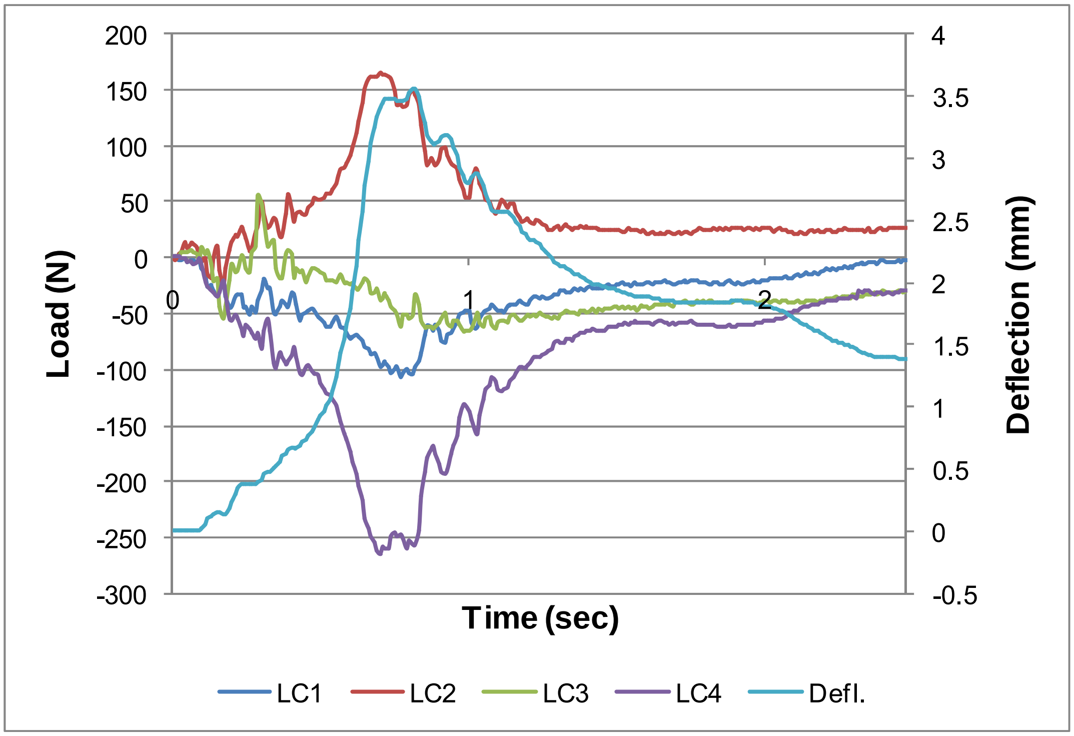

Figure B19: Load and deflection versus time for 30 cm wave lab trial, 0-1.0-WC-F-NE

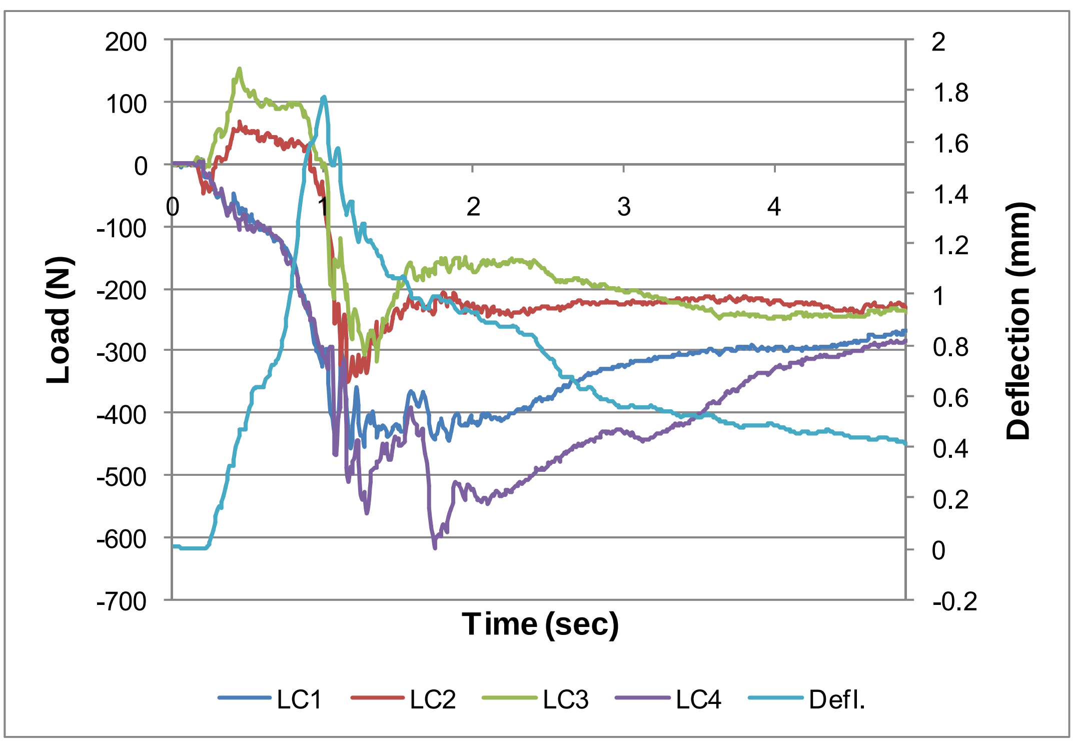

Figure B20: Load and deflection versus time for 40 cm wave lab trial, 0-1.0-WO-F-NE

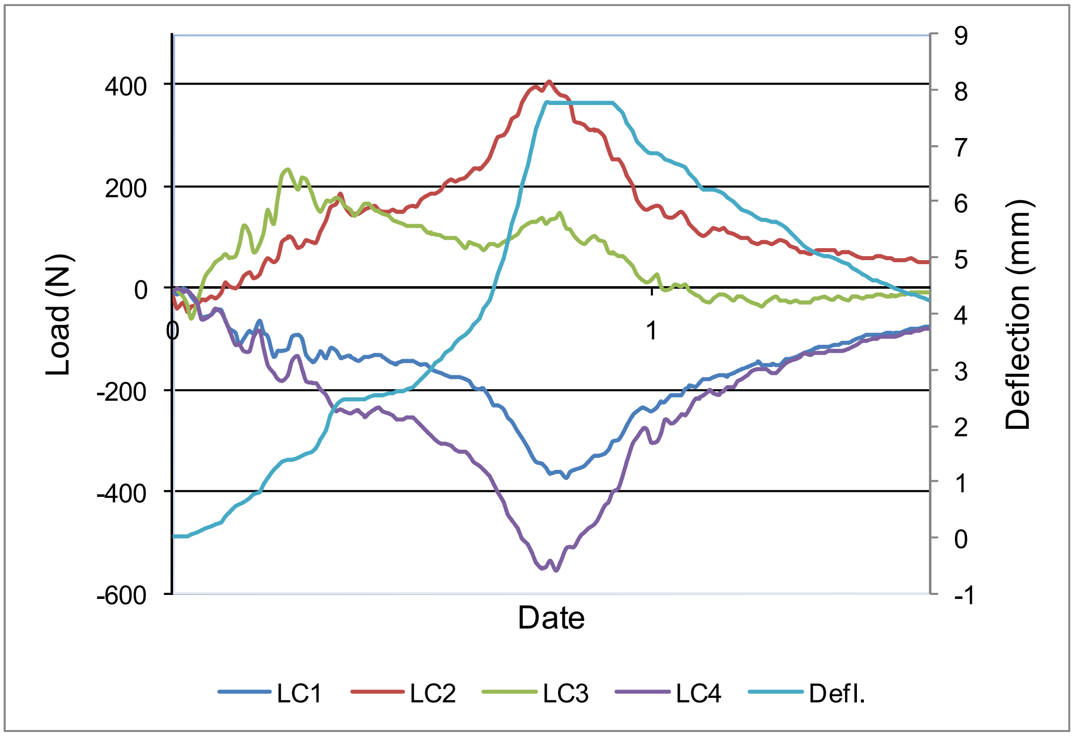

Figure B21: Load and deflection versus time for 50 cm wave lab trial, 0-1.0-WC-F-NE

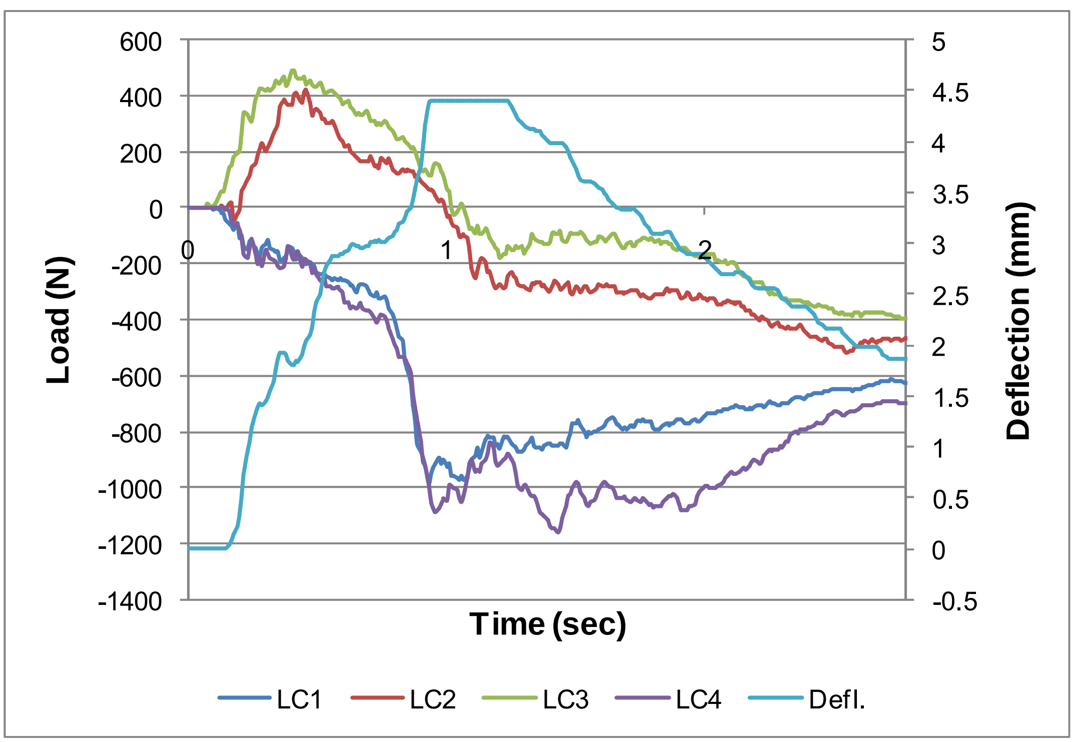

Figure B22: Load and deflection versus time for 60 cm wave lab trial, 0-1.0-WO-F-NE

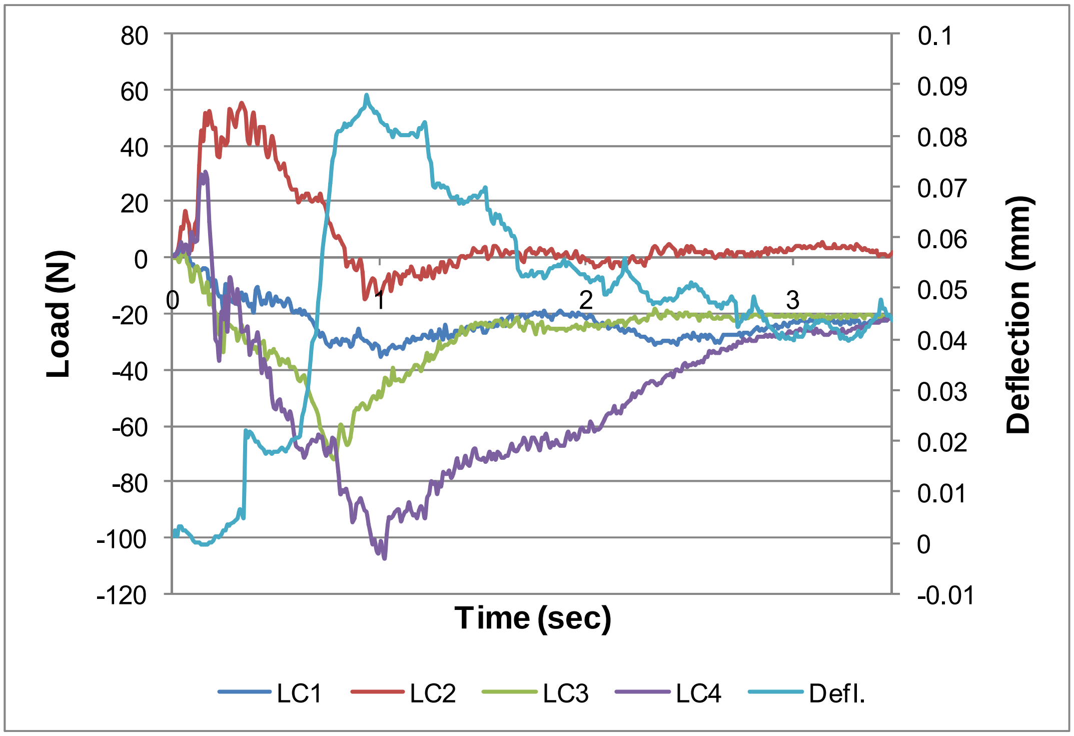

Figure B23: Load and deflection versus time for 40 cm wave lab trial, 90-1.0-WC-F-NE

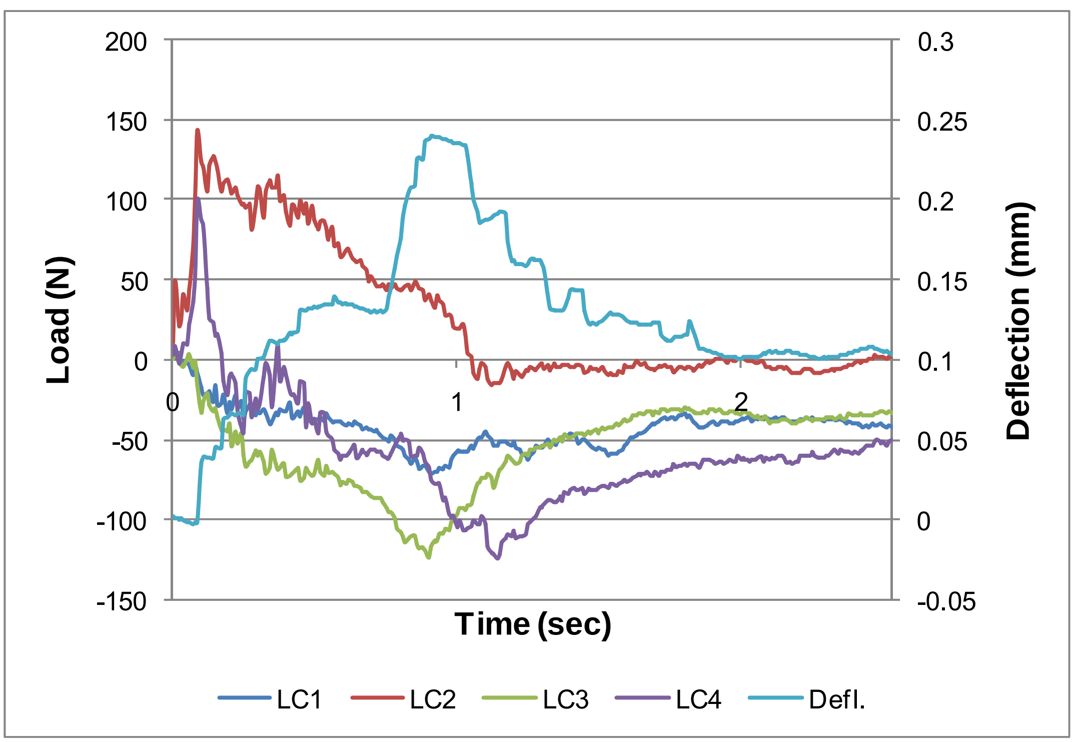

Figure B24: Load and deflection versus time for 60 cm wave lab trial, 90-1.0-WC-F-NE

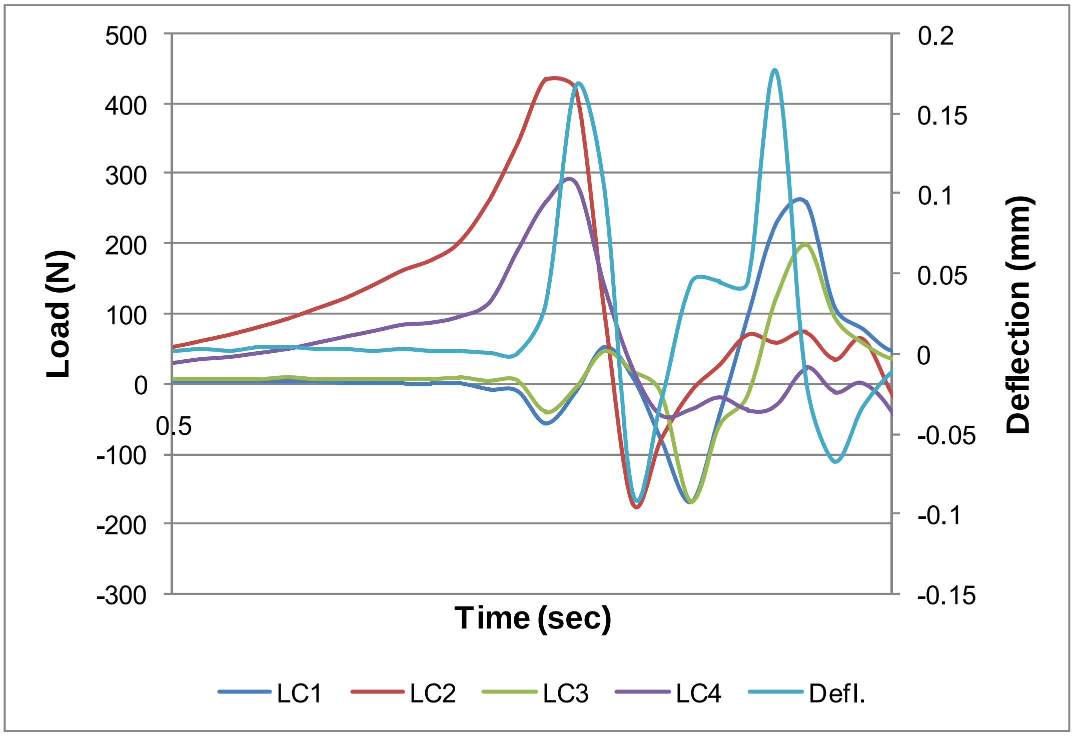

Figure B25: Load and deflection versus time for 10 cm wave lab trial, 90-1.1-WC-F-NE

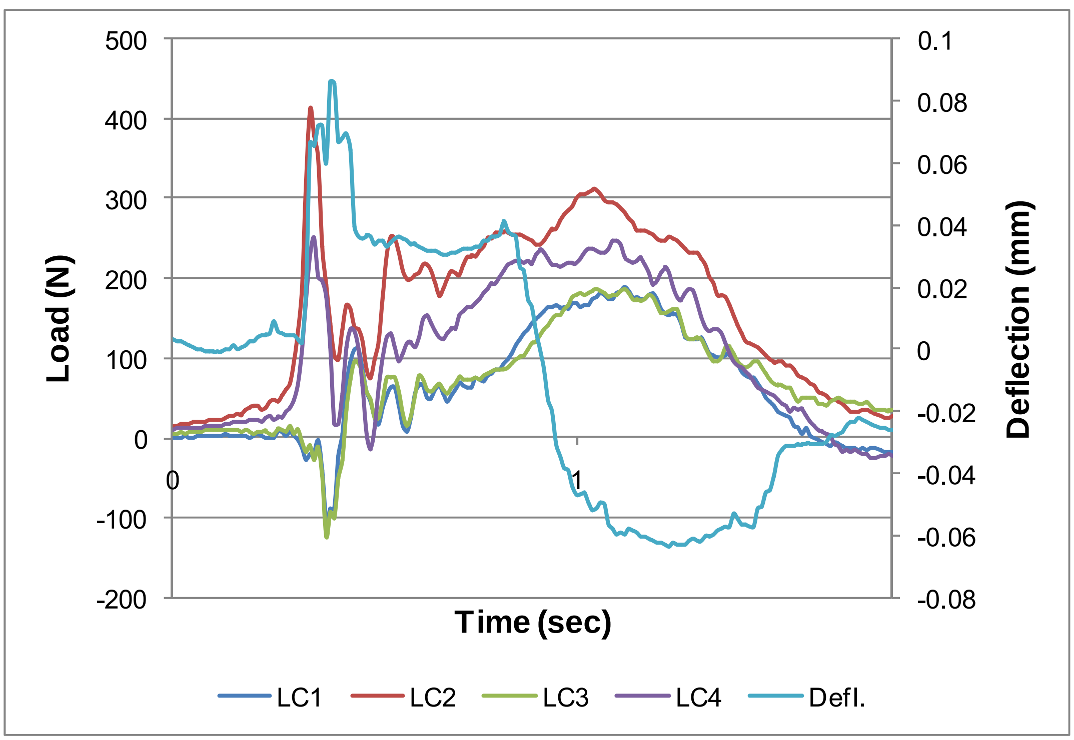

Figure B26: Load and deflection versus time for 12 cm wave lab trial, 90-1.1-WC-F-NE

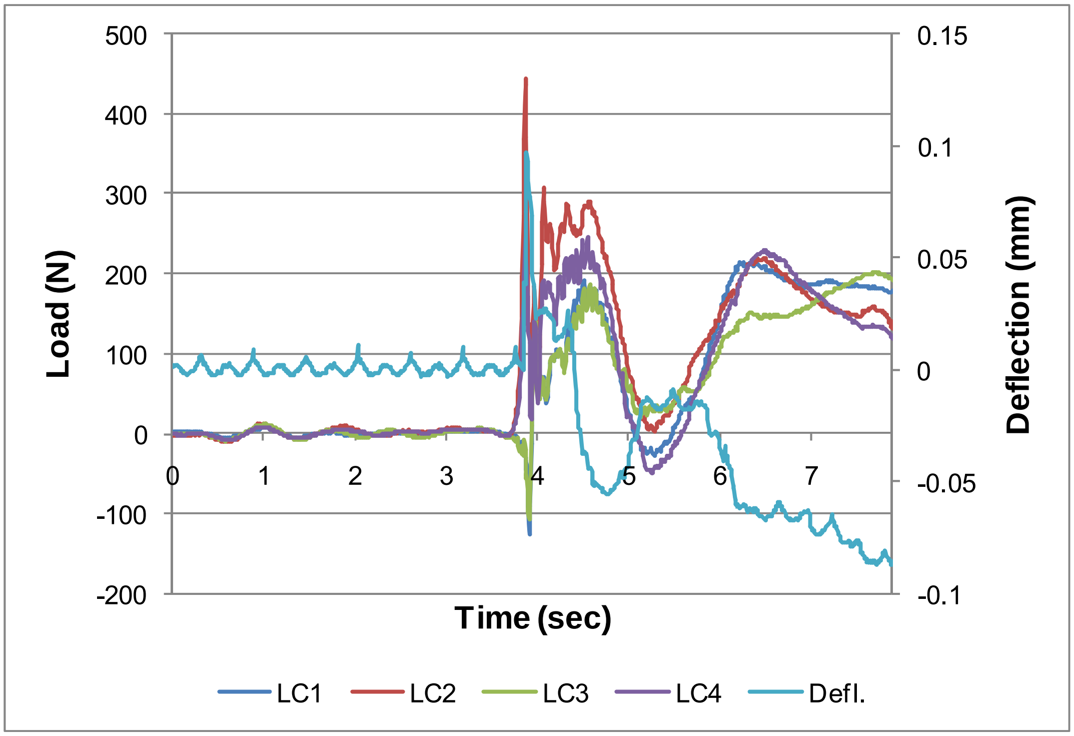

Figure B27: Load and deflection versus time for 15 cm wave lab trial, 90-1.1-WC-F-NE

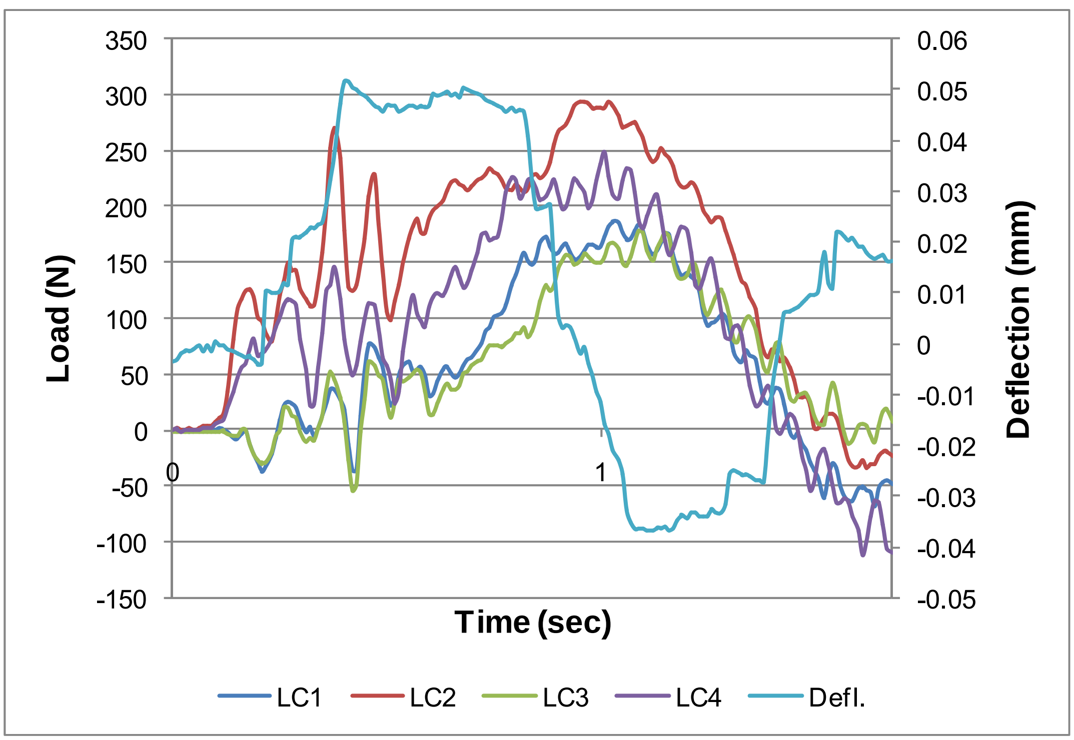

Figure B28: Load and deflection versus time for 20 cm wave lab trial, 90-1.1-WC-F-NE

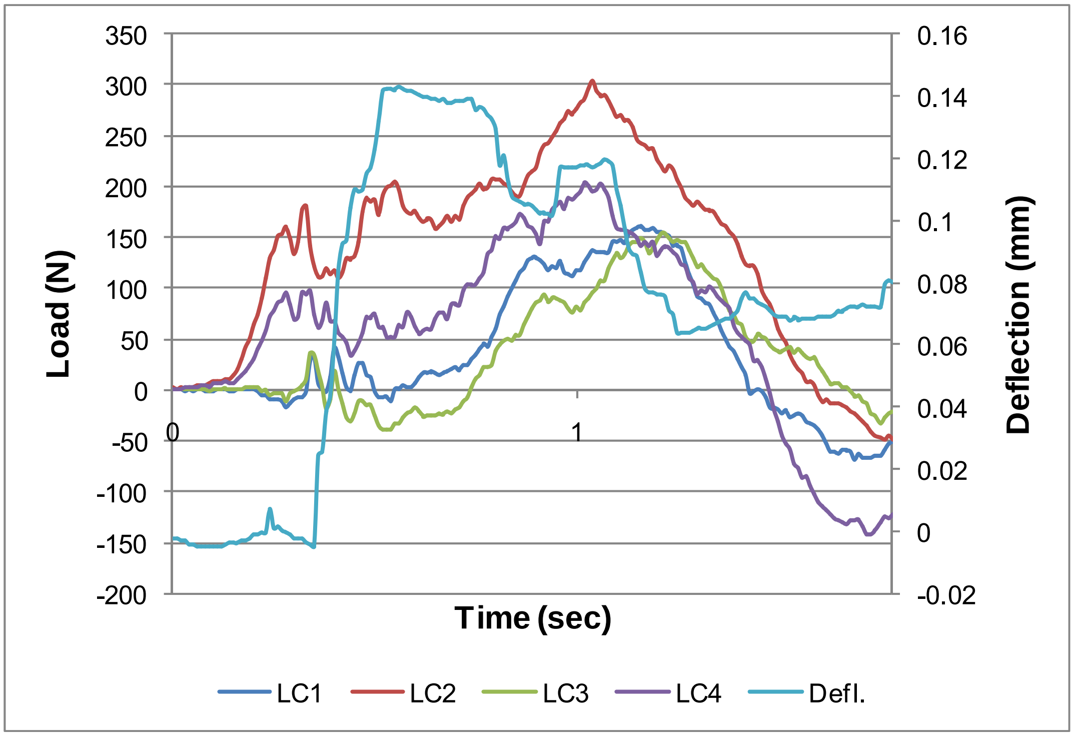

Figure B29: Load and deflection versus time for 30 cm wave lab trial, 90-1.1-WC-F-NE

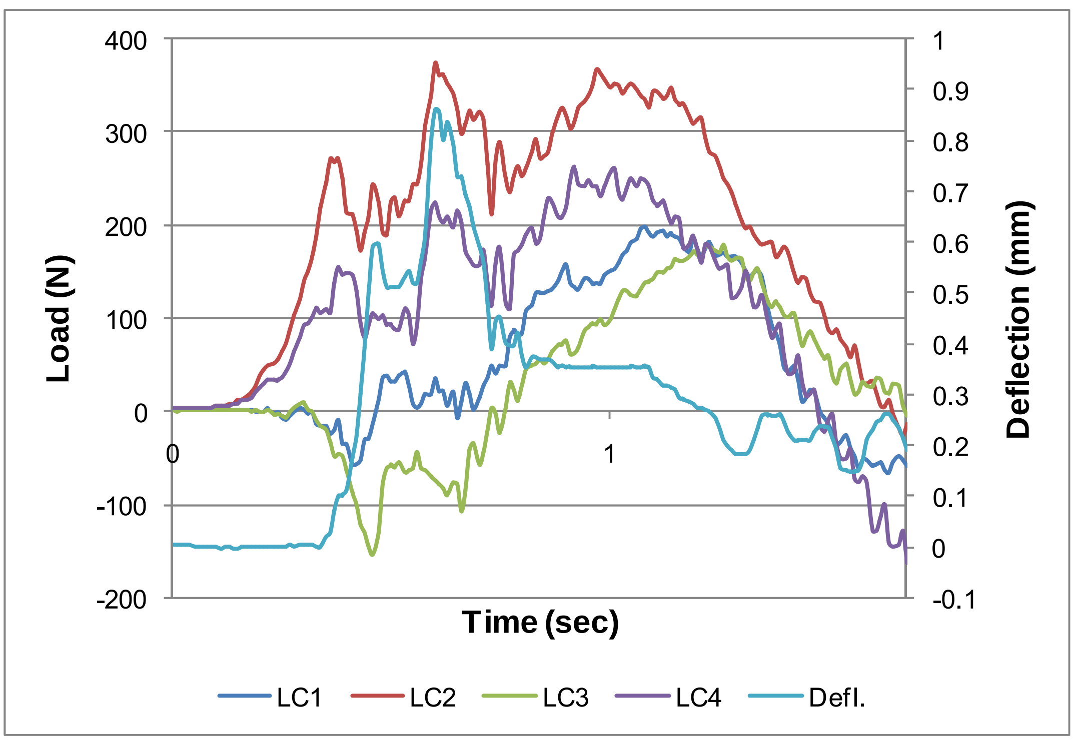

Figure B30: Load and deflection versus time for 40 cm wave lab trial, 90-1.1-WC-F-NE

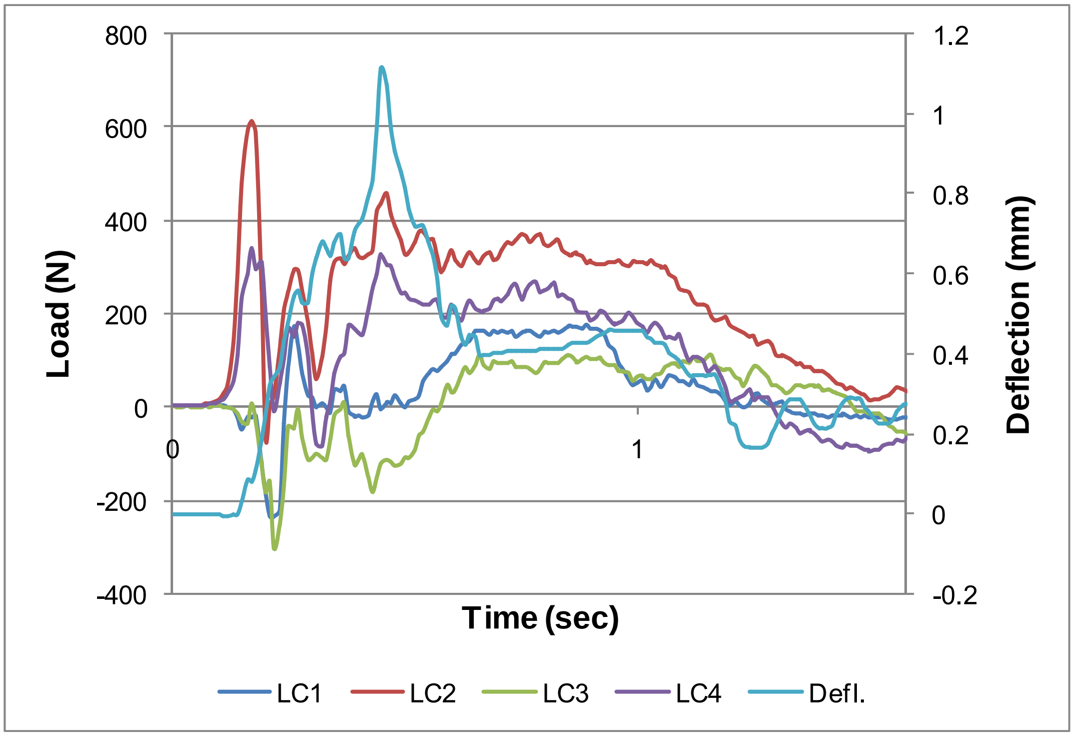

Figure B31: Load and deflection versus time for 50 cm wave lab trial, 90-1.1-WC-F-NE

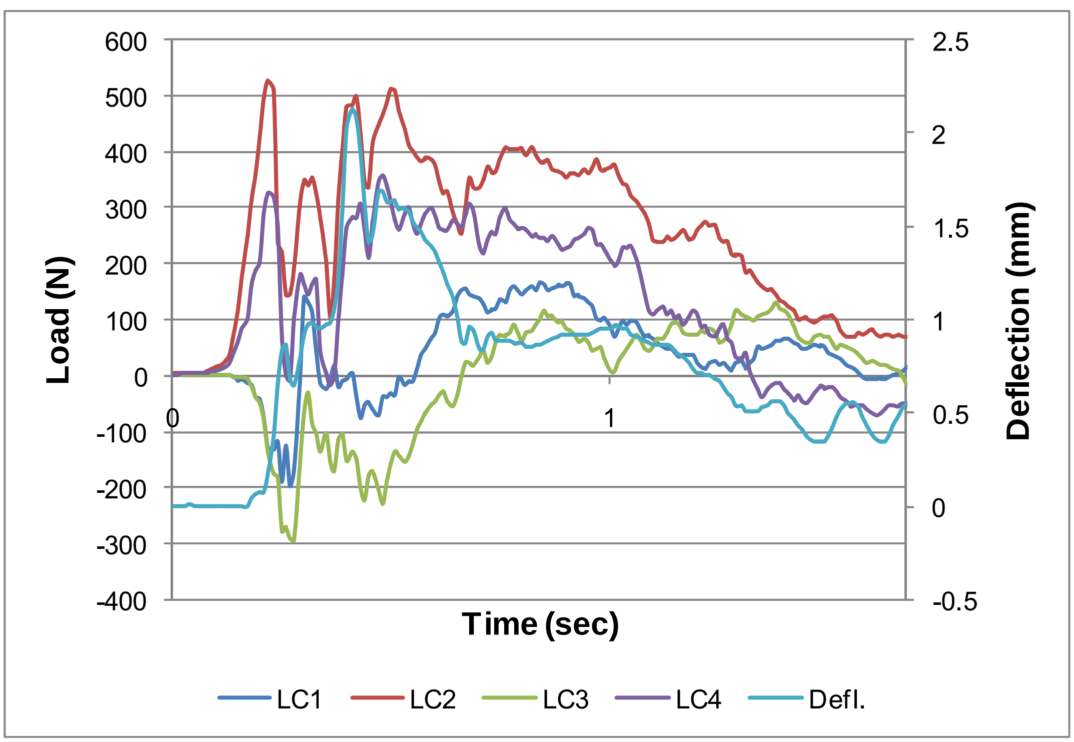

Figure B32: Load and deflection versus time for 60 cm wave lab trial, 90-1.1-WC-F-NE

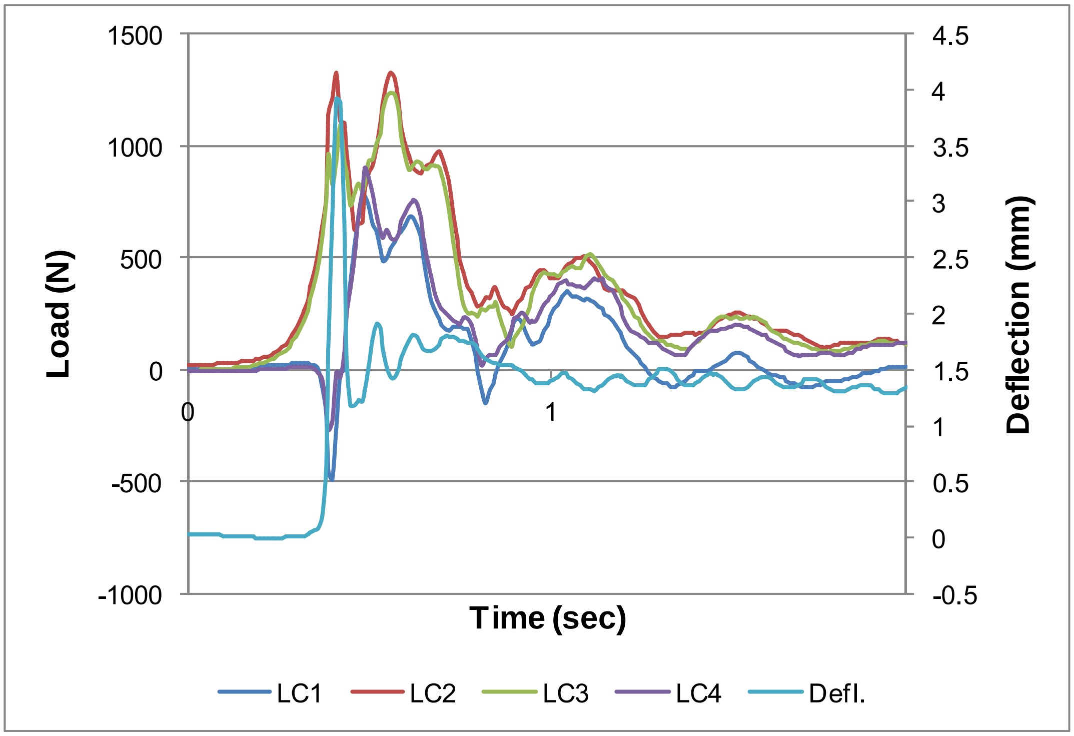

Figure B33: Load and deflection versus time for 10 cm wave lab trial, 0-1.1-WC-F-NE

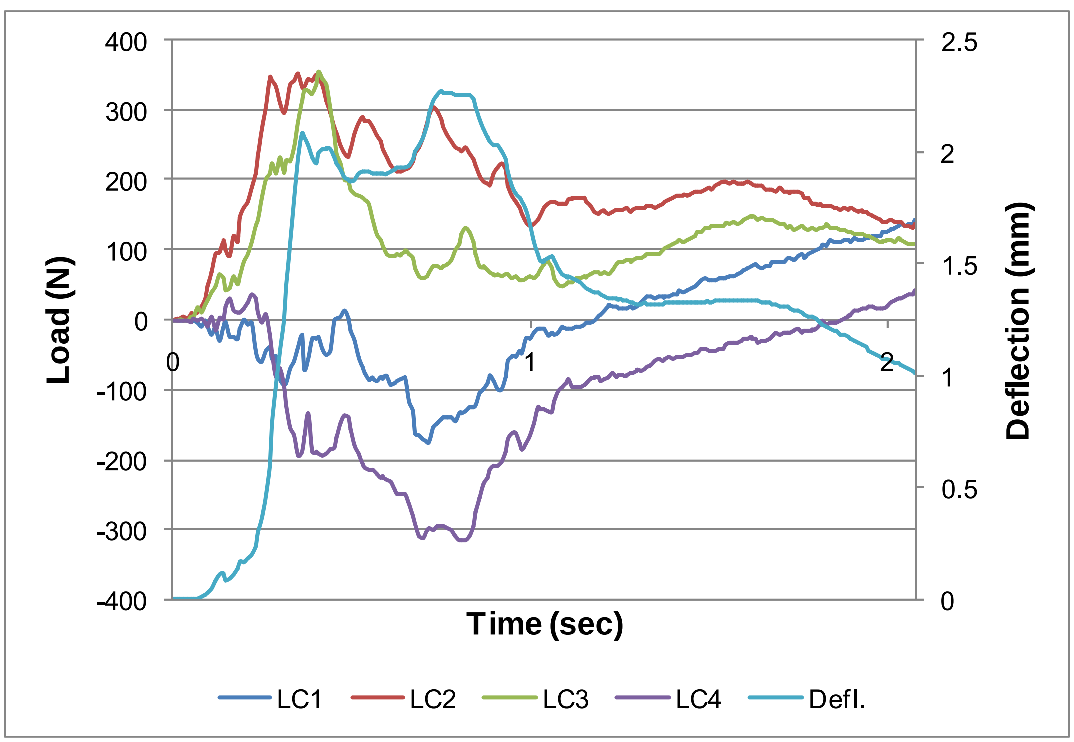

Figure B34: Load and deflection versus time for 20 cm wave lab trial, 0-1.1-WC-F-NE

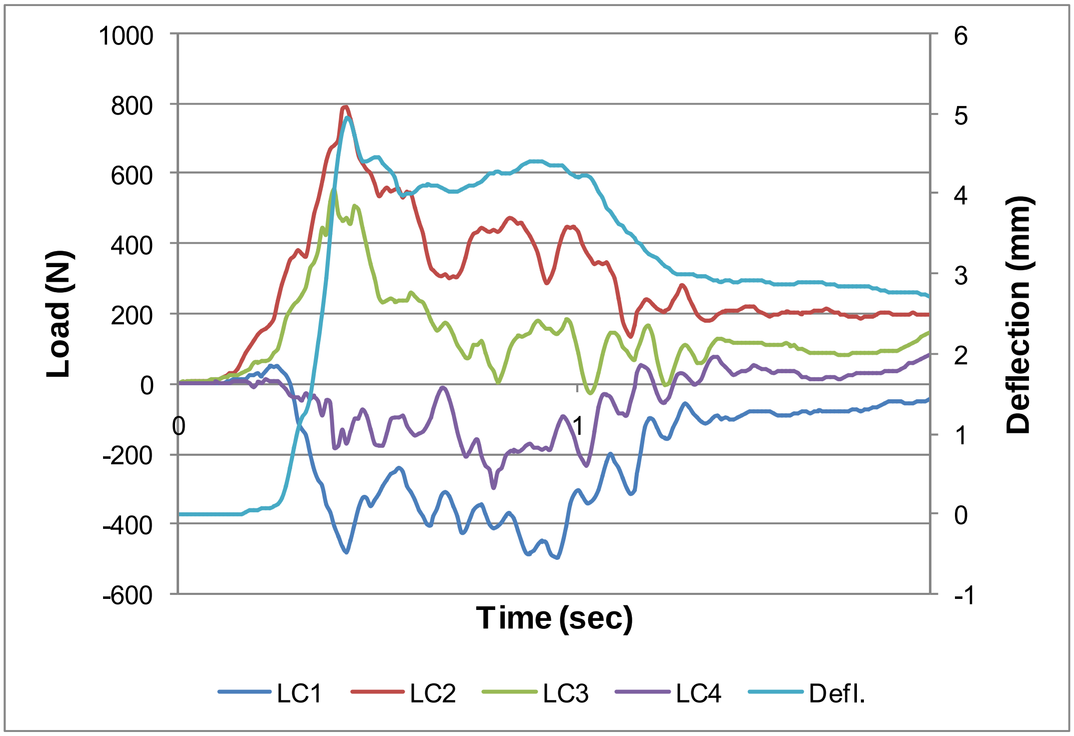

Figure B35: Load and deflection versus time for 30 cm wave lab trial, 0-1.1-WC-F-NE

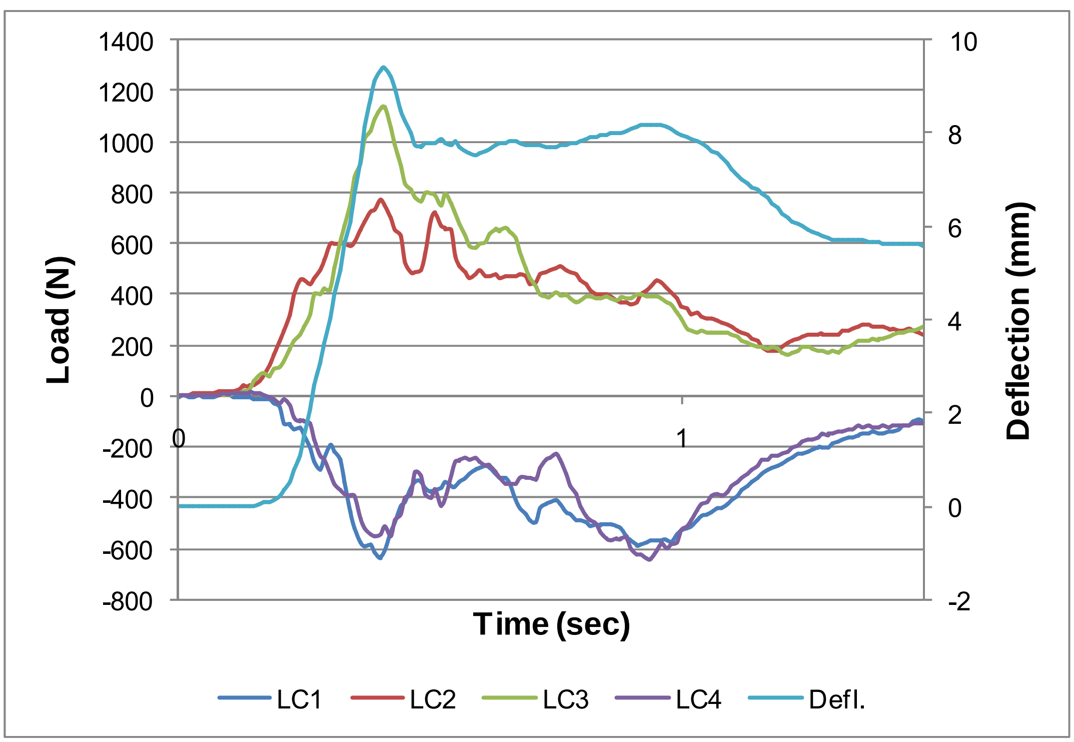

Figure B36: Load and deflection versus time for 40 cm wave lab trial, 0-1.1-WC-F-NE

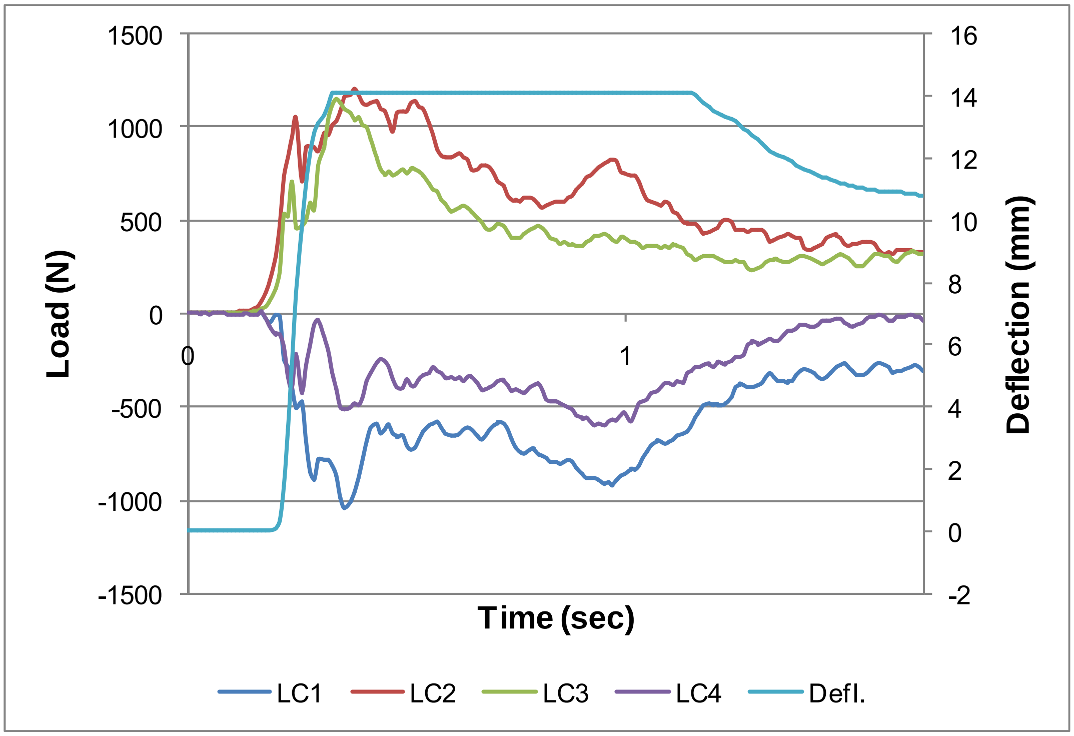

Figure B37: Load and deflection versus time for 50 cm wave lab trial, 0-1.1-WC-F-NE

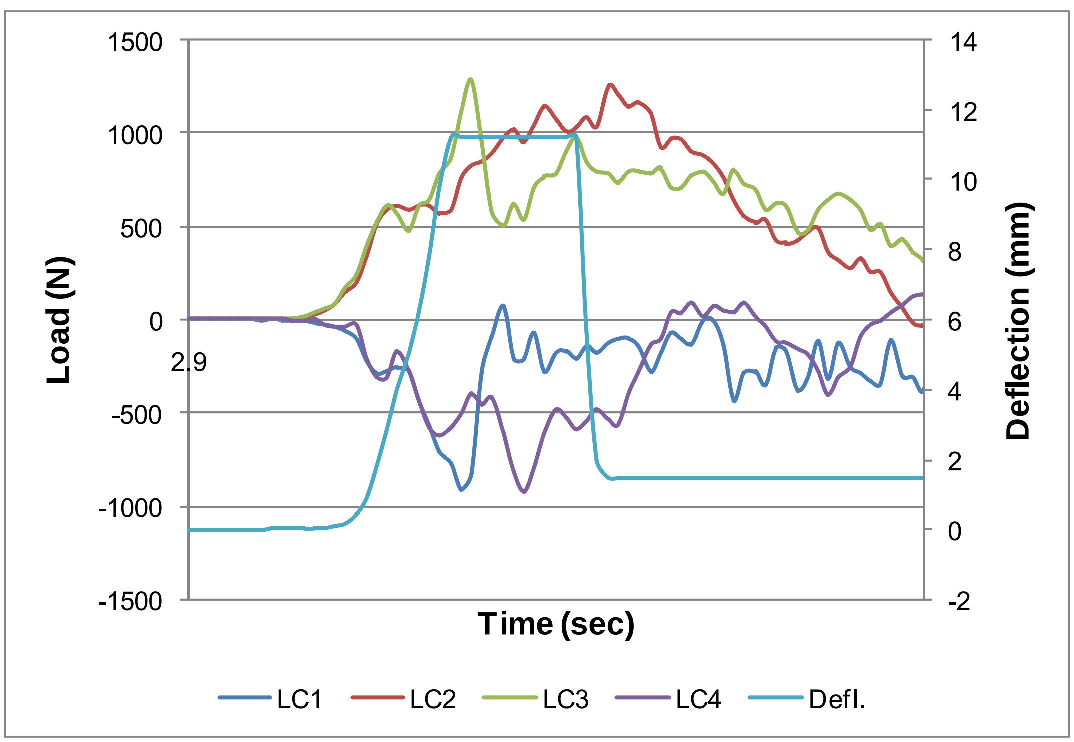

Figure B38: Load and deflection versus time for 60 cm wave lab trial, 0-1.1-WC-F-NE

Appendix D – Push Over Tests

Table C1: Averaged data from 0° orientation push over tests

Test	Slope	R^2	Max Load (N)	Rate of Loading (N/sec.)
0-DL-18-2	2.19	0.990	1591	60.6
0-DL-27-2	1.49	0.996	1420	47.7
0-DL-36-2	1.25	0.998	1417	38.0
0-DL-43-1	1.11	1.000	1429	28.6
0-DL-43-2	1.10	0.999	1641	22.2
0-DL-43-3	1.10	1.000	1416	25.9
0-PLC-43-2	1.28	1.000	1219	8.1
0-PLL-43-1	1.37	0.998	1419	11.5
0-PLL-43-2	1.10	0.999	1252	22.1
0-PLL-43-3	1.15	1.000	1177	18.2
0-PLR-43-1	1.34	0.998	1440	14.0
0-PLR-43-2	1.33	0.999	1334	16.0
0-PLR-43-3	1.22	1.000	1158	16.2

Table C2: Averaged data from 90° orientation push over tests

Test	Slope	R^2	Max Load (N)	Rate of Loading (N/sec.)
90-DL-21-2	5.14	0.998	2836	69.0
90-DL-26-2	4.21	1.000	2467	60.9
90-DL-32-2	3.42	0.999	2097	47.2
90-DL-38-2	2.76	0.995	2047	40.9
90-DL-43-1	2.78	0.998	2194	40.6
90-DL-43-2	2.70	0.998	2392	38.4
90-DL-43-3	2.80	0.998	2306	40.0
90-PLC-43-1	2.41	1.000	1983	34.5
90-PLC-43-2	2.28	1.000	1911	30.9
90-PLC-43-3	2.29	1.000	2044	31.5
90-PLL-43-1	2.69	0.999	2126	49.0
90-PLL-43-2	2.64	1.000	2179	61.8
90-PLL-43-3	2.84	0.999	2335	41.5
90-PLR-43-1	2.59	0.997	2090	40.5
90-PLR-43-2	2.56	0.997	1971	39.8
90-PLR-43-3	2.66	0.999	2011	34.5

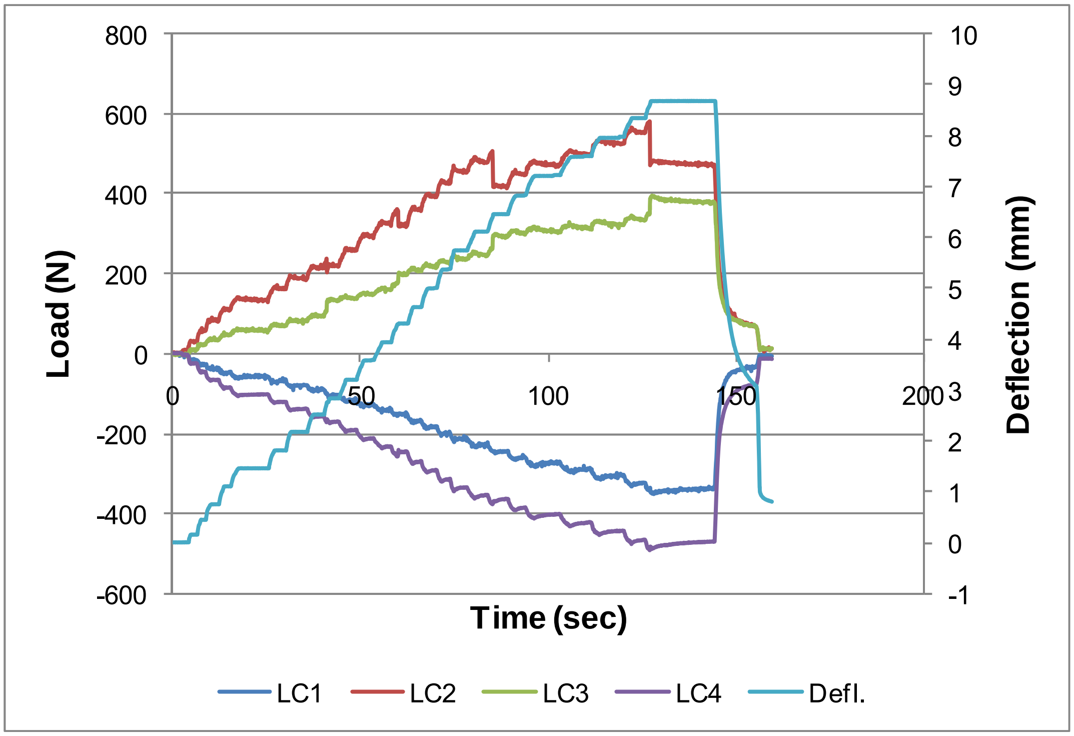

Figure C1: Load and deflection versus time for push over trial 0-DL-43-2

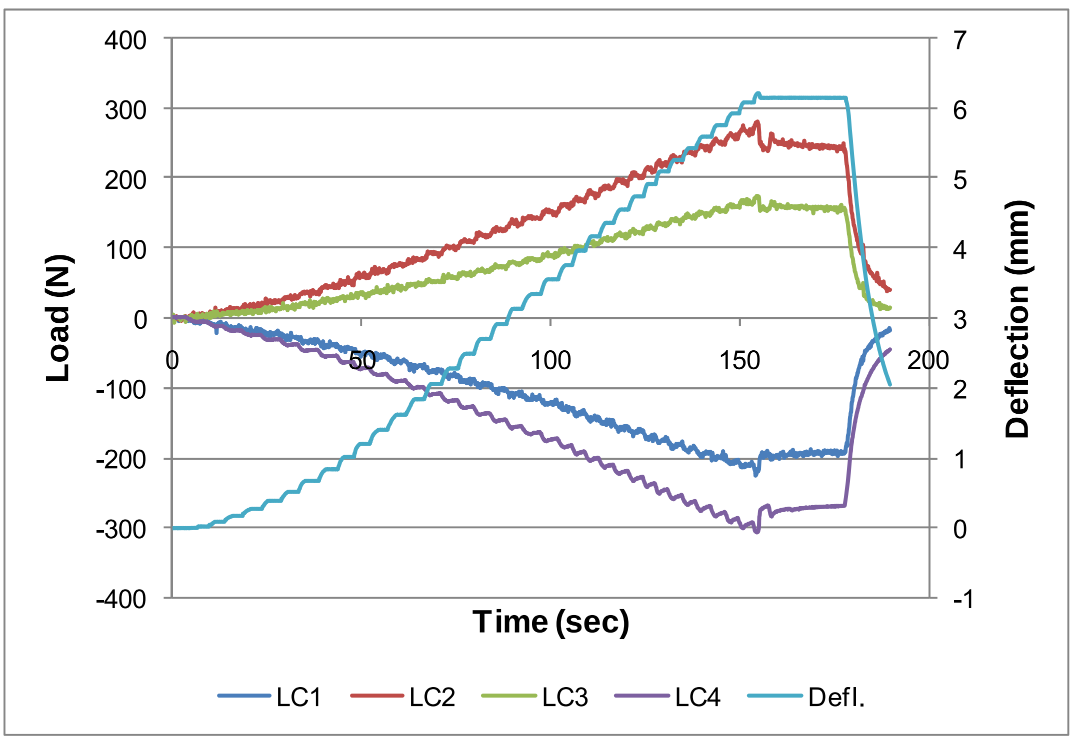

Figure C2: Load and deflection versus time for push over trial 0-PLC-43-2

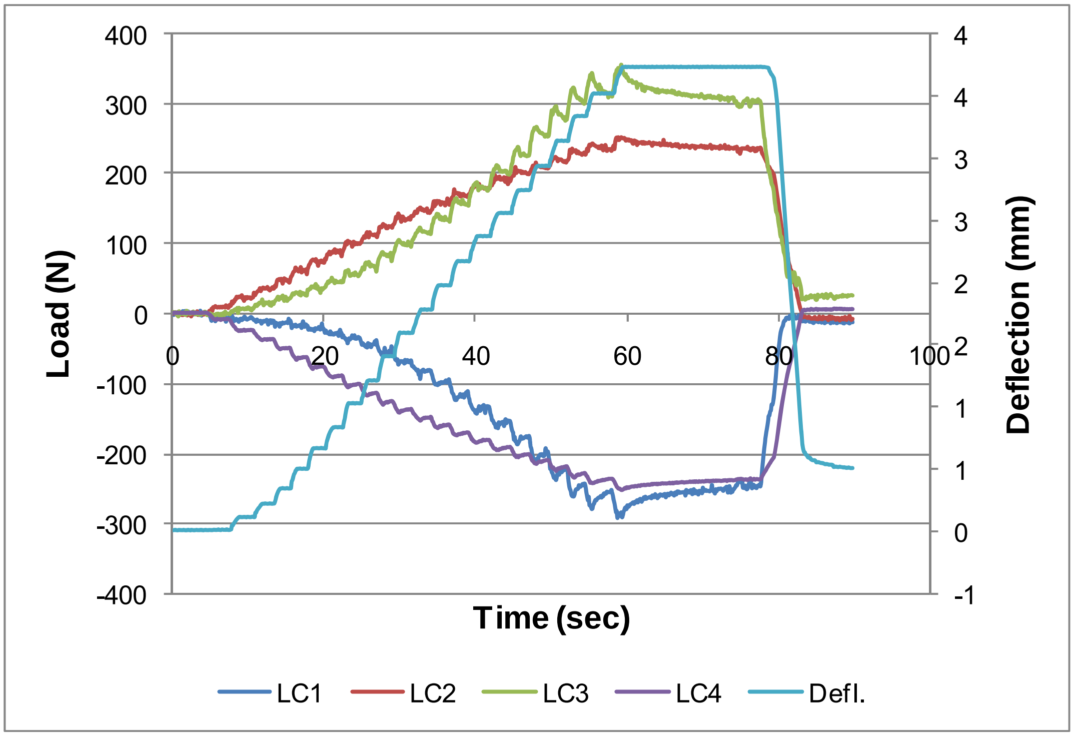

Figure C3: Load and deflection versus time for push over trial 0-PLL-43-2

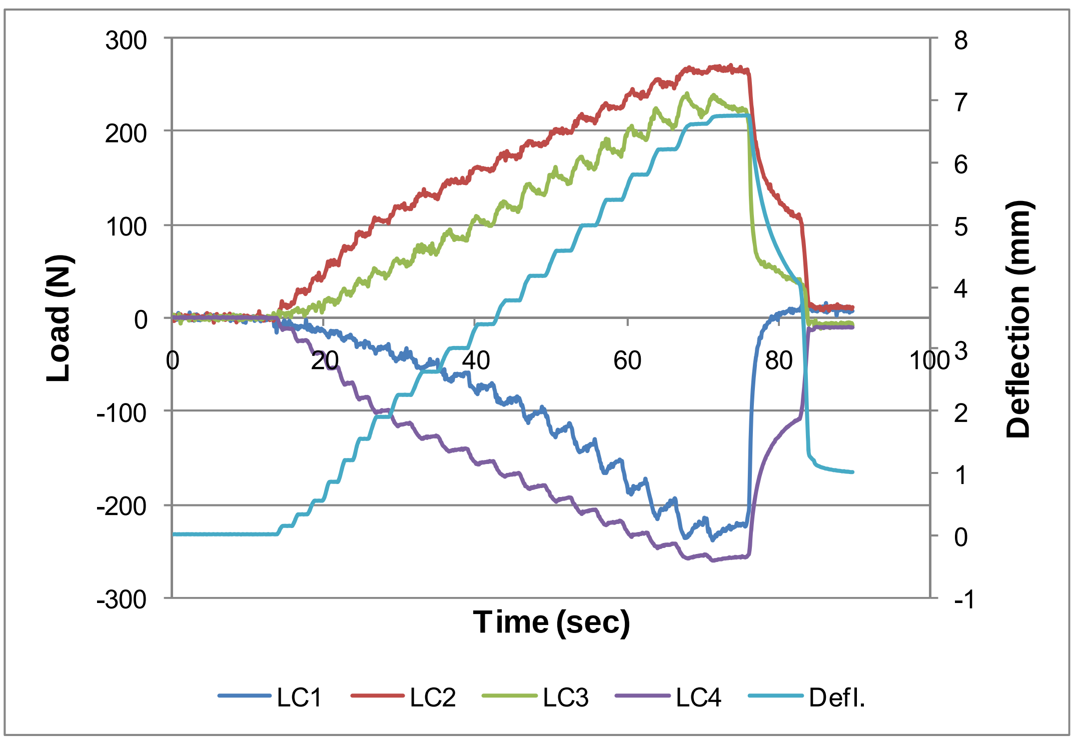

Figure C4: Load and deflection versus time for push over trial 0-PLL-43-3

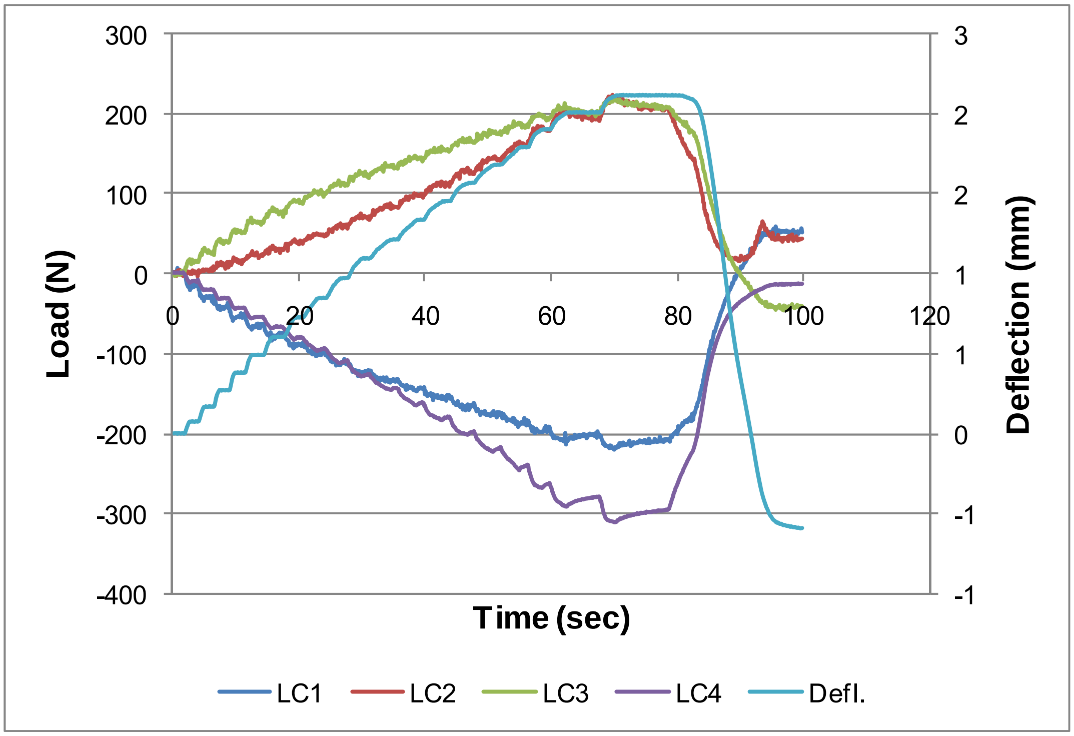

Figure C5: Load and deflection versus time for push over trial 0-PLR-43-3

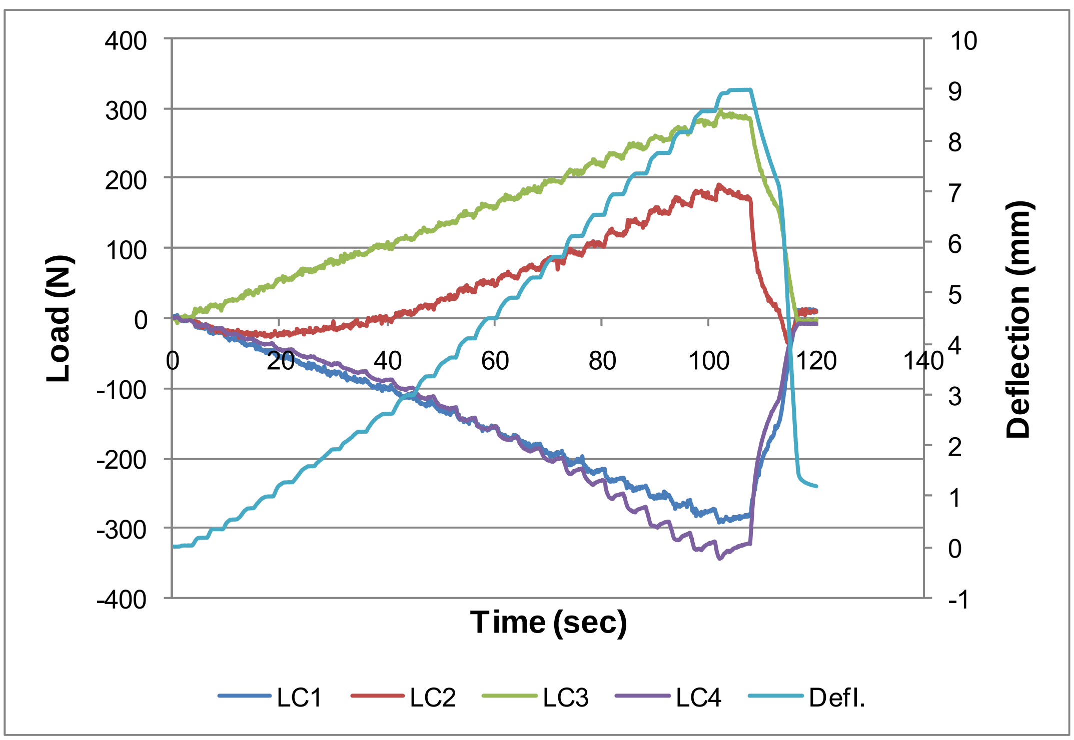

Figure C6: Load and deflection versus time for push over trial 0-PLR-43-1

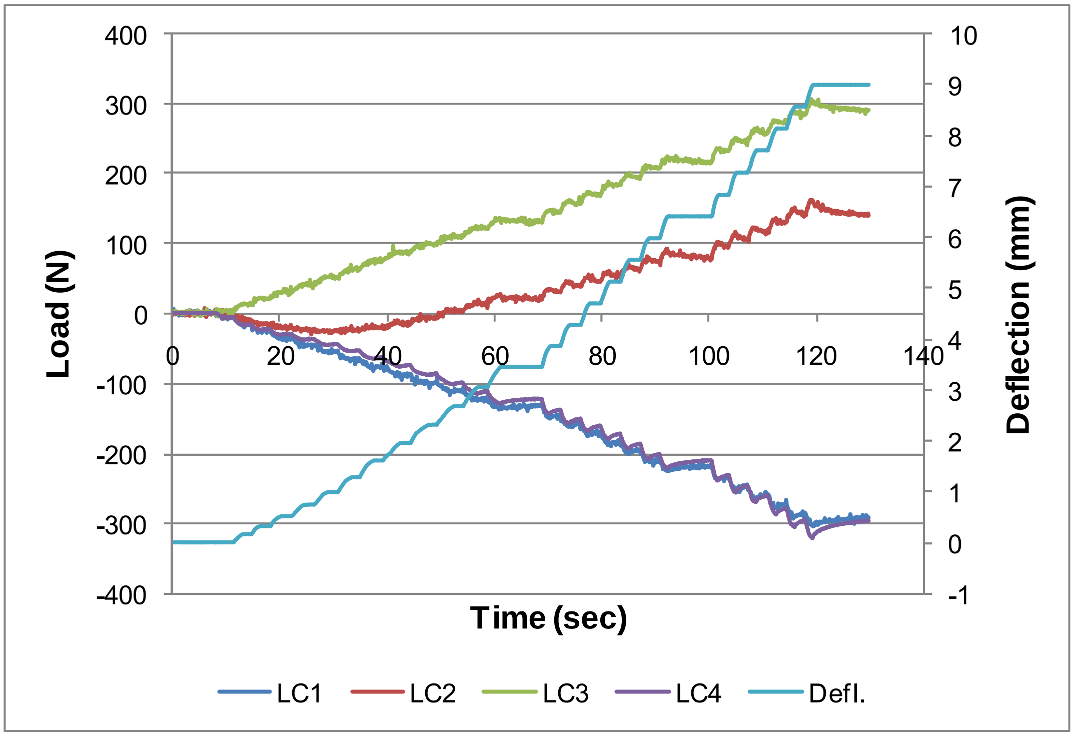

Figure C7: Load and deflection versus time for push over trial 0-PLL-43-1

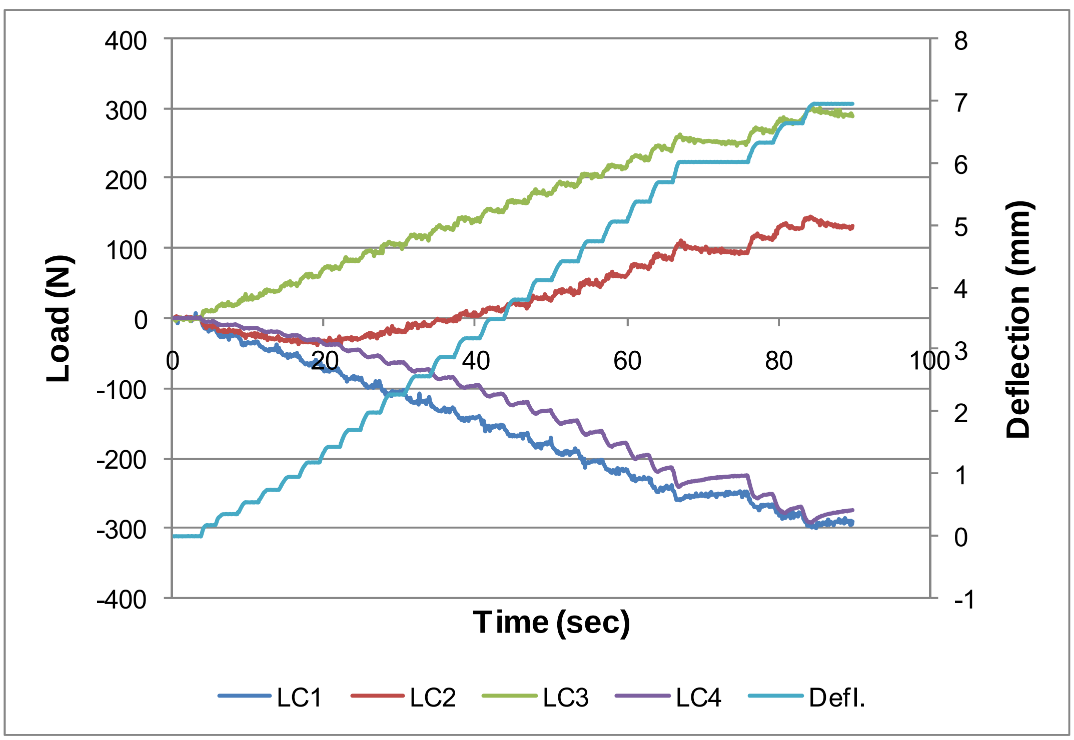

Figure C8: Load and deflection versus time for push over trial 0-PLR-43-2

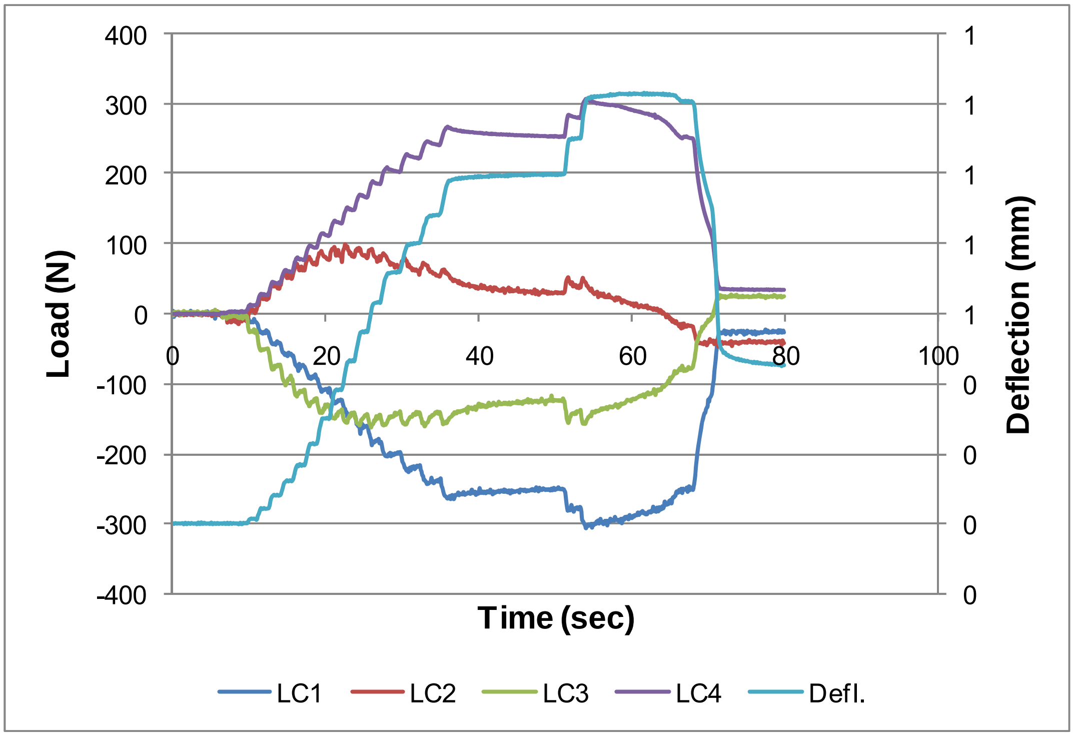

Figure C9: Load and deflection versus time for push over trial 90-PLL-43-1

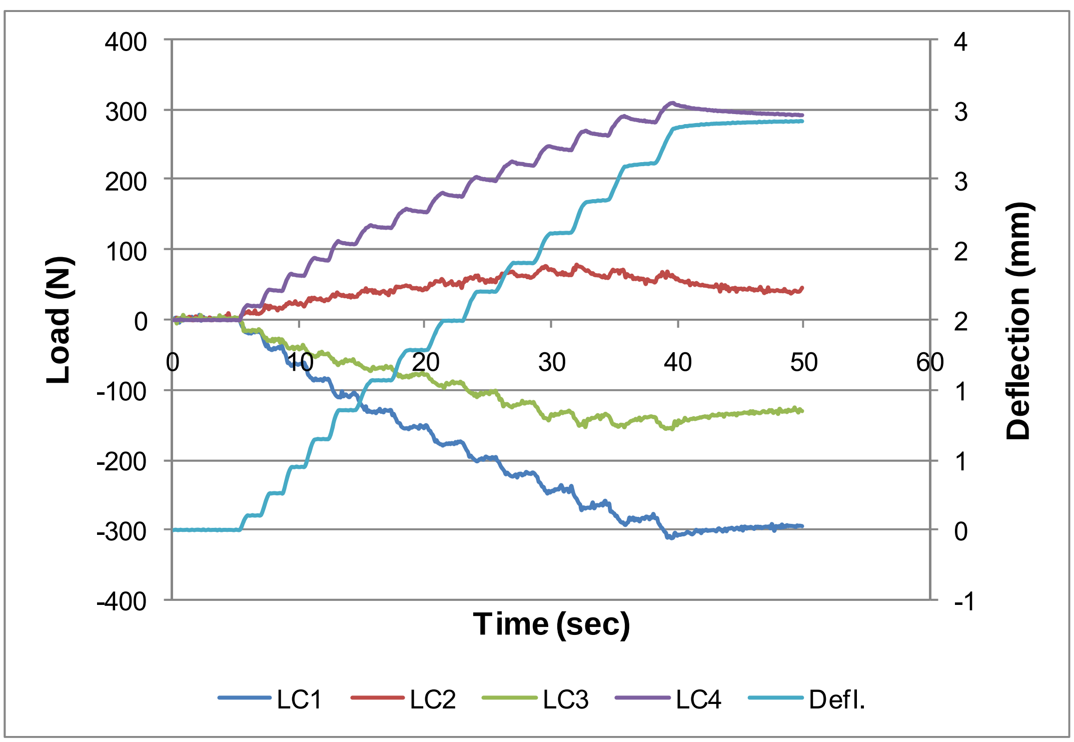

Figure C10: Load and deflection versus time for push over trial 90-PLL-43-2

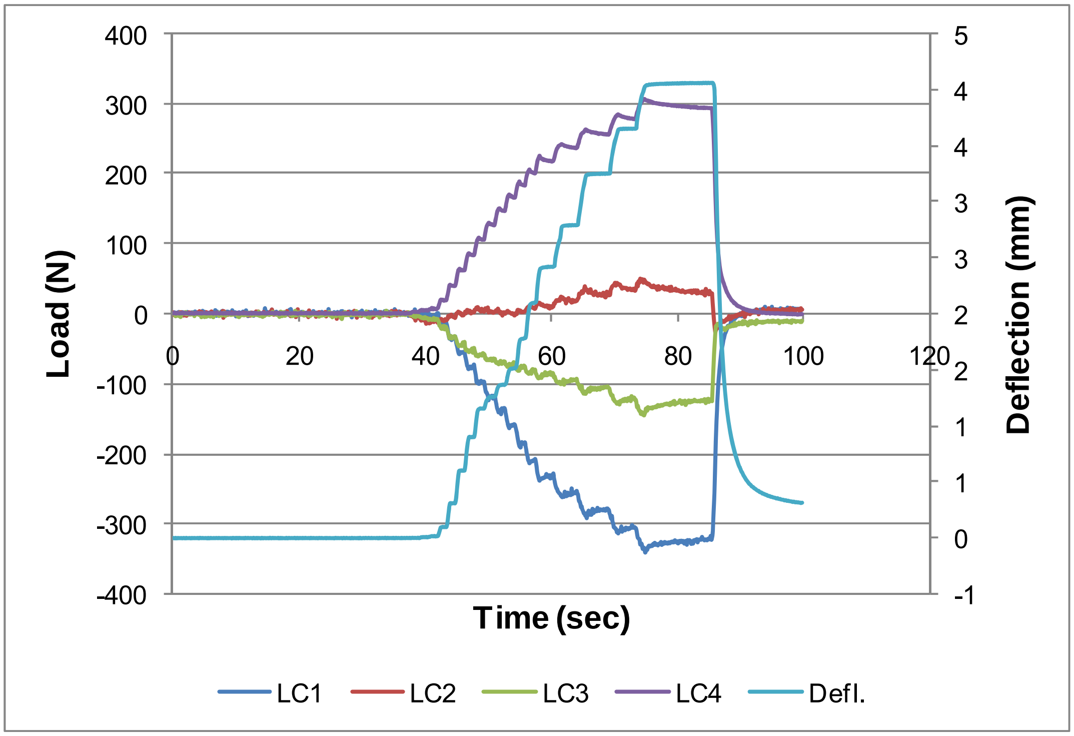

Figure C11: Load and deflection versus time for push over trial 90-PLL-43-3

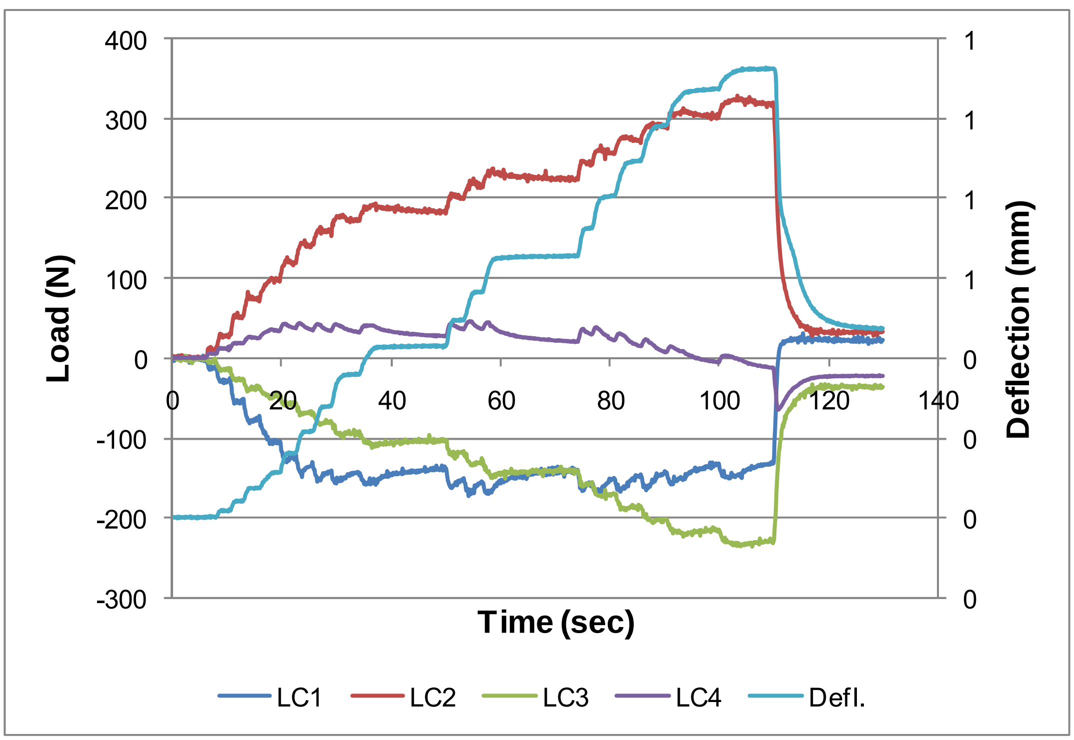

Figure C12: Load and deflection versus time for push over trial 90-PLR-43-3

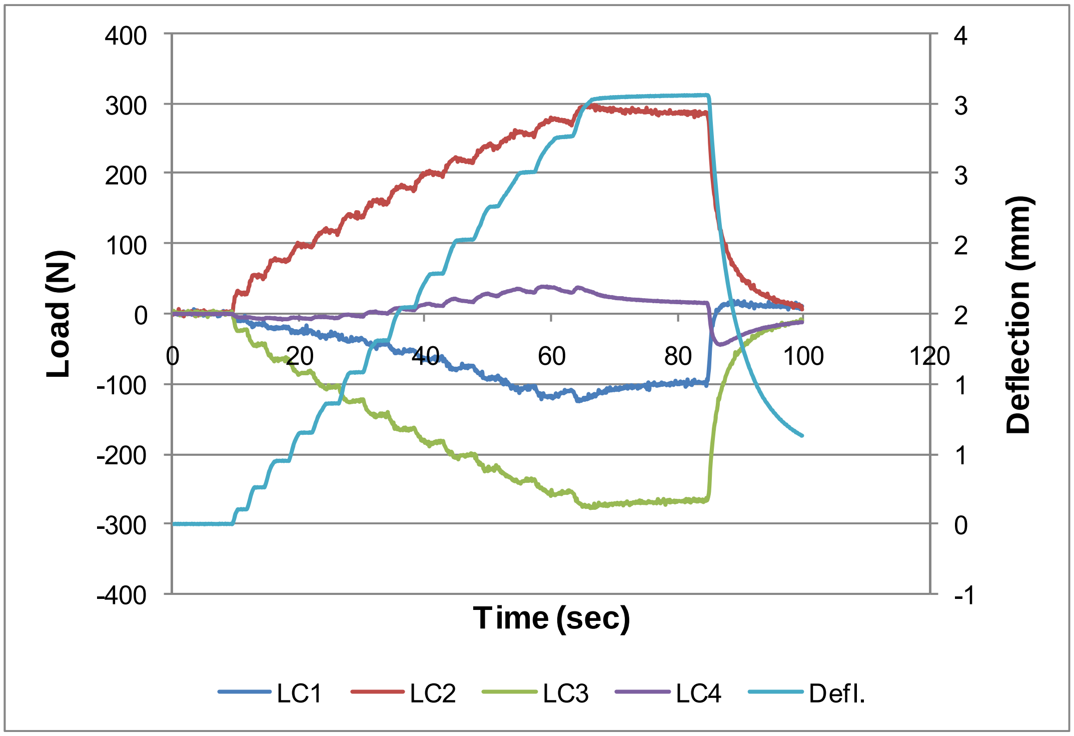

Figure C13: Load and deflection versus time for push over trial 90-PLR-43-2

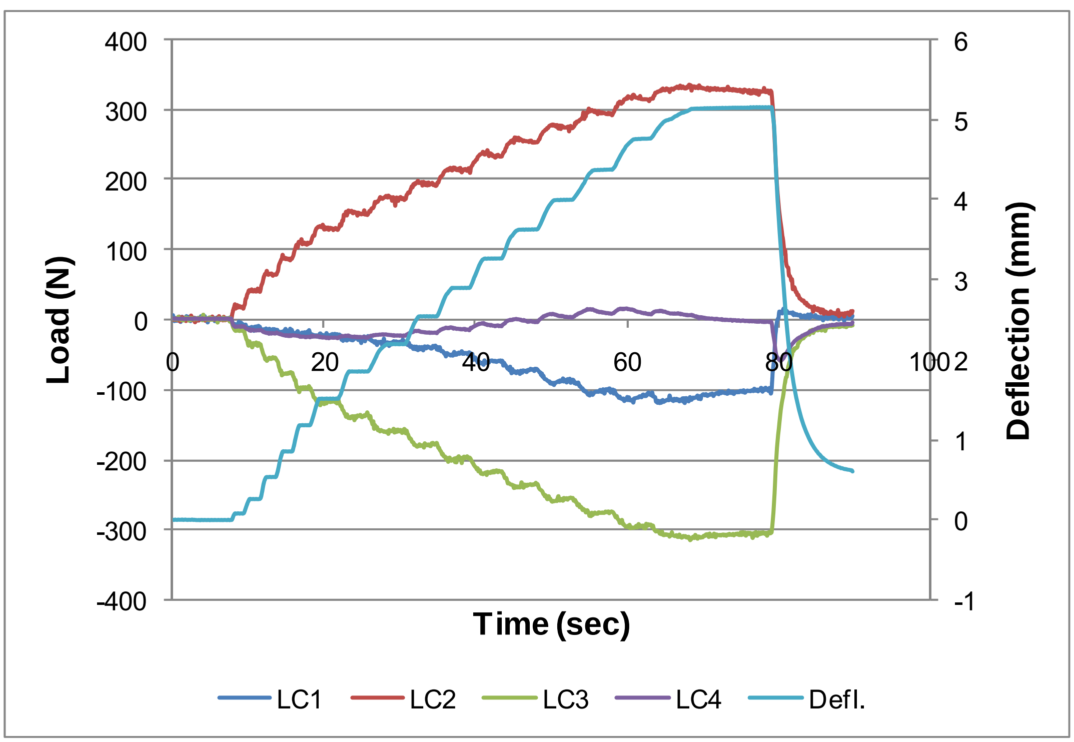

Figure C14: Load and deflection versus time for push over trial 90-PLR-43-1

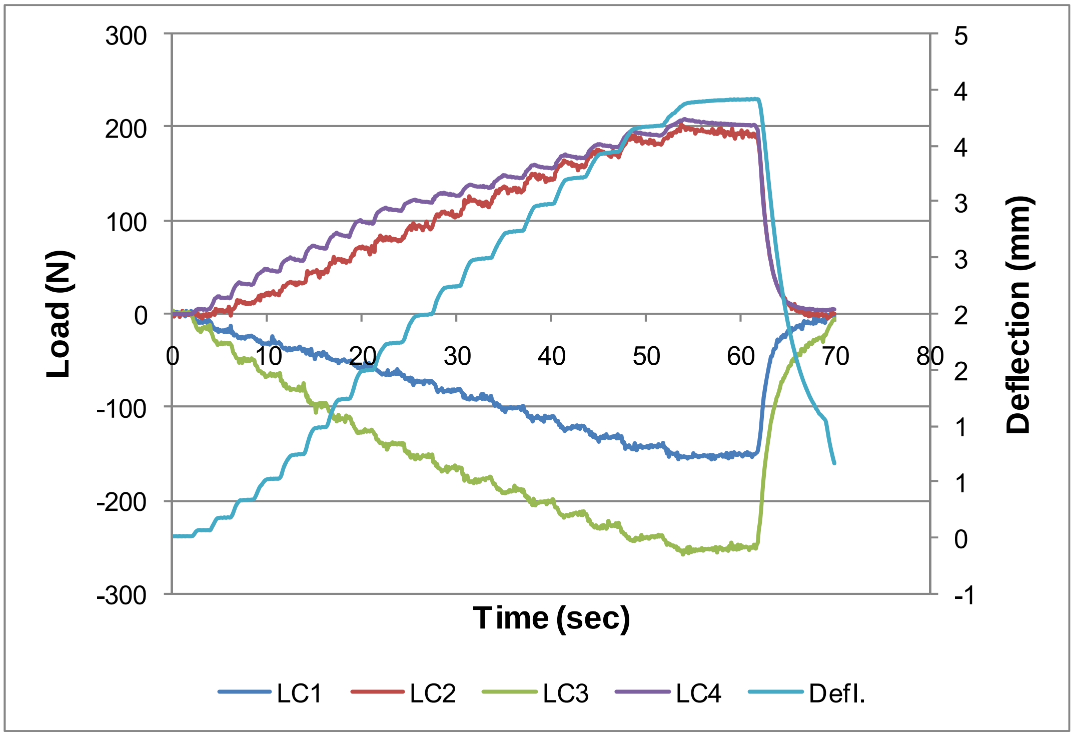

Figure C15: Load and deflection versus time for push over trial 90-DL-43-1

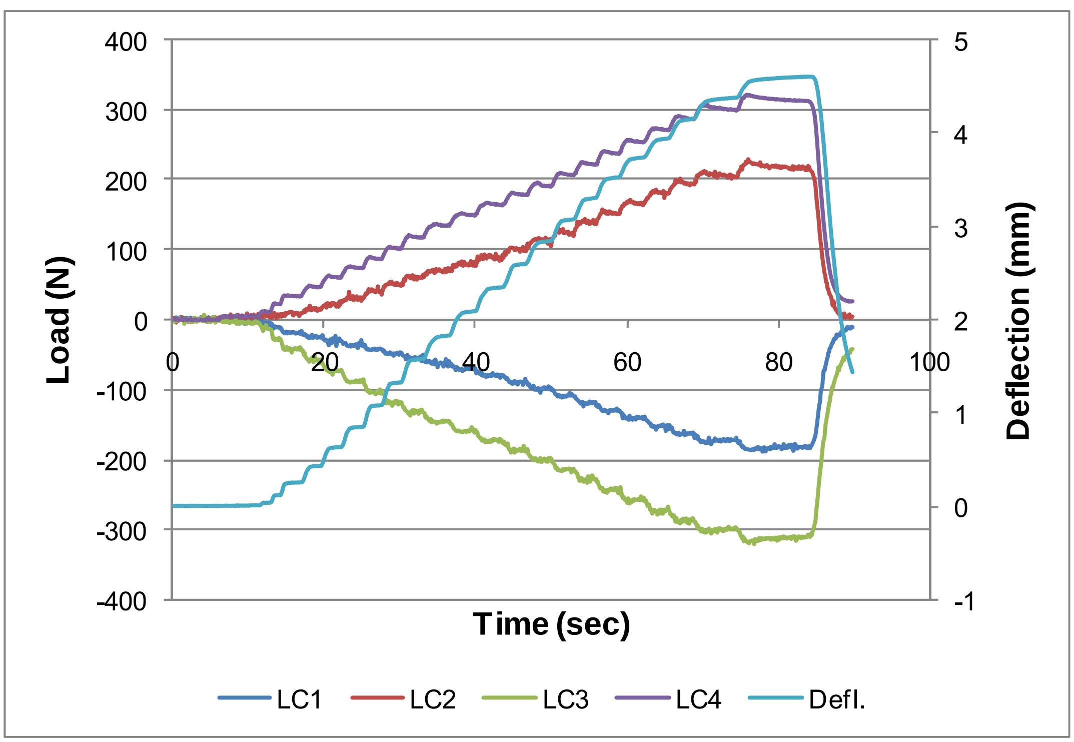

Figure C16: Load and deflection versus time for push over trial 90-DL-43-2

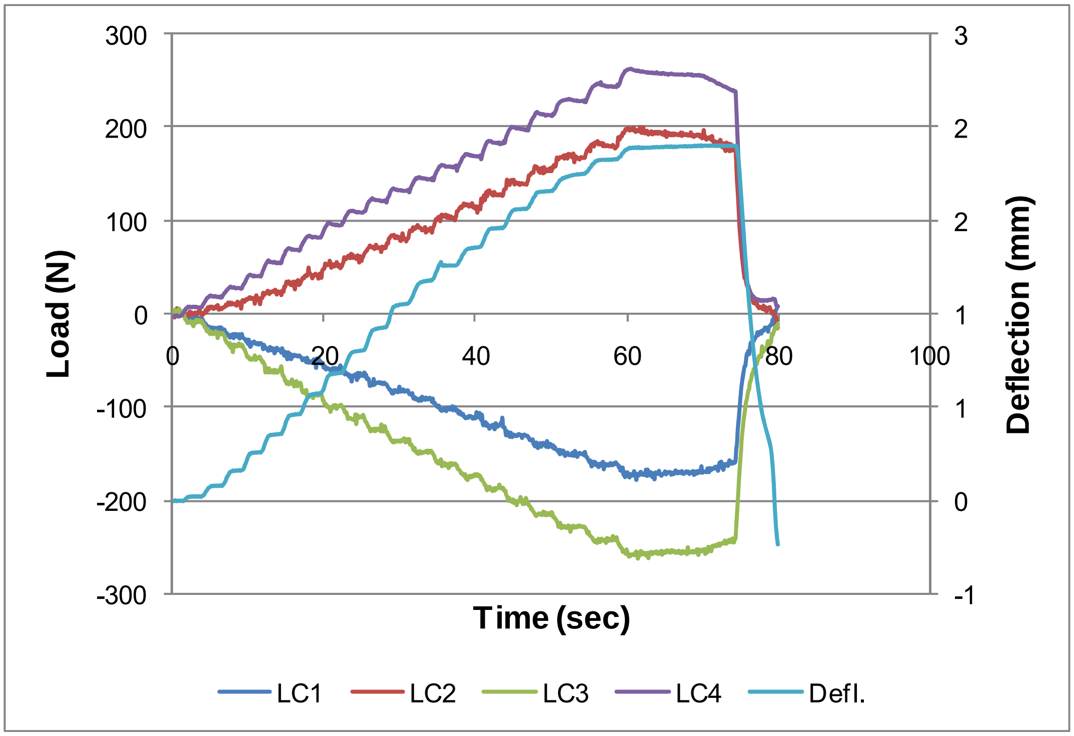

Figure C17: Load and deflection versus time for push over trial 90-DL-43-3

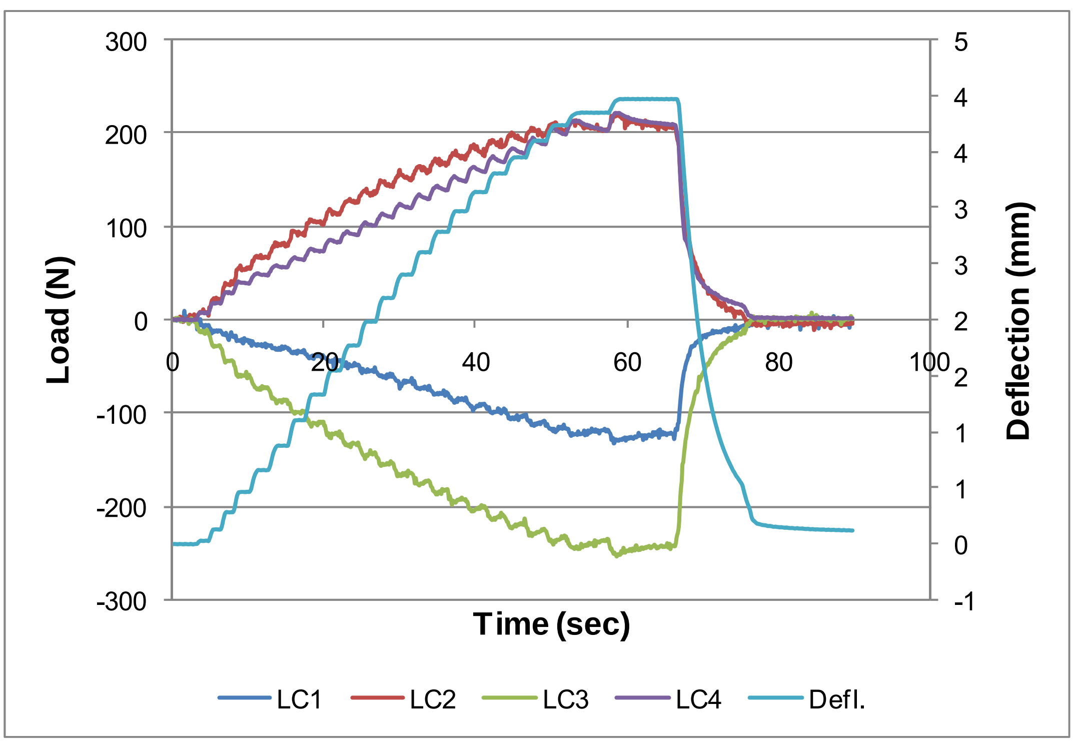

Figure C18: Load and deflection versus time for push over trial 90-PLC-43-1

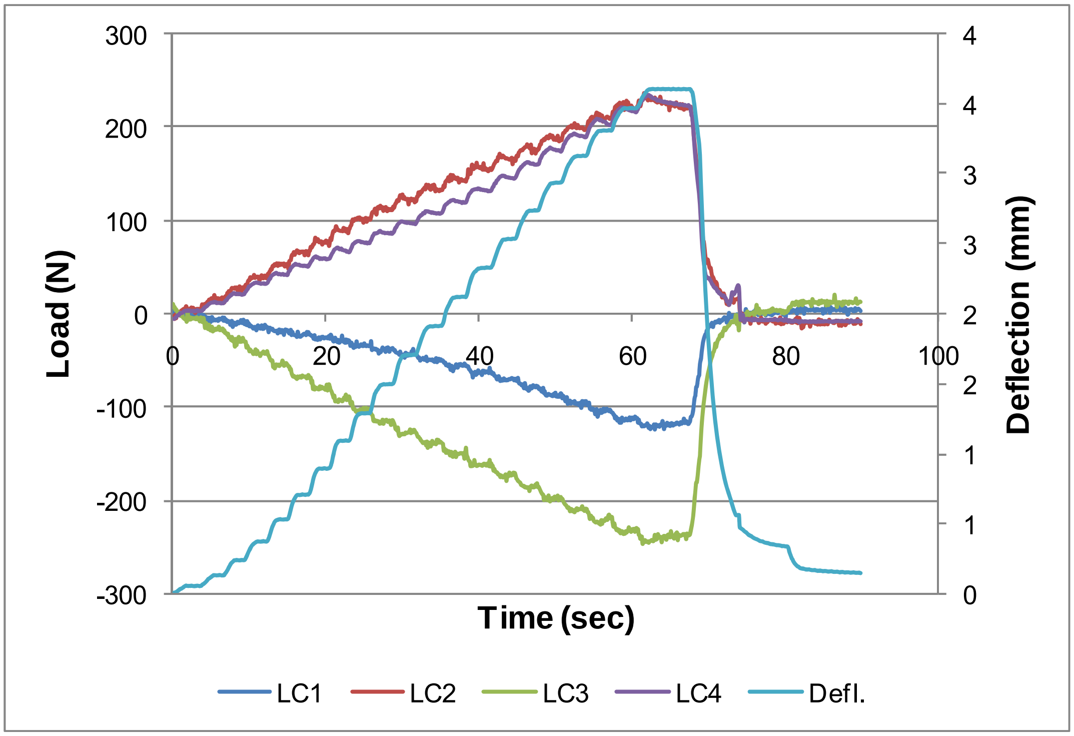

Figure C19: Load and deflection versus time for push over trial 90-PLC-43-2

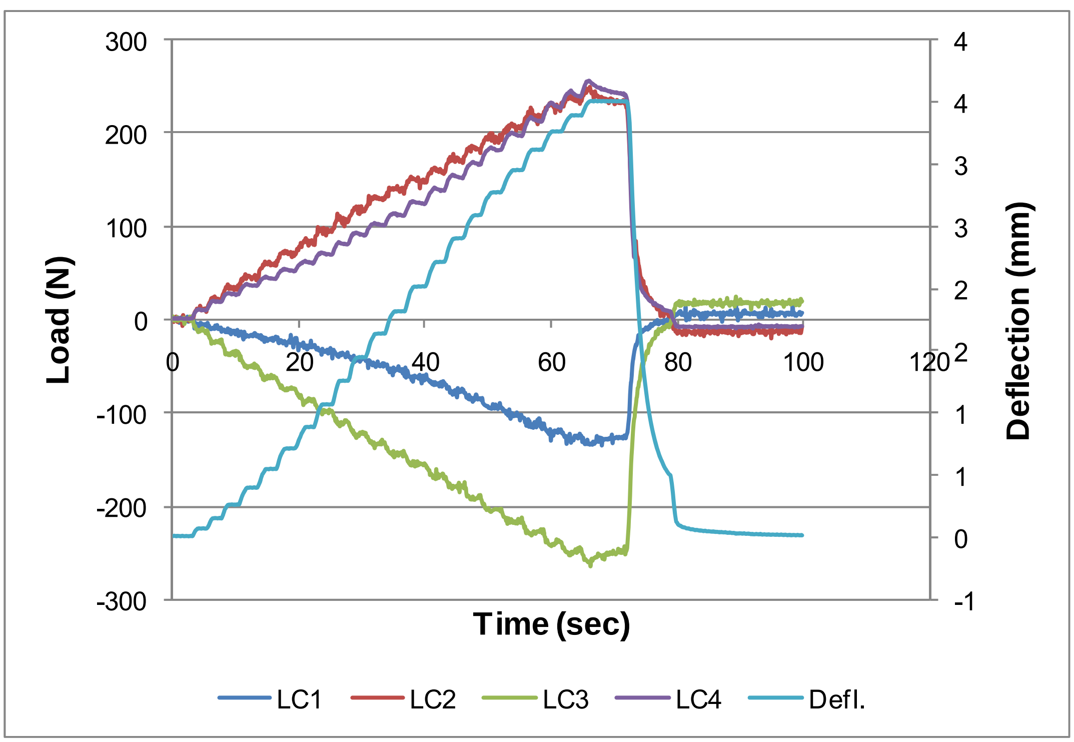

Figure C20: Load and deflection versus time for push over trial 90-PLC-43-3

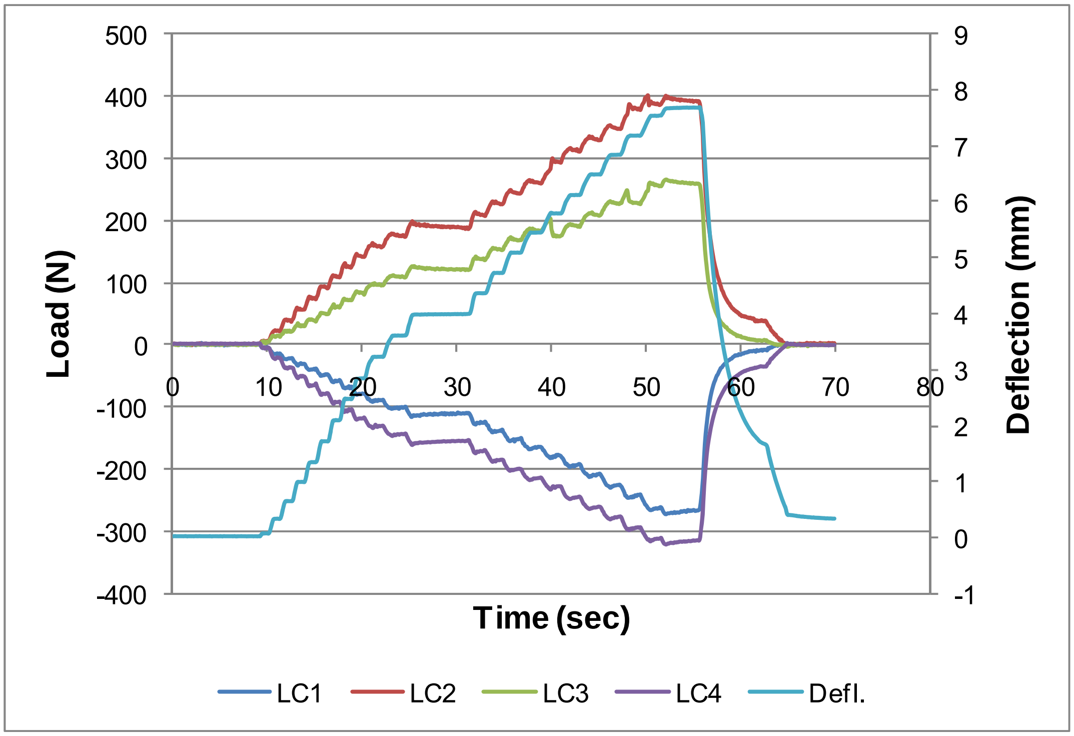

Figure C21: Load and deflection versus time for push over trial 0-DL-43-1

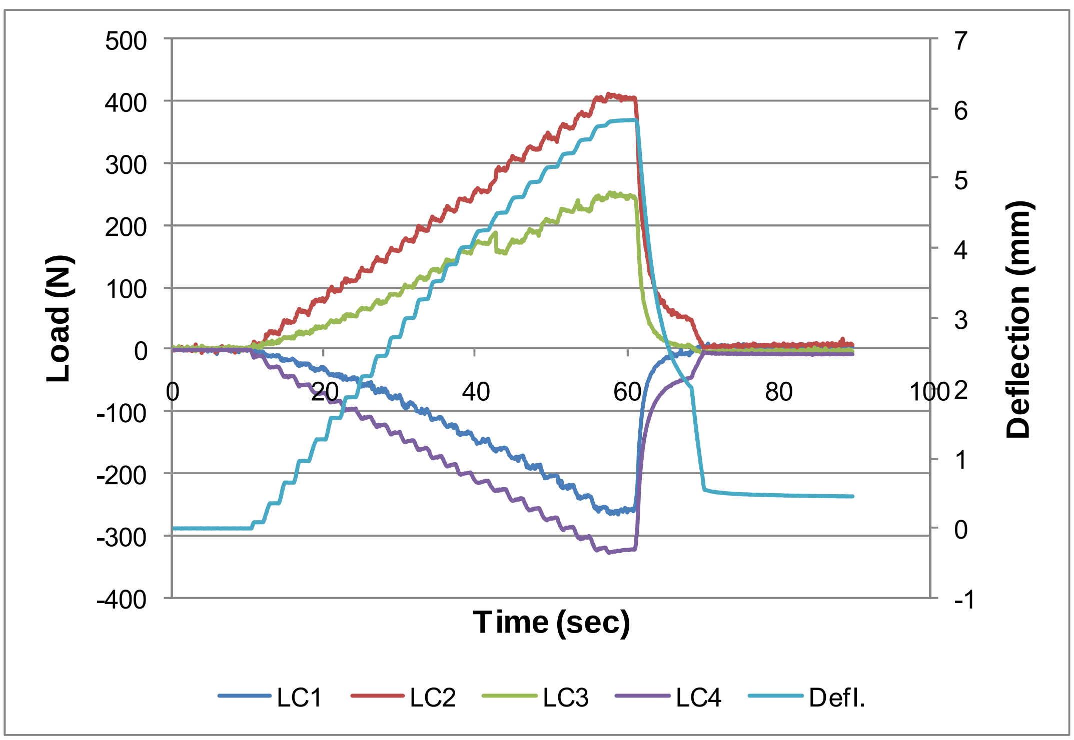

Figure C22: Load and deflection versus time for push over trial 0-DL-43-3

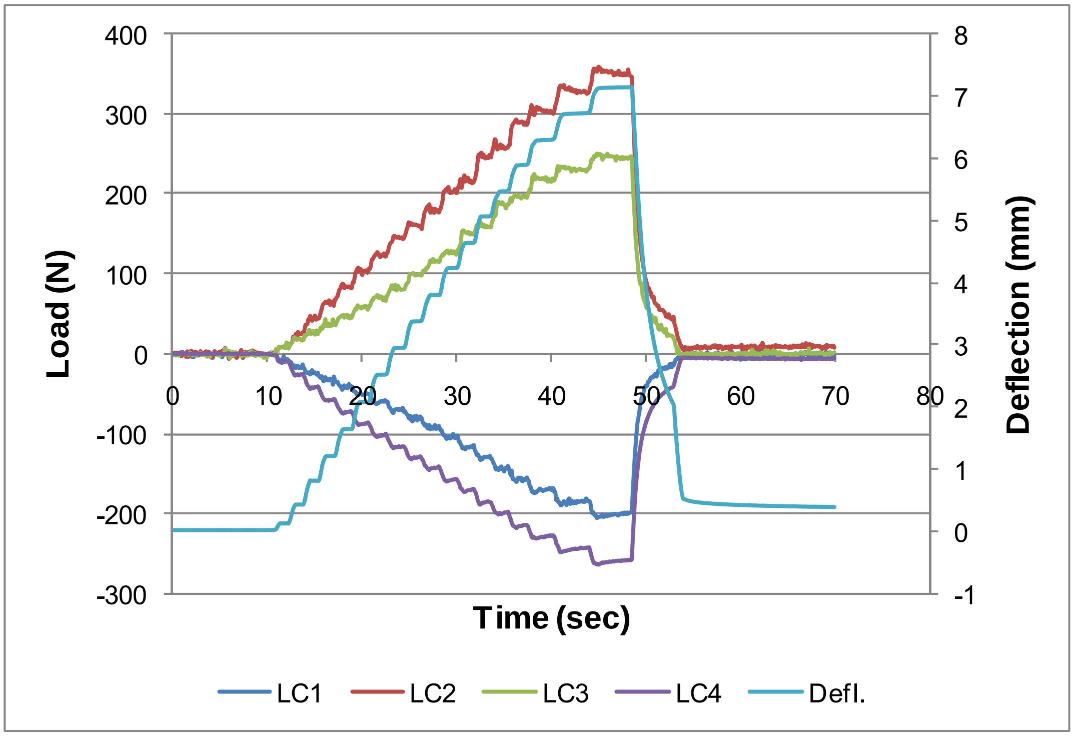

Figure C23: Load and deflection versus time for push over trial 0-DL-36-2

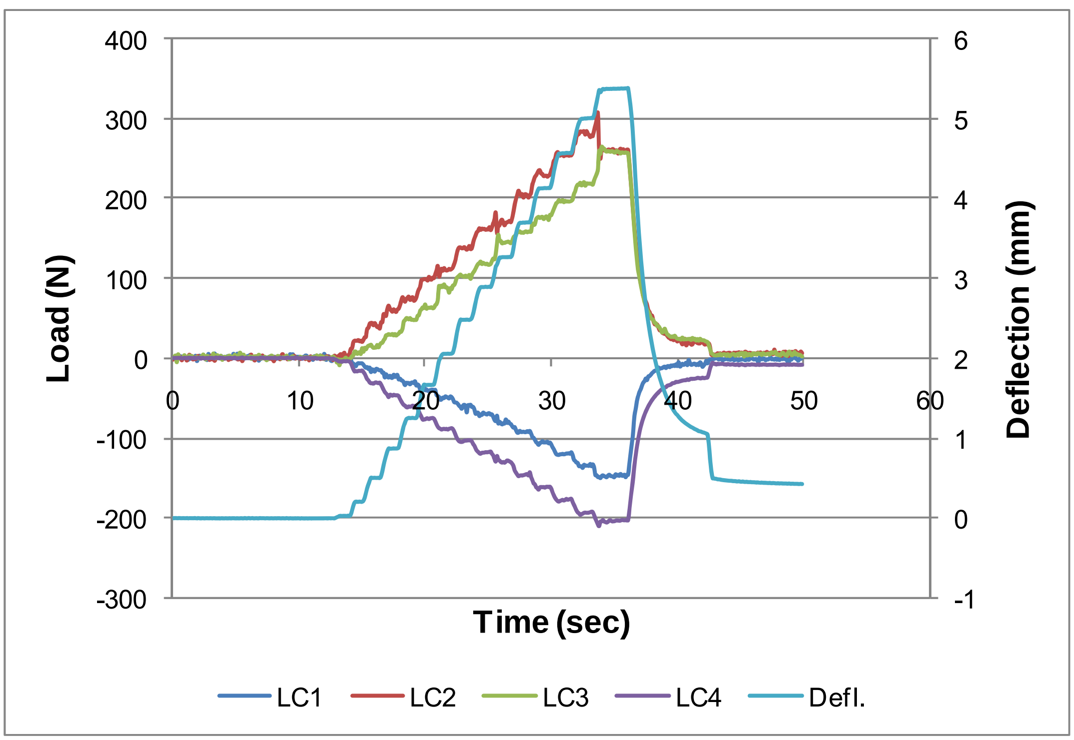

Figure C24: Load and deflection versus time for push over trial 0-DL-27-2

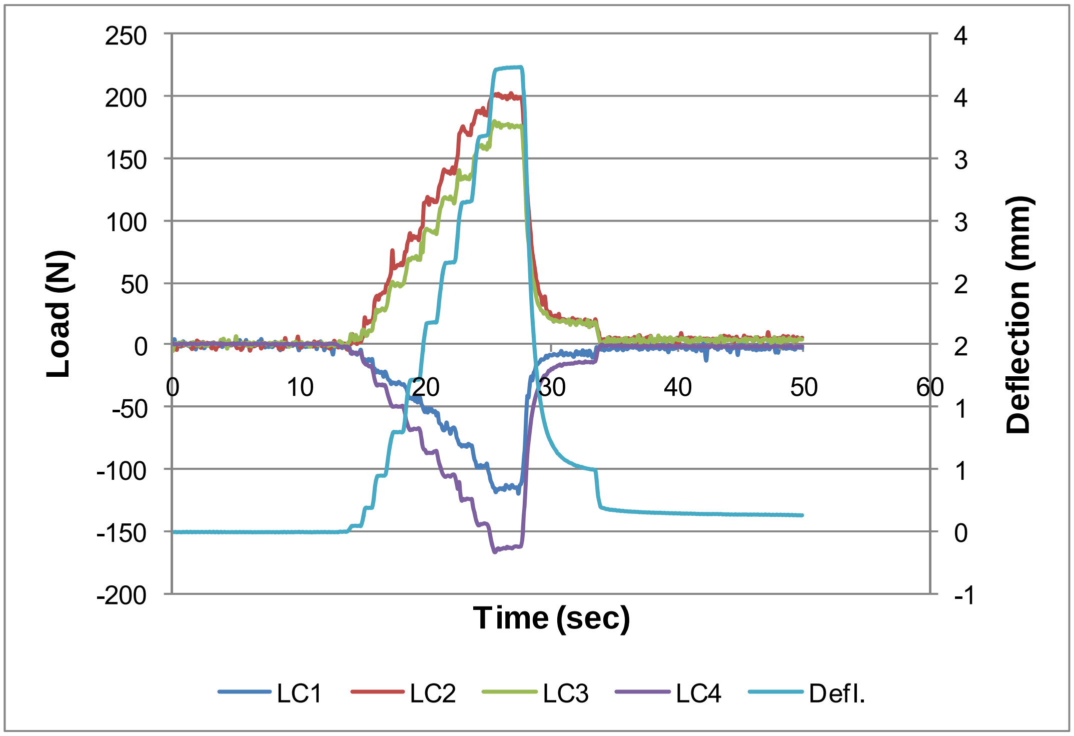

Figure C25: Load and deflection versus time for push over trial 0-DL-18-2

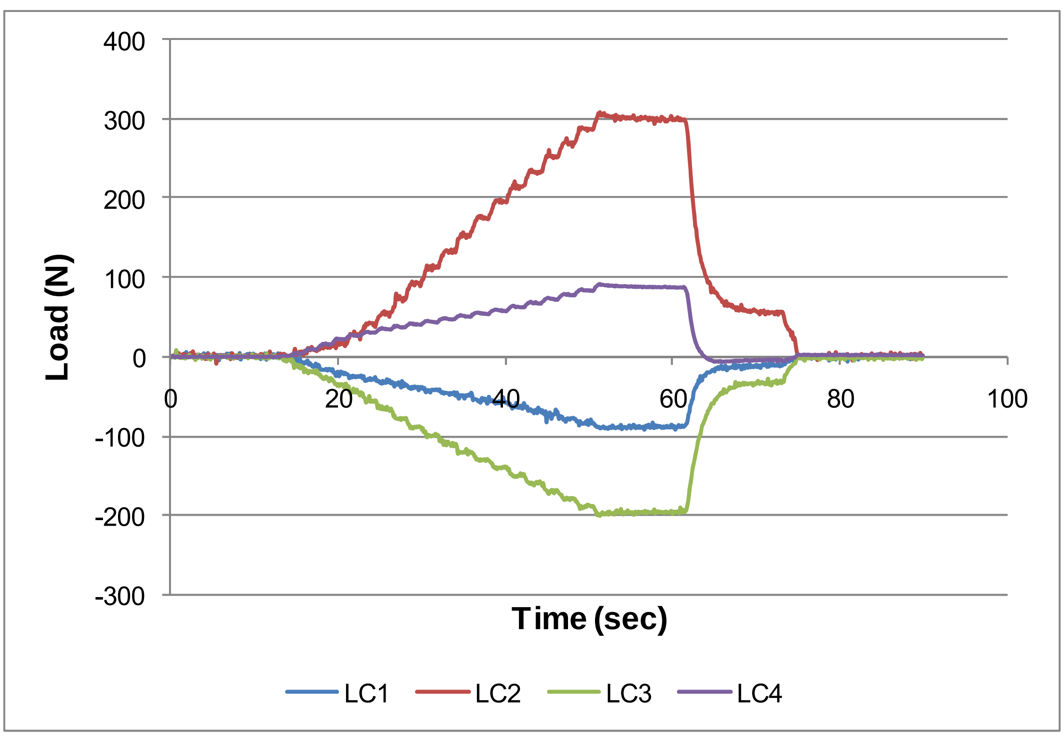

Figure C26: Load and deflection versus time for push over trial 90-DL-38-2

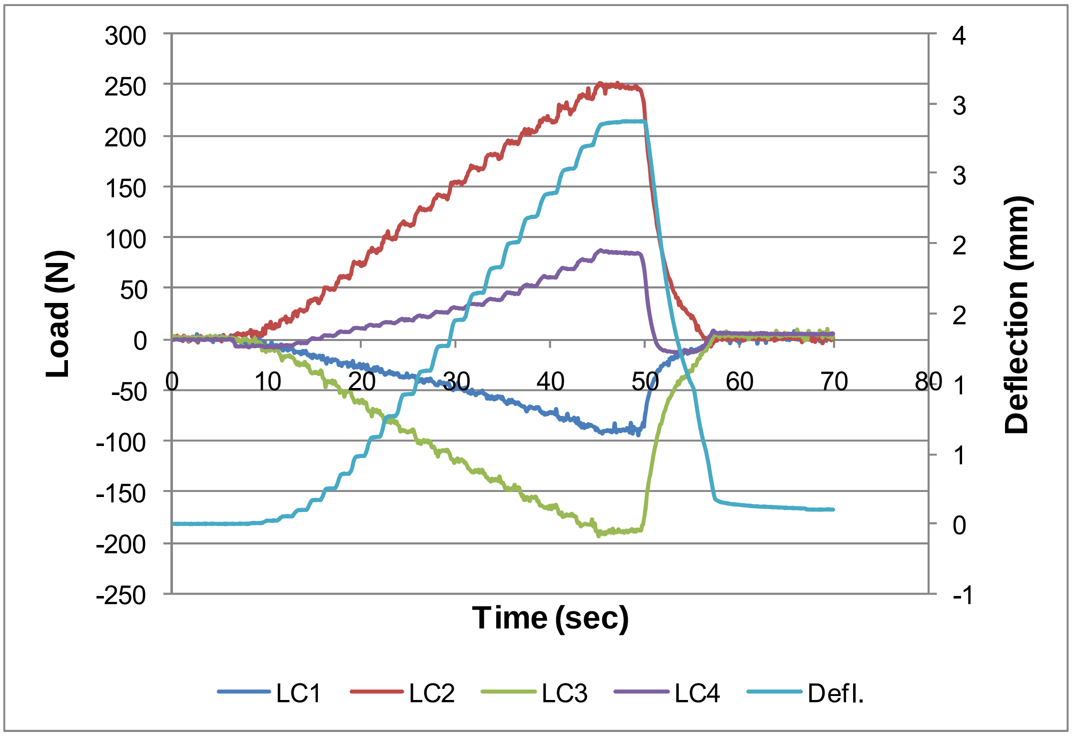

Figure C27: Load and deflection versus time for push over trial 90-DL-32-2

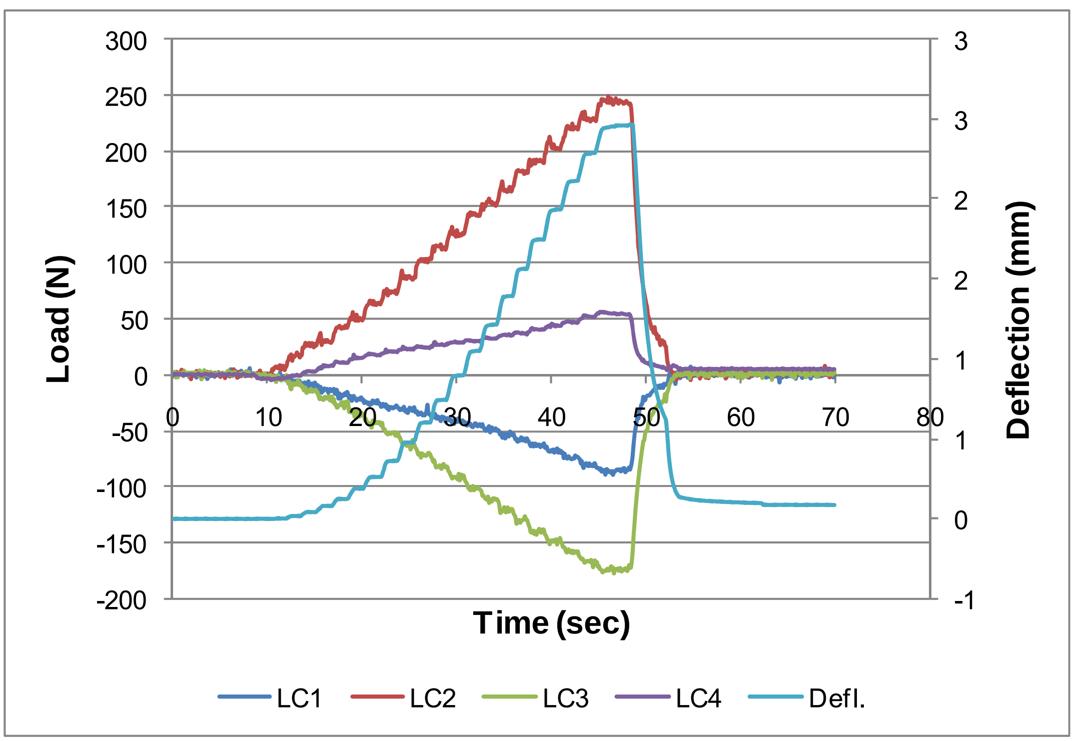

Figure C28: Load and deflection versus time for push over trial 90-DL-26-2

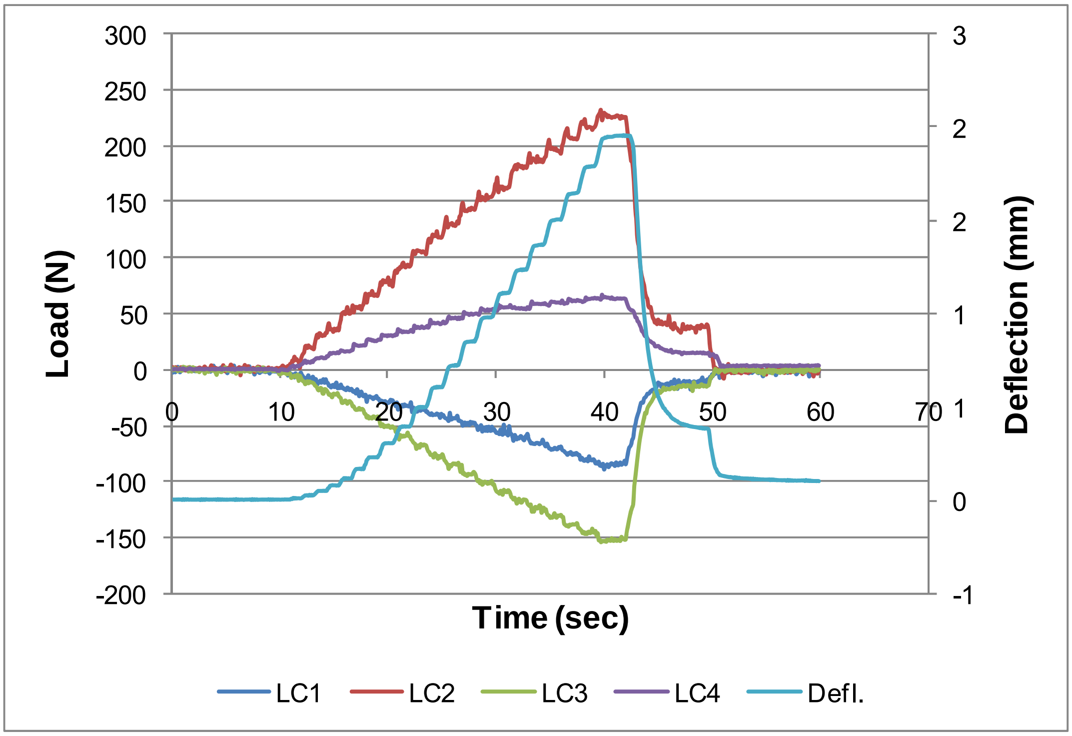

Figure C29: Load and deflection versus time for push over trial 90-DL-21-2

Appendix D – Data Analysis

Figures D1 and D2 demonstrate the methodology used to analyze the data from importing the raw data files into excel to extracting relevant data from the output.

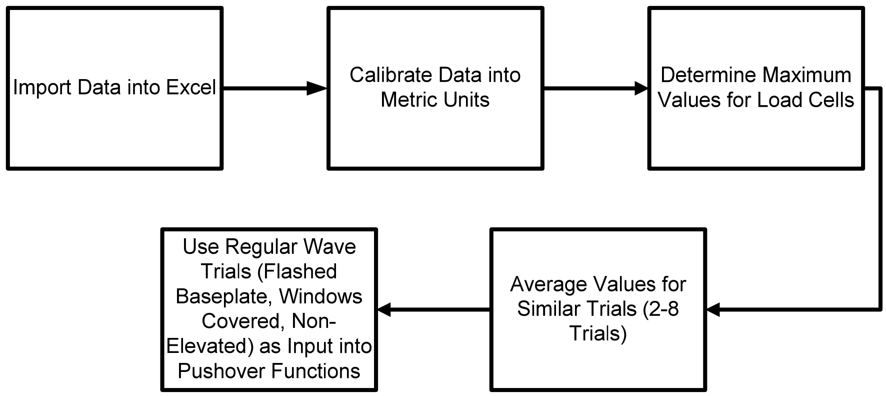

Figure D1: Flowchart describing analysis of wave lab data

.

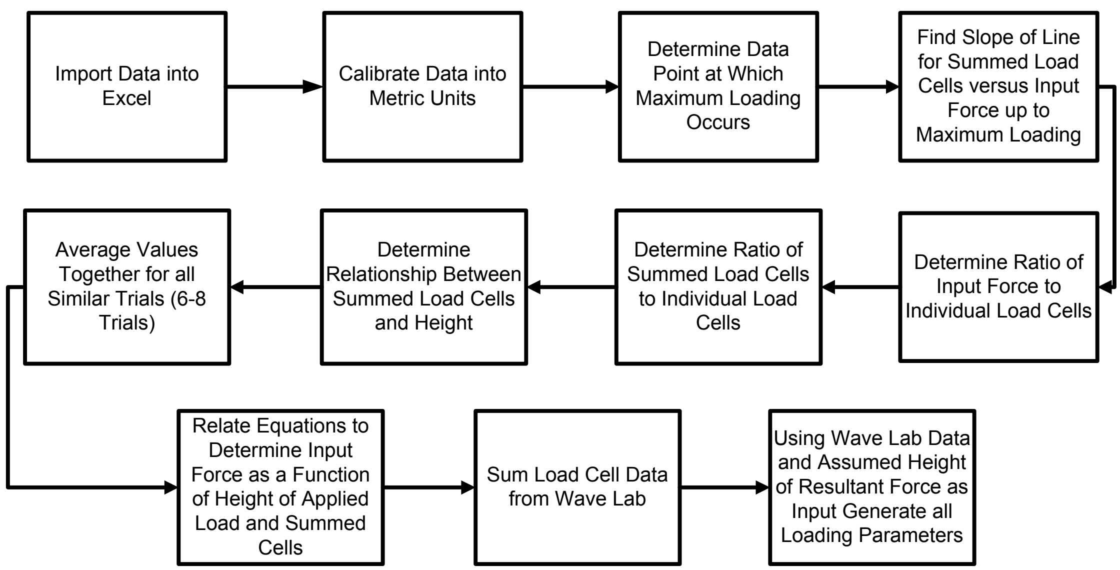

Figure D2: Flowchart describing analysis of push over test data and relating to wave lab data

Difference Between Wave Height and Bore Height

During the wave lab trials solitary waves of different amplitudes were generated by the wave maker. These waves travel towards the structure and break upon entering shallow waters in the sloped region of the wave basin. This broken wave is referred to as a broken bore, which is defined as a travelling wave with an abrupt vertical front or wall of water. In general, waves break when they enter water that 1.3 times as deep as the wave is high. In the results these are referred to as their initial wave height, e.g. 10 cm, not the bore height. The initial wave height is still a good indicator of the initial energy of the wave and therefore is still an appropriate measurement for discussing the results.

Table D1: Data from Arnason (2005), used in (3) and (4)

H_B (cm)	u (cm/s)	*F/b* (N/m)	*Eqn. 3* (N/m)	Over-Estimate	*Eqn. 4* (N/m)	Over-Estimate
5.08	57	18.9	113.9	6.0	29.2	1.5
5.85	70	30.4	151.1	5.0	45.5	1.5
6.58	82	43.8	191.1	4.4	65.5	1.5
7.27	93	59.8	233.3	3.9	88.8	1.5
7.92	104	73.8	276.9	3.8	116.4	1.6
8.55	114	95.2	322.7	3.4	147.0	1.5
9.15	124	117.7	369.6	3.1	181.8	1.5
9.74	133	145.1	418.8	2.9	218.8	1.5
10.3	142	165.9	468.3	2.8	259.7	1.6

Table D2: Undular bore data from Ramsden (1993), used in (3) and (4)

H_B (cm)	c (cm/s)	F/b (N/m)	*Eqn. 3* (N/m)	Over-Estimate	*Eqn. 4* (N/m)	Over-Estimate
14.28	146.8	328.1	900.2	2.7	407.8	1.2
13.45	144.7	349.2	798.6	2.3	370.3	1.1
14.28	146.7	328.5	900.2	2.7	407.3	1.2
13.45	143.8	349.7	798.6	2.3	366.9	1.0
14.25	146.5	322.8	896.4	2.8	405.4	1.3